SYNERGISTIC CO-PYROLYSIS OF BIOMASS AND

NATURAL GAS OVER HZSM-5 CATALYSTS

By

ZIXU YANG

Bachelor of Engineering in Thermal and Power Engineering
Huazhong University of Science and Technology
Wuhan, China
2009

Master of Engineering in Thermal Engineering
Huazhong University of Science and Technology
Wuhan, China
2012

Submitted to the Faculty of the
Graduate College of the
Oklahoma State University
in partial fulfillment of
the requirements for
the Degree of
DOCTOR OF PHILOSOPHY
May, 2016

SYNERGISTIC CO-PYROLYSIS OF BIOMASS AND

NATURAL GAS OVER HZSM-5 CATALYSTS

Dissertation Approved:

Dr. Ajay Kumar

Dissertation Adviser

Dr. Raymond L. Huhnke

Dr. Hasan Atiyeh

Dr. Clint Aichele

ACKNOWLEDGEMENTS

With the completion of this dissertation, my school career finally comes to an end. This is a great moment that is worth to be cherished forever in my life indeed. But more important, I owe my deepest gratitude to those who devote their time and effort to guide and help me to make this achievement.

First and foremost I am deeply indebted to my advisor, Dr. Ajay Kumar for his mentorship role during my whole doctoral work. I appreciate all his contributions of time, ideas, and funding to make my Ph.D. experience productive and stimulating. Dr. Kumar provided me with every bit of guidance, assistance, and expertise that I needed to improve my research skills and records. Dr. Kumar also offered me freedom to work on the area that attracted me, in the meantime contributed valuable feedback, advice, and encouragement.

I would like to thank Dr. Allen Apblett, from chemistry department, Oklahoma State University for assistance with catalysts synthesis. I am deeply grateful to him for his patience and rigorousness, and these attributes were contagious and motivational for me during the tough times in the Ph.D. pursuit. I gratefully acknowledge the members of my Ph.D. committee, Dr. Clint Aichele, Dr. Hasan Atiyeh and Dr. Raymond.Huhnke for their time and valuable advice on my Ph.D. research.

I am very thankful to Mr. Mark Gilstrap, lab manager of bioenergy lab where most of my Ph.D. research activities occurred, for substantial guidance and comments on lab safety and handling and repairing of analytical instruments. I also appreciate the support from the staff in

BAE lab, Mr. Wayne R. Kiner, Mr. Mike Veldman, and Mr. Jason Walker for fabrication of the experimental setup and temperature control systems used in my Ph.D. research and other research projects.

I have been blessed with a friendly and cheerful group of fellow students. Many thanks to Dr. Prakash Bhoi, Dr. Ashokkumar M Sharmar, Redemptus Tshikesho, Sunil Thapa, Nata Indrawan, Madhura Sarkar, Cody Collins and Mohit Dobhal for their assistance and collaboration on my Ph.D. research.

Finally, I would like to express my heart-felt gratitude to my family for their love, patience and sacrifices. Without them, none of this would have been possible. I am grateful to my parents for their continuous support and encouragement to all my pursuits. I am also thankful to my baby boy who is ready to arrive soon. His arrival definitely makes my family perfect, and at the same time stimulates me to strive harder and take more responsibility in the future life. This last word of acknowledgment I have saved for my dearest wife Kezhen Qian, who has been with me throughout my whole Ph.D. pursuit and has made them the best years of my life. Thank you.

Name: ZIXU YANG

Date of Degree: May, 2016

Title of Study: SYNERGISTIC CO-PYROLYSIS OF BIOMASS AND NATURAL GAS OVER
HZSM-5 CATALYSTS

Major Field: BIOSYSTEMS AND AGRICULTURAL ENGINEERING

Abstract: Bio-oil produced from pyrolysis of lignocellulose biomass is regarded as a potential intermediate to synthesize renewable hydrocarbon fuels and chemicals. However, the utilization of bio-oil has been challenged by undesirable attributes associated with its high oxygen content. The current study is focused on effective technologies that address the issues with unwanted properties of bio-oil and result in a product that is compatible to the current refinery infrastructures in long term. The mechanisms that lead to unstable properties of bio-oil during storage and recent developments on methods to improve storage stability of bio-oil were reviewed in Chapter 1. The pyrolytic behavior of eastern redcedar wood, an invasive plant in Oklahoma was investigated in Chapter 2. Results showed that pyrolysis conditions, such as reaction temperature and heating rate, and feedstock wood zones (heartwood and sapwood) had significant effects on the distribution and composition of pyrolysis products. In addition, alpha/beta-cedrene, a high-value product extracted from slow pyrolysis of eastern redcedar, was in higher amount from heartwood than from sapwood. Torrefied switchgrass (Chapter 3) yielded a higher H/C ratio and lower O/C ratio. Torrefaction enhanced the production of sugar-based compounds and phenols during pyrolysis. Densification enhanced the degradation of carbohydrate components in biomass feedstock thus yielded more secondary pyrolysis products, such as furans, ketones and acetic acids. Methane incorporated into the hydrodeoxygenation of lignin-derived phenols and increased the aromatics yield (Chapter 4). Molybdenum modified HZSM-5 catalysts were found to promote deoxygenation of lignin-derived phenols, resulting in more simple aromatics. In Chapter 5, catalysis of torrefied switchgrass with the intervention of methane was performed in presence of molybdenum modified bimetallic catalysts, MoAg/HZSM-5 and MoZn/HZSM-5. Bimetallic loading catalysts demonstrated a higher reactivity towards methane activation. The maximum aromatic carbon yield of 39.31 % was achieved from catalysis of raw switchgrass under methane atmosphere over MoZn/HZSM-5 at 700 °C. Torrefaction had no significant effect in improving the yield of aromatics from catalysis due to the loss of cellulose and concentration of lignin during torrefaction process. Catalysis of biomass with the intervention of cheap methane is a promising biomass upgrading technology.

TABLE OF CONTENTS

LIST OF TABLES

LIST OF FIGURES

CHAPTER I

INTRODUCTION AND LITERATURE REVIEW: RECENT DEVELOPMENTS TO

IMPROVE STORAGE AND TRANSPORTATION STABILITY OF BIO-OIL

This review paper was published as "Z. Yang, A. Kumar, R. Huhnke, Review of Recent

Developments to Improve Storage and Transportation Stability of Bio-oil, Renewable and

Sustainable Energy Reviews, 50 (2015) 859-870"

Abstract: The technology of fast pyrolysis is regarded as a promising route to convert lignocellulose biomass into liquid oil (bio-oil) which can be upgraded to transportable fuels and intermediate chemicals. However, the bio-oil is a complex mixture of organic compounds that are obtained in a non-equilibrium state. Therefore, the physical properties of bio-oil such as density, acidity, viscosity and chemical compositions change during storage and transportation. This change in properties during storage and transportation, also known as instability, is one of the most challenging problems in using bio-oil for any applications including as transportation fuels. This paper summarizes phenomena that lead to unstable properties of bio-oil and reviews recent developments in techniques used to improve the bio-oil properties for making bio-oil a stable intermediate product that can be easily handled and processed.

Keywords: Biomass; Biofuels; Fast Pyrolysis; Bio-oil; Stabilization; Storage; Review

1.1. Introduction

The research and development of renewable energy has gained much attention since the rise of crude oil price in 1970`s, especially on developing alternative fuels to satisfy both the rapid growth of worldwide economies and environmentally concerns[1, 2]. Biomass is considered as a sustainable resource for producing energy, fuels and alternative chemicals. Bio-based products prevail over conventional fossil-based products in reducing green-house gas effects because the production and use of biomass completes the carbon cycle in a short duration.

Biomass can be converted into different forms of energy and fuels through numerous processes (e.g. biological, thermochemical and mechanical processes) according to the types of raw materials and objective products. Among various conversions, thermochemical methods, such as combustion, gasification, pyrolysis and hydrothermal pyrolysis, provide the most efficient and convenient ways to convert biomass into multiple forms of fuels and products in terms of power, renewable gaseous, liquid and solid fuels, and chemicals. In addition, most of the thermochemical conversions are flexible in accepting diverse feedstocks and are simpler systems than biochemical conversion systems. In the cadre of thermochemical conversions technologies, pyrolysis techniques offer efficient ways to produce solid, liquid and gaseous products depending on the need. The liquid product, known as bio-oil, has been regarded as a carrier of energy and a source of intermediate chemicals which can be substituted for conventional fossil fuels and chemicals.

Pyrolysis cracks biomass thermally in the absence of oxygen resulting in solid (char), gaseous (syngas) and liquid (bio-oil) products. It is also the first step that occurs in combustion and gasification processes. Pyrolysis processes can be differentiated into three types according to operation conditions and objective products, as indicated in Table 1.1 [3-5]. Generally, low temperatures and long residence times facilitate high char yields. High temperatures and long residence times lead to high gas yields, while short residence times at moderate temperatures favor high production of liquid bio-oil.

Table 1.1. Types of pyrolysis [3, 6].

Pyrolysis processes	Residence time	Heating rate	Temperature (K)	Products
Carbonization	Days	Very low	~673	Charcoal
Torrefaction	10-60 min	Low	~563	Solid
Fast pyrolysis	0.5-5 sec	Very high	~723	Bio-oil
Flash pyrolysis	<1 sec	High	<723	Bio-oil, gas

Fast pyrolysis depolymerizes biomass at a rapid heating rate (~1000K/s) in the absence of oxygen. The generated vapors and aerosols are then quickly quenched to recover liquid oil (bio-oil), which accounts for 60~95 wt. % of overall products, depending on the feedstock composition [6, 7]. The incondensable gases and solid residues lead to syngas and char, respectively, as byproducts. High liquid yields require high heat and mass transfer rates and short residence times (usually less than 2s) to hinder secondary cracking of vapors. Reducing feedstock particle size helps increase heat and mass transfer rates. Finally, the char residue must be separated from the reactor system to prevent vapors from cracking [8]. Numerous pyrolysis reactor configurations, such as ablative reactor, fluidized bed, circulating fluidized bed, fixed bed, vacuum reactor and auger reactor, have been investigated to enhance yield and quality of the bio-oil [9-11]. Designs of new reactor configurations promising high liquid yield and optimum control are receiving significant attention, scale up and commercialization face major challenges.

Bio-oil is a mixture of products of degradation of cellulose, hemicellulose and lignin performed with rapid heating and cooling. Bio-oil can be produced from various types of forest and agricultural wastes and energy crops, including rice husk, wheat straw, wood, paper and switchgrass [12, 13]. The yield and chemical composition of bio-oil depends on the distribution of cellulose, hemicellulose and lignin in the feedstock. Compared to biomass, bio-oil has a higher energy density and can be readily transported and stored. Compared to fossil fuels, bio-oil is not a contributor of new CO_2 introduced into the atmosphere, since CO_2 is consumed during the growth of the biomass feedstock. SO_x and NO_x emissions from combustion of bio-oil are also negligible because most biomass feedstocks contain trace amount of sulfur and nitrogen. Therefore, bio-oil is considered a clean and renewable liquid fuel which can serve as a direct substitute for fossil

fuels in boilers and turbines for heat and power generation. In addition, bio-oil can be a potential resource and platform for production of transportation fuels and chemicals with higher added value [14]. A summary of possible applications of bio-oil is given in Figure 1.1 [2]. Despite these promises, commercialization of bio-oil for fuels and chemicals production is limited due to its notoriously undesirable characteristics, such as high and changing viscosity, high water and oxygen contents, low heating value and high acidity.
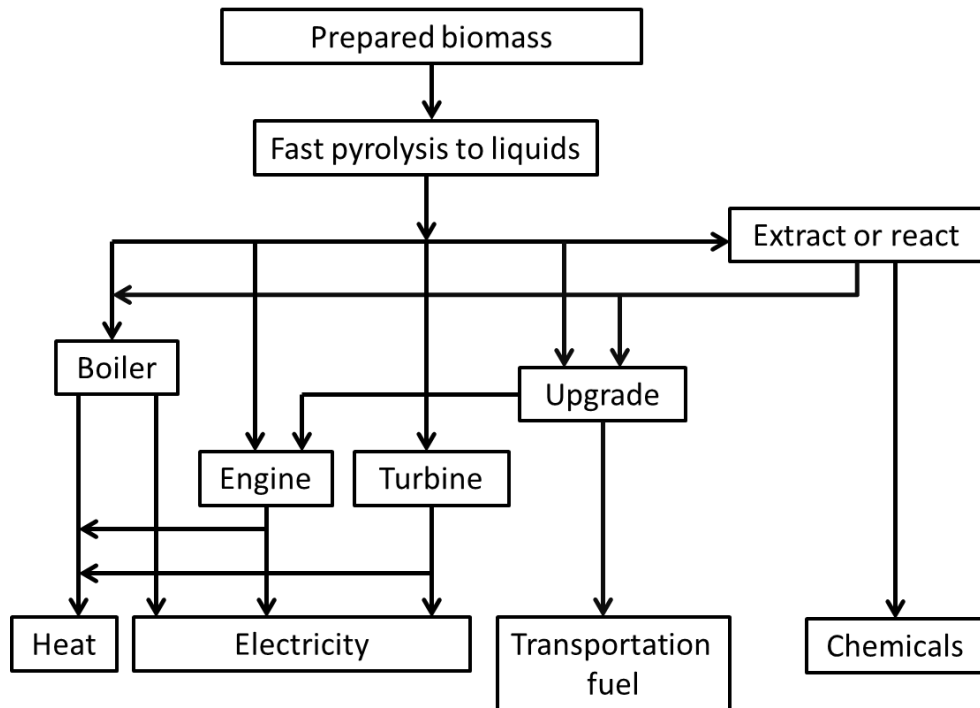
Figure 1.1 Applications of bio-oil. Adapted from [2]

Compared to conventional fossil fuels, bio-oils are not chemically or thermally stable due to their significant contents of reactive oxygenates, low boiling point volatiles and solid residues [15]. Consequently, the chemical reactions continue to occur during recover, storage and transportation of the pyrolysis liquids. These reactions lead to the changes in bio-oil physical and chemical properties that include increase in viscosity, phase separation, increase in average molecular weight and varying chemical composition. Previous studies [16, 17] indicated that the bio-oil viscosity and average molecular weight increased significantly as the storage temperature and time increased. In particular, the impacts of storage temperature were much stronger than

5

those of storage time. For example, the increase in average molecular weight[17] after storage at 80 °C for a week was equal to that after storage at room temperature for a year. In addition, the significant quantity of solid residue aggregates the changes in viscosity and average molecular weight of bio-oil discussed above, which makes bio-oil even more difficult to process and handle with. The changing viscosity with temperature creates additional challenges in feeding and injecting the fuel in a combustor, especially at low temperature. Clogging of filters and agglomeration of fuel transportation lines and the fuel circulation system frequently occur, [18] leading to major issues in operation and safety. In practice, bio-oils have to be preheated before injected into the combustor to reduce the viscosity. However, this method has been proved to be unsatisfactory since it raises another problem due to growth of particulates in the fuel feeding system[15]. The changing physiochemical properties of bio-oil during storage will require corresponding adjustments in the fuel feeding system and operation conditions, which may sacrifice performance of the combustor [15]. Therefore, the storage and transportation stability of bio-oil must be improved before it is stored, or transported to the end user or to the refineries for processing.

The storage and transportation stability is one of the most critical properties of bio-oil that hinder its successful commercialization for fuels, chemical and power production. The bio-oil stability can be improved by reduction of oxygen content, especially removal of the oxygen heteroatoms that contribute to the high acid number, and also substantial removal of char fines[19]. A stabilized bio-oil should have a total acid number of less than 10 and char fines content of less than 0.5 wt. %. Considerable efforts during the last five to ten years have contributed to the development of measuring standards and methods of bio-oil stability so that improvements in the storage and transportation stability of bio-oil can be quantified [20, 21]. So far, extensive studies have been focused on the upgrading of bio-oil into advanced bioproducts and/or biofuels, and the state-of-art of bio-oil upgrading has been critically reviewed [22, 23]. However, only limited information is available on the comprehensive understanding of bio-oil

stability, including the mechanisms leading to instability, methods to quantitatively measure

stability, the difference between stabilization and upgrading of bio-oil, and recent developments

in techniques and methods to improve the storage and transportation stability of bio-oil.

This review focuses on the recent developments in technologies to overcome challenges

in using bio-oil with a special focus on its stabilization for storage and transportation. Economic

and environmental issues and other challenges associated with these techniques are also

discussed.

1.2. Properties of bio-oil

Bio-oil, also known as pyrolysis oil, bio-crude-oil, wood liquids, wood oil, liquid smoke,

pyroligneous acid and liquid wood, is composed of a wide range of chemicals that are derived

from depolymerization and degradation of cellulose, hemicellulose and lignin. The chemical

composition of bio-oil is highly dependent on the pyrolysis conditions and variety of feedstock.

Proximate and elemental analyses of bio-oil are similar to those of biomass from which it is

derived, and contains a large number of oxygenated species and considerable water (as indicated

in Table 1.2). These properties make bio-oil significantly different from conventional fuel oil.

Table 1.2 Typical properties of bio-oil [13].

Physical property	Bio-oil	Heavy fuel oil
Moisture content (wt. %)	15-30	0.1
pH	0.5	-
Specific gravity (@ 15 °C)	1.2	0.94
Elemental compositions (wt. %)		
C	54-58	85
H	5.5-7.0	11
O	35-40	1.0
N	0-0.2	0.3
Ash	0-0.2	0.1
HHV (MJ/kg)	16-19	40
Viscosity (@ 50°C) (cP)	40-100	180
Solids (wt. %)	0.2-1	1
Distillation residue (wt. %)	Up to 50	1

*cP: centipoise, 1 cP=1 mPa·s

1.2.1. Water content

The water content of bio-oil varies from 15 to 30 wt. % depending on the feedstock and the pyrolysis cooling conditions[6]. Bio-oil water is mainly the result of the original moisture content of feedstock and dehydration reactions during pyrolysis. The solubilizing effects of hydrophilic compounds (acids, alcohols, aldehydes and ketones) in the liquid products make it difficult to separate water from bio-oil. The water content has both positive and detrimental effects on bio-oil properties. Water lowers the heating value and flame temperature; however, it also lowers viscosity and increases pH which improves bio-oil quality. Typically, the water content of bio-oil is analyzed using Karl Fischer titrimetric method [24] following the ASTM E 203.

1.2.2. Oxygen content

Although water is the most abundant compound in bio-oil contributing to bio-oil's high oxygen content, bio-oil also contains up to 400 oxygenated organic compounds that contribute 45~50 wt. % of the oxygen content in bio-oil [25]. High oxygen content results in bio-oil's properties being different from those of conventional fossil fuels (hydrocarbons). For example, the heating value of bio-oil is less than half of that of conventional fuels. Moreover, bio-oil is immiscible with hydrocarbon fuels, and most of the oxygenated species are very reactive leading to its instability during storage and transportation [13]. Typically, the oxygen content of bio-oil is measured by performing an elemental analysis of C, H, S, and N in percent of weight, and the difference is considered as the oxygen content.

1.2.3. Viscosity

The viscosity of bio-oil varies widely [14] (35~1000 cP at 40 °C) depending on the feedstock and processing conditions used to generate bio-oil. Also, unlike hydrocarbon fuels, viscosity of bio-oil decreases rapidly above room temperature [6, 26] and changes with time during storage. As stated above, the addition of water can decrease the viscosity. Viscosity is also reduced with the addition of polar solvents such as methanol or acetone [27]. The bio-oil

viscosity test can be performed using capillary or rotary viscometers at different temperatures, but temperature of 20 and 40 °C are usually recommended [6].

1.2.4. Acidity

Bio-oil is acidic (pH ranging from 2 to 3) due to the carboxylic acids formed during decomposition of biomass polymers[14]. This high acidity makes bio-oil very corrosive to materials used for transportation fuel pipelines and tanks which add to challenges in using bio-oil. The acidity of bio-oil is usually evaluated following ASTM D664 by measuring the total acid number (TAN, mg of KOH g^{-1}) [9], which is the quantity of KOH in milligrams needed to neutralize the acids in one gram of the bio-oil.

1.2.5. Ash Content

Bio-oil ash content can cause problems in some applications. The ash composition is dominated by alkali metals (potassium and sodium), which are responsible for the severe corrosion of turbines and deposition of heating surfaces and pipes during combustion [13]. Also, some metals are highly catalytic (e.g. potassium) and facilitate secondary reaction of pyrolysis vapors, which leads to loss of liquid yield. Biomass pretreatment, such as washing with water or dilute acid, is effective in removing ash from the raw biomass [28]. The ash content is determined by measuring the amount of non-combustible residues in the bio-oil following ASTM D482.

1.2.6. Aging and instability

Bio-oil is an intermediate product that is generated by first thermal degradation of biomass at a very rapid heating rate and then condensation of vapors and aerosols into liquid at a fast quenching rate. The process; however, does not reach a thermodynamically equilibrium. Therefore, some of the species are still highly active, leading to changes in physical and chemical properties of bio-oil during storage and transport [16, 29, 30]. Bio-oil tends to age at room temperature once it is collected, especially with increasing temperature. The result can be an increase in viscosity, decrease in water content, loss of volatiles, and phase separation [3]. The

9

degree of change in these physical properties is due to the chemical reactions that increase the average molecular weight of the bio-oil [29, 31]. Oasmaa et al [32, 33] found that the principal compositional changes during aging include a decrease in carbonyl compounds, such as aldehydes and ketones and an increase in the water-insolubles which are mainly composed of lignin fragments, extractives and solid residue.

The changes in chemical properties of bio-oil are usually associated with presence of highly active organic functional groups, such as aldehydes, alcohols, carboxylic acids, phenols and unsaturated hydrocarbons. Several chemical reactions that favor the thermodynamic equilibrium occurring during storage among these active compounds, are categorized into the following [17, 31, 34]: (1) formation of esters by esterification of alcohols and acids or by transesterification of two esters; (2) homopolymerization of aldehydes to form polyacetal oligomers; (3) addition of alcohol to aldehyde to form hemiacetals or acetals; (4) polymerization of phenol and aldehyde to form resins; (5) polymerization of furan derivatives; (6) reaction of alcohol with unsaturated aldehydes to form alkoxy aldehyde/acetal; (7) olefinic condensation; and (8) oxidation of alcohols and aldehydes to carboxylic acids. Besides these mechanisms mentioned above, Kim et al also [35] found that the low molecular weight components may participate in the polymerization with pyrolytic lignin, contributing to the increase of average molecular weight. Recently, few studies[36, 37] confirmed that the existence of free radicals was responsible for the bio-oil instability during storage. Solid char residues, that are comprised mainly of oxides and salts of metals, contribute to changes in bio-oil properties [22]. While char increases the viscosity of bio-oil, it offers plenty of catalytic sites for promoting several reactions [13]. It should also be noted that bio-oil is highly sensitive to heat and oxygen because some of bio-oil compounds are more reactive with the availability of heat and oxygen [14, 38]. Therefore, bio-oil must be sealed and kept away from heat sources.

1.3. Methods to measure the stability of bio-oil

As discussed in earlier sections, bio-oils are not as chemically or thermally stable as the conventional fossil fuels due to the high amount of reactive functional groups, solid residue and low boiling point volatiles[15, 21]. Changes of physical and chemical properties (e.g. phase separation, viscosity increase, increase of molecular weight, and change of acidity and moisture content, etc.) will occur in bio-oil during the storage, transportation and utilization in various conditions. The term "fuel stability" has been used to evaluate the resistance of a fuel to change[39]. Particularly, it can refer to "storage stability" at ambient conditions, defined as the ability of a fuel to retain its original properties during storage over an extended period of time without significant degradation [40]. Procedures for testing the storage stability of hydrocarbon fuels are available in ASTM standards [41, 42]. Generally, these standards are followed to test the fuel stability towards thermal and/or oxidizing environment. In addition, procedures for stability tests performed with accelerated methods [43, 44] are available in the standards so that the degree of aging is equivalent to if bio-oil had been stored in ambient conditions for a set time.

Similar to hydrocarbon fuels, research activities on evaluation of bio-oil stability are focused on two aspects, that is, thermal stability and oxidative stability. Aging experiments have been carried out at various research institutions to assess the fuel stability of bio-oil [15, 45-52]. Nevertheless, no standardized methods for measuring the stability of bio-oils are available.

1.3.1. Thermal stability test methods

Thermal stability of a fuel is defined as the capability of the fuel to withstand elevated temperature stress for a reasonable time period without noticeable deterioration[39]. Accelerated thermal aging processes have been broadly adopted for thermal stability tests [21, 47, 48]. In an accelerated thermal aging experiment, the bio-oil is stored at an elevated temperature for a certain time, and the physical and chemical properties prior to and after the aging process are analyzed [53]. An example of the accelerated aging were described in a round robin study on bio-oil viscosity and stability from International Energy Agency (IEA) [21]. Briefly, the bio-oil samples

were heated in sealed bottles at 80°C for 24 h, and then cooled at room temperature for 1.5 h before analysis. Based on the results from accelerated aging experiments, different methods of measuring bio-oil stability were developed and evaluated. Since the aging process causes substantial changes in water-insolubles and carbonyl products, the compositional changes in these products are used to evaluate the thermal stability of bio-oil. Instead of measuring these changes directly, correlations have been developed between these compositional changes and measurable parameters. For instance, the increase in water-insolubles [53] can be correlated with the increase in the average molecular weight and the increase in viscosity of the wood bio-oil. Similarly, the change in carbonyl content can be correlated with the change in viscosity measured by accelerated aging test (24 h @80 °C)[15]. Consequently, stability test methods based on measurements of the thermal stability indicators, such as viscosity change, average molecular weight change, the change in carbonyl content have been established [21, 24, 33].

1.3.1.1. Stability test method based on viscosity change

Bio-oil viscosity is a key parameter to evaluate its practical application and fuel quality. The changing viscosity with time increases the difficulty and cost of fuel-pumping and combustor operation. The change in viscosity of bio-oil over time are usually associated with the increase in molecular weight resulted from the polymerization reactions that proceed in the bio-oil [46]. Hence, the measurement of viscosity increment has been considered as a direct indicator of bio-oil stability [17, 21, 40, 45, 47, 54-56].

Stability test based on viscosity change assesses the stability of bio-oil by measuring the absolute increase in viscosity during an accelerated aging test (24 h @80 °C). To develop analytical standards for measuring physical and chemical properties of bio-oil[21], IEA suggested that in order to achieve a good repeatability, the amount of bio-oil sample and the sample bottle must be carefully controlled so that the mass loss due to volatilization is less than 0.05 wt % [21]. In addition, viscosity of bio-oil samples should be measured as kinematic viscosity at 40 °C

12

following ASTM D 445. The stability value can be calculated as the percent of increase in viscosity after the aging test compared with the original viscosity [21, 53].

1.3.1.2. Average molecular weight test method

In addition to the increased viscosity, increasing average molecular weight is another characteristic of bio-oil aging process. The main reason for the increase in molecular weight is the polymerization and condensation reactions of low molecular weight components during storage[31, 53]. The most common method for measuring the molecular weight distribution of bio-oil is gel permeation chromatography (GPC), also known as size exclusion chromatography (SEC) [10, 21, 24, 53]. In a GPC test, the bio-oil sample is prepared in a solution of tetrahydrofuran (THF). The injected sample is passed through two columns in series for separation and then detected by a refractive index (RI) detector[21]. The GPC must be calibrated against polystyrene standards for quantification. By evaluating the applicability of GPC methods to analyze pyrolysis oils and hydrodeoxgenated pyrolysis oils, Hoekstra et al. [57] suggested that GPC should not be used as a quantitative method to characterize bio-oil samples, because the RI detector response factors were not consistent among low and high molecular weight fractions. In addition, GPC was recommended to compare the bio-oil samples with similar composition, e.g. bio-oils prepared with only incremental changes in reaction conditions [57].

1.3.1.3. Carbonyl products test methods

Carbonyl compounds (aldehydes and ketones), sugars, acids and water are the four major components of the water-soluble fractions of bio-oil [58]. Aldehydes and ketones are considered as the primary contributors of the bio-oil instability during storage. Due to their high reactivity, esterification, acetalization, aldol-condensation and other reactions that lead to the formation of dimers or polymers occur in the water-soluble fractions of bio-oil. Moreover, aldehydes could react with pyrolytic lignin in the water-insoluble fraction through phenol-formaldehyde condensation [48]. A linear correlation was observed between the change in carbonyl content and water-insoluble content [15] during the accelerated aging of bio-oil.

13

Carbonyl contents can be measured by chemical titration or using analytical instruments. Oximation is one of the most general chemical titration methods used to determine the total carbonyl functional groups [59]. This method uses the reactions between hydroxylamine and aldehydes/ketones to form the corresponding oximes while carboxylic acids or esters do not react[60]. El Mansouri et al[59] measured carbonyl content in five different lignins using both oximating method and the differential UV-spectroscopy, and concluded that oximating method was more reliable for total carbonyl quantification. VTT[15] described detailed procedures on carbonyl titration tests, and a good repeatability was achieved. In addition, they found that the carbonyl content determined by carbonyl titration was not affected by the amount of acid compounds in the bio-oil. Although oximation titration was confirmed to be applicable for measuring the total carbonyl content in bio-oil, this method has not been confirmed by others.

Besides chemical titration, typical analytical spectroscopy methods such as Fourier Transform Infrared spectroscopy (FTIR), Gas Chromatography/Mass Spectrometry (GC/MS) and ^{1}H and ^{13}C Nuclear Magnetic Resonance (NMR) are also widely used to determine the change in bio-oil carbonyl contents [47, 61, 62]. FTIR spectroscopy is a direct method to measure the compositional and structural changes of bio-oil during aging[45]. Due to complex nature of bio-oil, FTIR spectral is not applicable to perform quantitative analysis[56]. Instead, FTIR is commonly used to provide the qualitative information on change in carbonyl by comparing the corresponding absorbance intensities prior to and after the aging process.

GC/MS has been commonly used to identify and quantify the volatile components of bio-oil[61]. However, due to the chemical complexity of bio-oil, it is impossible to perfectly separate all the compounds using a single column in GC. In Hilten`s study [45], no substantial compositional changes were observed in GC-MS results from whole bio-oil sample prior to and after aging even though noticeable physical changes occurred during aging. They concluded that such inconsistency was due to the narrow range of volatile compounds that GC-MS was able to detect. Oasmaa et al[58] recommended separating bio-oil into multiple fractions using solvent

14

fractionations, and then characterizing the compositional changes in each individual fraction. For example, carbonyl groups fall into the ether-solubles fraction, which are GC-eluted compounds[58]. Then, the change in carbonyl groups of bio-oil during aging can represent the compositional change in that fraction. To get quantitative information, a calibration must be performed for the selected compounds using corresponding calibration standards. However, calibration standards are not available for few target compounds. The variations in calibration procedures lead to poor reproducibility. Moreover, the poor separation of overlapping peaks poses challenges in identification of compounds with similar retention time. Hence, GC/MS is recommended as a qualitative or semi-quantitative tool to measure the change in carbonyl groups during aging process.

Unlike GC/MS, which can only detect GC-eluted compounds, NMR analysis can be used to interpret structural information of whole bio-oil samples [63]. Different NMR analytical methods have been developed for specific applications. Among all the NMR methods, ^{1}H, ^{13}C-NMR and distortionless enhancement polarization transfer (DEPT) methods are the most frequently used to characterize the bio-oil samples [64]. The percentages of carbon or hydrogen in different chemical functional groups (based on chemical shift) are interpreted, and hence, the relative concentration of functional groups in bio-oil can be estimated. NMR analysis has been used to characterize the compositional change in bio-oil during accelerated aging test [47, 48, 56, 65]. The poor solubility of bio-oil in NMR solvents was one of the main challenges for the analysis [47].

1.3.2. Oxidative stability test methods

Oxidative stability refers to the susceptibility of a fuel to oxidative degradation. The oxidative aging leads to the formation of carboxylic acids, esters and reactive peroxides that catalyze the polymerization of unsaturated compounds [31]. Only limited information is available for measuring oxidative stability of bio-oil [45, 51, 52]. In Hilten`s study [45], two hydrocarbon fuel ASTM standard methods (D5340 and E2009) were compared to evaluate the oxidative

stability of bio-oil. The D5340 method is based on the measurement of solid contents formed during oxidative accelerated aging [66]. In this method, the original solids in bio-oil must be removed before test. ASTM E 2009, also known as oxidation onset temperature (OOT) test, determines the temperature at which oxidation starts by running the sample in a differential scanning calorimetry (DSC) [67]. The higher OOT indicates the higher oxidative stability and, vice versa. Hilten [45] concluded that determination of solid formation can be used as a standard method to measure the oxidative stability, but the filtration of bio-oil increased the difficulty of using this method. OOT method was considered a quick and easy method to determine the oxidative stability, and was also confirmed by other researchers [51, 52].

1.4. Approaches to Improve the Stability of Bio-oil

It is critical to develop effective approaches to maintain the stability of bio-oil during storage and transport because unstable bio-oil with high viscosity creates challenges in pumping and handing the bio-oil during storage and transportation to the biorefinery or end-use application. The keys to improving the stability of bio-oil, as discussed above, are associated with viscosity reduction, eliminating the highly reactive organic compounds, mildly modifying bio-oil to reduce its reactivity and acidity and removal of the solid char residue. The latest developments in bio-oil stabilization techniques, categorized as physical and chemical methods, are discussed below.

1.4.1. Physical methods

1.4.1.1. Solvents addition

Typically, the addition of polar solvents has been shown to decrease the viscosity and rate of increase in the viscosity over time. Diebold et al [46] investigated effects of adding ethyl acetate, methyl isobutyl ketone and methanol, acetone, methanol, acetone, methanol and ethanol to reduce viscosity and aging rate of bio-oil. The results indicated that these additives not only lowered the initial viscosity but also reduced the rate of increase in the viscosity with time, among which methanol was the most effective additives tested to decrease the rate of aging.

Oasmaa et al [68] studied the change in bio-oil properties with age by adding three alcohols: methanol, ethanol and isopropanol. Among these alcohols tested, methanol was the most effective solvent in reducing the viscosity, and the bio-oil fluidity improved significantly as methanol concentration increased. Furthermore, the addition of alcohols effectively enhanced the solubility of the hydrophobic compounds, which consisted of high molecular weight lignin derivatives and extractives. The overall mechanism of alcohols addition to bio-oil can be summarized as follows. The chemical reaction [69] that leads to increase in average molecular weight of bio-oil was undermined by diluting the reactive chemical species (e.g. aldehydes and acids). In the meantime, the polymerization reactions of aldehyde groups which contribute to the increase of molecular weight of bio-oil could be reduced by competing reactions, such as acetalization and esterification between alcohols and aldehydes, ketones, and anhydrous sugars[70, 71]. Moreover, additives enhance depolymerization of large compounds into low molecular weight compounds through transesterification and transacetilization. One of the problems with adding solvents for improved viscosity appears to be a decrease in flash point [31, 68] that must be addressed to avoid fire hazards. Nonetheless, due to low cost and potential to improve energy content and aging properties of bio-oil, solvent addition has been recognized as one of the most efficient approaches to obtain a homogenized and less viscous product.

1.4.1.2. Emulsification

Another promising approach to decrease bio-oil viscosity is emulsification with other petroleum fuels, such as diesel. Interestingly, biodiesel which is a renewable fuel consisting of esters of fatty acids, has become one of the most popular fuels to decrease bio-oil viscosity because the resulting products are environmentally-friendly and compatible to fossil fuels. Emulsification involves two immiscible liquids in which droplets of one phase (the dispersed or internal phase) are encapsulated within a layer of another phase (the continuous or external phase) with the help of agitation and emulsifying agent (also known as surfactant). The quality of the final mixture is highly dependent on agitation intensity, surfactant concentration, operation

temperature and bio-oil to bio-diesel ratio[72, 73]. By investigating mixture stability at different operation conditions, Jiang et al [74, 75] concluded that viscosity at room temperature decreased significantly from 67.39×10^{-3} to 4.665×10^{-3} Pa·s and energy content was also improved from 15.28 to 34.57 MJ/kg when 60% vol. of biodiesel was mixed with bio-oil Moreover, the results indicated that emulsification was a novel method to extract the pyrolytic lignin fraction from bio-oil. Aging tests of the mixture with 60% vol. of biodiesel indicated that viscosity increased slightly within first 10~60 hours and then decreased in the next 120 hours until the end of the test, and the higher volumetric fraction of bio-oil in the mixture led to higher final viscosity.

Garcia-Perez et al [76] carried out the blending of bio-oil and biodiesel by heating the mixture at 60°C using a water bath. They found that the compounds in organic phase of bio-oil, such as furans, sugars and oligomers, were more soluble in biodiesel than the compounds in aqueous phase. The viscosity of the bio-oil/biodiesel mixture increased slightly as the bio-oil concentration increased; however, it was much lower than that of original bio-oil. For example, the viscosity of organic phase of bio-oil obtained from pine chips dropped from 140.2 to 9 cP when mixed with 35 wt. % of biodiesel. However, the phase equilibrium of the two blends was dependent on temperature. More information on the effects of temperature on the phase equilibrium is needed.

Zapata et al [77] found that the aqueous/oil emulsions can be stabilized by metal supported nanohybrid catalysts, and these catalysts further enhanced the simultaneous aldo-condensation/hydrogenation reactions of carbonyl compounds, such as furfurals and ketones. The aqueous/oil biphasic emulsion also proved to be more advantageous for condensation than single phase which was due to the improved mass transfer between the phases that resulted from the extended interfacial area by the nanohybrid catalyst.

In summary, emulsifying bio-oil with biodiesel is an effective way of improving bio-oil quality in terms of reduced viscosity and profoundly improved energy content. However, high

consumption of emulsification agents and energy input to generate sufficient agitation are current challenges for using this approach [3, 78].

1.4.1.3. Removal of solid char residue

One of the main reasons for instability of bio-oil during storage is the metal ions hidden in char particles that act as catalysts triggering reactions, such as polymerization and condensation, resulting in an increase in viscosity [79]. Moreover, the alkali metals retained in char particles cause corrosion problems and deposit on the inner wall of transportation lines and can cause plugging problems. Char particles must be removed from bio-oil, especially for use as fuels. Cyclone separators are commonly used for char removal, but these are not effective in trapping fine particles (<10 μm).

(a) Hot gas vapor filtration

Hot gas vapor filtration is considered a promising technique to reduce the char content in bio-oil. Char particles are stripped from pyrolysis vapors before entering the quenching unit. The bio-oil obtained from using hot vapor filtration was found to have improved quality, such as lower solid contents, viscosity and alkali metal content compared with that obtained from using conventional cyclone separators [80-82].National Renewable Energy Laboratory (NREL) [83] tested vapor-phase filtration of bio-oil using two filter elements (porous sintered stainless-steel metal powder and sintered ceramic powder provided by Pall Corporation). Researchers found that alkali metal contents decreased significantly using hot gas filtration, and the bio-oil obtained through the ceramic filter was stable with viscosity increase rate being only one tenth than that of the bio-oil obtained through conventional cyclone system. In an accelerated aging test, Adisak et al[81] found that the bio-oil stability index, which was measured as the percent of viscosity change after aging decreased from 24.8 to 1.4 when hot vapor filter was applied during the production of rice straw derived bio-oil.

(b) Microfiltration

Microfiltration, as one of the membrane-based particle removal techniques, has been widely used for removal of fine particles (0.02-10µm) in petroleum [84, 85] and water industries [86]. The membrane acts as a barrier that separates two bulk phases and controls the transportation of chemical components through both sides, which is driven by a driving force, such as electric field, pressure, temperature or concentration difference across the membrane [84]. Using tubular ceramic membranes (pore size: 0.5 and 0.8 µm) for microfiltration of bio-oil char particles, Javaid et al [85] showed that most of the char particles was removed, and bio-oil ash content decreased by nearly 60%. No significant variation was observed in chemical composition of bio-oil after microfiltration. Microfiltration is a promising method for removal of fine char particle from bio-oil. However, the mechanisms of char removal and the effect of operation conditions on fouling process are still unclear.

In summary, char, the solid byproduct of fast pyrolysis, can act as a catalyst to crack volatiles reducing the yield of bio-oil. Therefore, there is a need to separate solids before the condensation of volatiles. Cyclone separators are most frequently used techniques to sequestrate the solids from gas streams; however, they are not effective for fine particles (<10 µm). Microfiltration is useful for trapping very fine particles (0.02-10 µm). However, selection, recovery and cost of membrane are barriers in using this technology.

1.4.1.4. Other physical methods

High-pressure homogenization (HPH) has also been widely used to stabilize bio-oil emulsions [87]. He et al [88] investigated using high-pressure homogenization (up to 300 MPa) to treat bio-oil. Aging tests were also conducted at 40°C for 60 days to compare the storage stability of the homogenized bio-oil. The results indicated that the bio-oil viscosity decreased up to 30% at 100 MPa homogenization pressure; however, no significant viscosity decrease was observed at pressures above 100 MPa. This is because high pressure (>100 MPa) breaks weak bonds in macro molecules (e.g. partially degraded holocellulose, pyrolytic lignin polymers and

char) but is not capable of breaking strong covalent bonds. The aging test indicated that the rate of increase in viscosity of bio-oil treated with homogenization at 100 MPa was 0.0661 centistrokes (cSt)/day, which was approximately 20% of untreated bio-oil. Similarly, a linear correlation was observed between the bio-oil viscosity and its molecular weight. Compared to emulsification and solvents addition, HPH aims to chemically transform the bio-oil composition. Technically, traditional physical methods, such as emulsification and solvents addition, do provide a short-term and simple solution to decrease the viscosity of raw bio-oil; however, the approaches that focus on changing composition of the bio-oil appear more effective for long-term stabilization of bio-oil.

Most aging reactions involve reactive functional groups in water-soluble phase; therefore, physical separation of water-soluble phase from bio-oil is a promising method to improve the stability. Zheng et al. [78] separated the rice husk derived bio-oil into water-soluble phase (19 wt%), distilled bio-oil (61 wt%) and residue (10 wt%) using reduced pressure distillation (80 °C, 15mmHg). The properties of the distilled bio-oil were significantly improved compared with those of raw bio-oil. For example, the water content decreased from 25.2 to 0.01 wt%; the oxygen content reduced from 50.3 to 9.2 wt%; pH value increased from 2.8 to 6.8. Viscosity based stability tests also indicated that the viscosity change in distilled bio-oil was negligible. Reduced pressure distillation was a simple and efficient way to separate the reactive species from raw bio-oil, which has the potential to improve the bio-oil stability. However, more up-scaled studies are required to identify optimum parameters to maximize distillation efficiency.

1.4.2. Chemical methods

As discussed above, the instability of bio-oil during storage is due to the interaction between reactive oxygenated functional groups, such as carboxylic acids, alcohols, aldehydes and phenols. To improve bio-oil stability, removal of these functional groups has been extensively researched [89-94]. Table 1.3 summarizes current techniques for reactive oxygenated functional groups removal.

Table 1.3 Summary of current technologies to remove reactive oxygenated functional groups from bio-oil.

Methods	Process condition	Reaction mechanism	Advantages	Disadvantages	References
Esterification with alcohol and mineral acid catalysts	Mild conditions	Chemical reactions between acids and alcohols	Applicable to improve oil qualities with low cost	Only address acidity issues	[95-98]
Mild HDO	Mild conditions (100~280 °C/low pressure), chemical needed: H_2/CO, catalyst(e.g.,CoMo, HDS, NiMo,HZSM-5)	Hydrogenation under mild conditions	Reduced hydrogen input, reduced handling cost of stabilized intermediates	Carbon loss to the gas and solid phase	[99-107]
Catalytic cracking	Severe conditions (>350 °C, 100–2000 Psi), chemical needed: H_2/CO or H_2 donor solvents, catalyst (e.g., Ni/Al_2O_3-TiO_2)	Crack large molecules into small molecules through decarboxylation and decarbonylation	No hydrogen input, low cost	Poor fuel quality, high coking	[108, 109]
Catalytic fast pyrolysis	Mild conditions (350~600 °C, atmospheric pressure), zeolite catalysts	Upgrade biomass derived volatiles through dehydration, deoxgenation, decarboxylation and decarbonylation	Does not require hydrogen, high hydrocarbon conversion	Catalyst coking	[90, 91, 110-113]

1.4.2.1. Esterification

Bio-oil reacts with alcohols at room temperature through esterification or acetalization as shown in Figure 1.2.
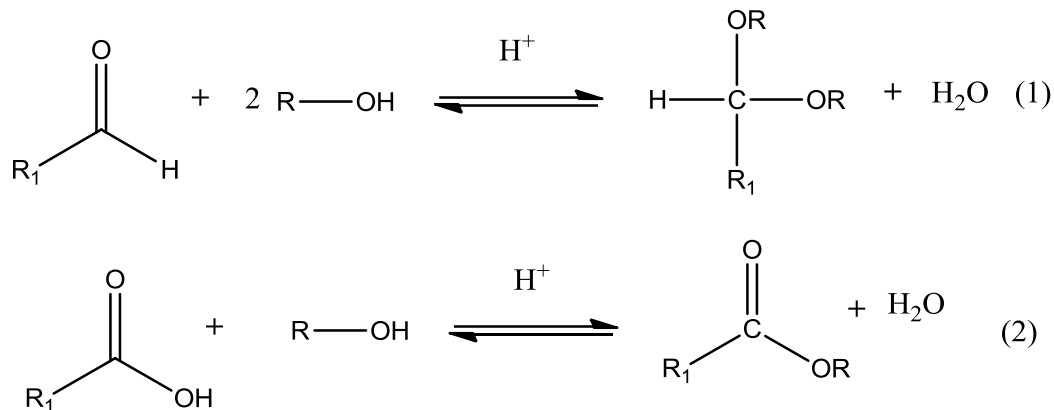
Figure 1.2 Reactions of esterification (1) and acetilization (2). Adapted from [8]

The compounds that contain carboxylic acids and aldehydes in bio-oil can react with alcohols and are converted into esters and acetals, respectively. This process converts high polar organic compounds into low polar organic compounds leading to polarity difference in the bio-oil mixture, thus increasing the tendency of phase separation during storage. In addition, these reactions also lead to other desirable changes, such as reduced acidity, improved volatility and heating value, and better miscibility with diesel fuels [8]. Numerous researches have focused on catalytic esterification. The conversions of esters and acetals depend on reaction temperature, reaction time, and amounts and types of catalyst and alcohol used [96]. Traditionally, heterogeneous acid/base catalysts, homogeneous ionic liquid catalysts and aluminum silicate catalysts have been used for esterification of bio-oils[114]. Solid catalysts have been used for bio-oil esterification to lower viscosity, increase HHV value, and decrease pH and water content. However, catalyst coking and poor recyclability limit its applications; therefore, novel catalysts are needed. Xiong et al [95] showed that after esterification, no carboxylic acids were detected in the upgraded bio-oil, and significant improvements in properties were also observed. These improvements included HHV increasing from 17.3 to 24.6 MJ/kg, kinetic viscosity decreasing

from 13.03 to 4.9 mm^2/s, pH value increasing from 2.9 to 5.1 and moisture content decreasing from 32.8 to 8.2. In addition, the selectivity to esters was still high (over 92 %) after recycling the catalysts for five times. However, the most critical issue with this approach is the complex synthesis of the catalysts. Recently, bifunctional catalysts have been investigated for simultaneous esterification and acetalization of acids and aldehydes in bio-oil [90, 97]. Li et al [97] investigated the simultaneous catalytic esterification and acetalization of bio-oil with methanol using a commercial Amberlyst-70 catalyst (Rohm & Haas, Philadelphia, PA, USA.). In this condition, not only light fractions of bio-oil but also medium (e.g. phenols, furans and sugars) and heavy fractions (oligomeric compounds from cellulose, hemicellulose and lignin) of bio-oil react with alcohols, forming products with more stability and more volatility.

1.4.2.2. Mild hydrodeoxygenation

Challenges in using bio-oil are related to its high oxygen content, which can be overcome by hydrodeoxygenation (HDO). HDO treats the bio-oil at a moderate temperature range (300 ~ 600 °C) under high pressure hydrogen atmosphere in the presence of heterogeneous catalysts[115]. During hydrodeoxygenation, the oxygen in the bio-oil was rejected in the form of water through a series of C-C, C-O-C and C-OH bond cleavage, and hydrogenation reactions [116, 117]. After HDO, the bio-oil is upgraded into an energy dense and non-corrosive product, such as naphtha, with oxygen content less than 2 wt. %[99]. However, cost of hydrogen consumption becomes one of the barriers in using HDO as this process requires high partial pressures of hydrogen. Like other catalytic processes, coking of catalysts under high temperature provides additional challenges.

As an alternative of complete HDO, mild hydrodeoxygenation (mild HDO) reduces hydrogen consumption and catalysts cost, which makes the bio-oil a better intermediate feedstock that can be further processed in petroleum refineries. The overall strategy is to divide the original deoxygenation process into two stages: (i) raw bio-oil is stabilized at low temperature (100-280°C) with trivial quantity of hydrogen, and then (ii) the intermediate is fed into a secondary

reactor at higher temperature (350-400°C) for further oxygen removal [100, 107, 118-120]. Mild HDO refers to the first low temperature stabilization step, in which carbonyl groups were hydrogenated into more stable alcohols[107]. French et al [101] used a sulfided Ni-Mo/γ-Al$_2$O$_3$ catalyst to upgrade bio-oil in a two-stage hydrotreating process. In the first stage, bio-oil and catalyst were co-fed into a reactor and stabilized at 1000 psig and 280°C for one hour. Then, the reactor was heated to a final temperature 400°C and held at the temperature for 1 hour. The oxygen content in the product decreased to 6.7 wt. %. The results suggested that mild HDO at these conditions was a feasible and economical method to remove the water and water-soluble compounds (e.g. carboxylic acids) with benefits of less hydrogen consumption and decreased acidity.

Mild HDO does not result in final products, but provides a new route to produce a stabilized intermediate that can be accommodated in the existing petroleum refinery system for further processing. Considering both the quality and economics of bio-oil derived products, mild HDO holds promise and requires more research. Recently, a combined one-step hydrogenation/esterification (OHE) process was proposed to stabilize two major reactive functional groups in bio-oil, aldehydes and carboxylic acids [102]. Bifunctional mesoporous catalysts [104], e.g. hybrid silicas with platinum and organic acid groups (Pt/SBA15-PrSO$_3$H), were used for OHE reaction. Using two bifunctional catalysts, Pt/SBA15-PrSO$_3$H and Pt/SBA15-ArSO$_3$H, for OHE reaction of acetaldehydes and acetic acid as model compounds, Tang et al [103, 104] demonstrated that the arenesulfonic acid groups resulted in higher catalytic activity than propylsulfonic acid groups due to increased acid strength. In summary, mild HDO can be a cost-effective approach to partially remove bio-oil oxygen and produce a liquid compatible with petroleum refinery. However, more information on how hydrogen consumption impacts the oxygen removal efficiency is needed.

1.4.2.3. Catalytic cracking

At a temperature range of 350-650°C [8] and relatively high pressure (up to 2000 psi), catalytic cracking rejects bio-oil oxygen in the form of CO_2 using, typically, zeolite catalysts (e.g. HZSM-5). Two types of catalytic cracking are frequently used for bio-oil treatment: catalytic cracking without hydrotreatment and hydrocracking. Catalytic cracking without hydrotreating removes a certain amount of oxygen through decarboxylation and decarbonylation reactions [99, 121], which compromises the carbon conversion efficiency, leading to a lower H/C ratio and higher O/C ratio in the product compared to bio-oil upgraded through HDO[121]. HDO combines the catalytic cracking reactions under hydrogen atmosphere with the help of bifunctional catalysts, which enhances cracking reaction and hydrogenation reaction. Using $Ru/ZrO_2/SBA$-15 and $Ru/SO_4^{2-}/ZrO_2/SBA$-15 for cracking bio-oil in supercritical ethanol under hydrogen atmosphere, Tang et al [108] showed that bio-oil composition changed to stable simple organic compounds mixtures, including phenols, guaiacols, and esters. In addition, the HHV value increased from 27.87 MJ/kg to 34.94 MJ/kg. The hydrocracking suppressed the polymerization reaction, mitigating the catalyst coking problem.

Catalytic hydrocracking is another approach to break down high molecular weight compounds of bio-oil. Qu et al [109] used a two-stage hydrotreating/cracking method to treat viscous heavy bio-oil. The bio-oil was evaporated at 250°C and then passed through a catalytic bed mixed with both hydrotreating catalyst and zeolite under hydrogen atmosphere at a temperatures ranging from 250 to 400°C. The results showed that the viscosity of bio-oil treated with hydrotreating/cracking at 400°C decreased from 8710 to 70 cP. Other bio-oil properties, such as higher heating value (HHV) and oxygen content, also improved and the proportion of lighter aromatic compounds, such as benzene, phenol and their derivatives, increased significantly. However, the properties of bio-oil during aging were not provided.

1.4.2.4. Catalytic fast pyrolysis

Catalytic fast pyrolysis can convert biomass directly into aromatic hydrocarbons that fit into existing refinery infrastructure with zeolite catalysts [90, 91]. Fluidized bed reactors are typically used for pyrolysis due to their flexibility in accepting a wide variety of feedstocks and effective heat and mass transfer. In catalytic pyrolysis condition, biomass is thermally decomposed to volatiles (vapors) that pass over a catalyst bed, converting the vapors into stable and deoxygenated compounds. The cellulose and hemicellulose primarily decomposes into anhydrosugars, and lignin mainly forms coke [90]. The evolved anhydrosugars are converted into furan compounds through dehydration and rearrangement reactions. These furan compounds are then absorbed into the pores of zeolite catalysts, where multiple chemical reactions, such as decarbonylation, decarboxylation, dehydration and oligomerization, take place, resulting in aromatics and olefins [91]. The aromatic and olefin intermediate hydrocarbons can be further converted into polycyclic aromatic compounds through chemical reactions with other oxygenated compounds. Torren et al [91] summarized the conversion pathways of cellulose during catalytic fast pyrolysis, as shown in Figure 1.3.

Anhydrous sugars

$-xH_2O;-yCO_2;-zHCOH$

Furan compounds

Polyaromatics

$-xH_2O$

$-xH_2O$
$-yCO_2$

$-xH_2O$
$-yCO_2$
oligomerization
decarboxylation
decarbonylation

$-xH_2O$
$-yCO_2$
polymerization

$-xH_2O$
$-yCO_2$

Cellulose

$-xH_2O$
$-yCO_2$

Coke

$-xH_2O$
$-yCO_2$

Hydrocarbon pool

Monoaromatics

Olefins
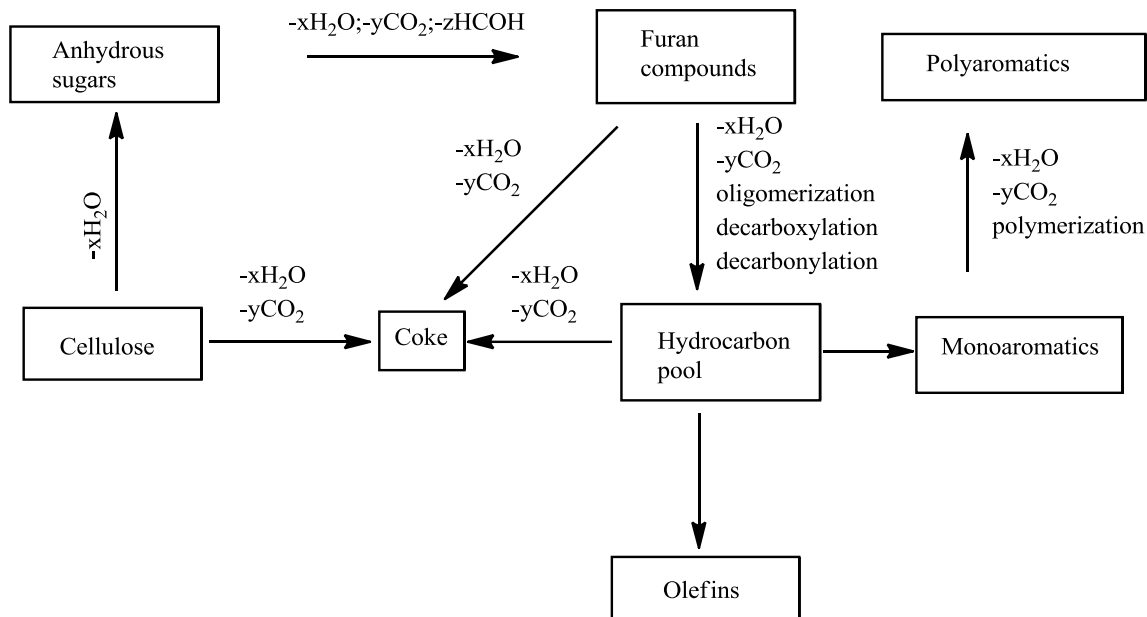
Figure 1.3 The conversion path of cellulose during catalytic fast pyrolysis. Adapted with modification from [41]

Mullen et al [112] investigated the catalytic pyrolysis behavior of lignin using analytical pyrolysis methods (Py-GC/MS) with two heterogeneous catalysts, HZSM-5 and CoO/MoO$_3$. Lignin is a complex polymer of three aromatic monomers, p-coumaryl alcohol, coniferyl alcohol and sinapyl alcohol. These monomers degrade into complex methoxyphenols, such as guaiacols and syringols, which can be further converted into simple phenols or aromatic hydrocarbons depending on the types of catalysts used.
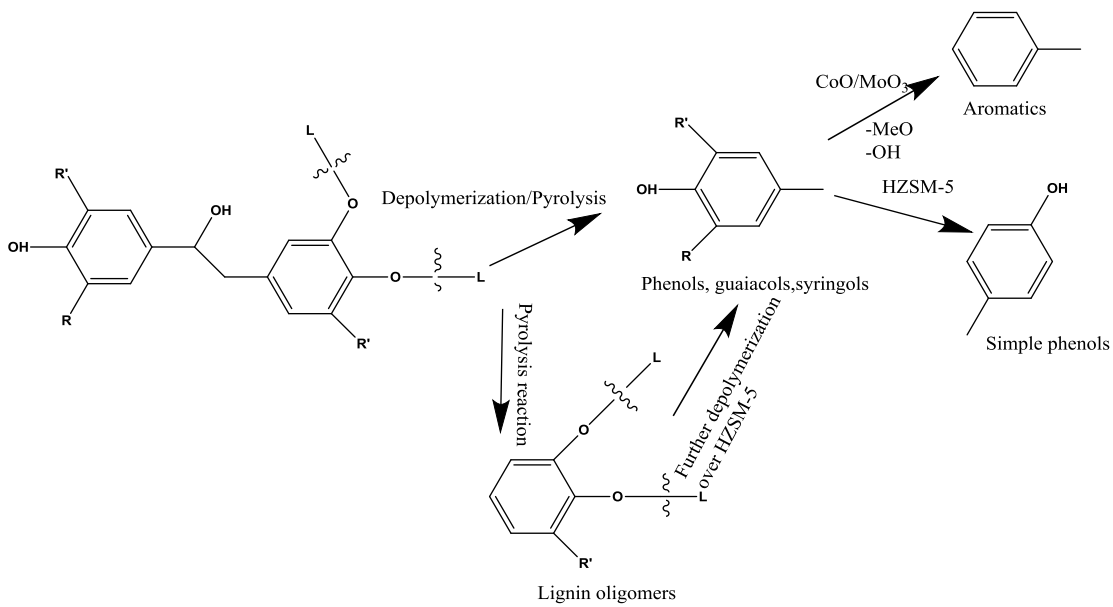
Error! Reference source not found. [112] shows the detailed conversion pathways of lignin during catalytic fast pyrolysis. Simple phenols are the main products derived from zeolite catalysis and are not likely to further convert into aromatic hydrocarbons because the phenols are easy to bond with active acid sites of zeolite catalysts, resulting in deactivation or choking of the catalyst [122]. The CoO/MoO_3 catalyst tends to produce aromatics directly via deoxygenation of methoxyphenol groups. By co-pyrolysis of pine wood with alcohols (methanol, 1-propanol, 1-butanol and 2-butanol) using ZSM-5 catalyst in a bubbling fluidized bed reactor, Zhang et al [90] found that selectivity of petrochemicals including benzene, toluene, xylene, ethylene and propylene can be optimized by manipulating the hydrogen to carbon effective (H/C_{eff}) ratio of the feed. H/C_{eff} is defined in   d   **Equation 1.1**; where H, C and O are the mole percent of hydrogen, carbon and oxygen, respectively.
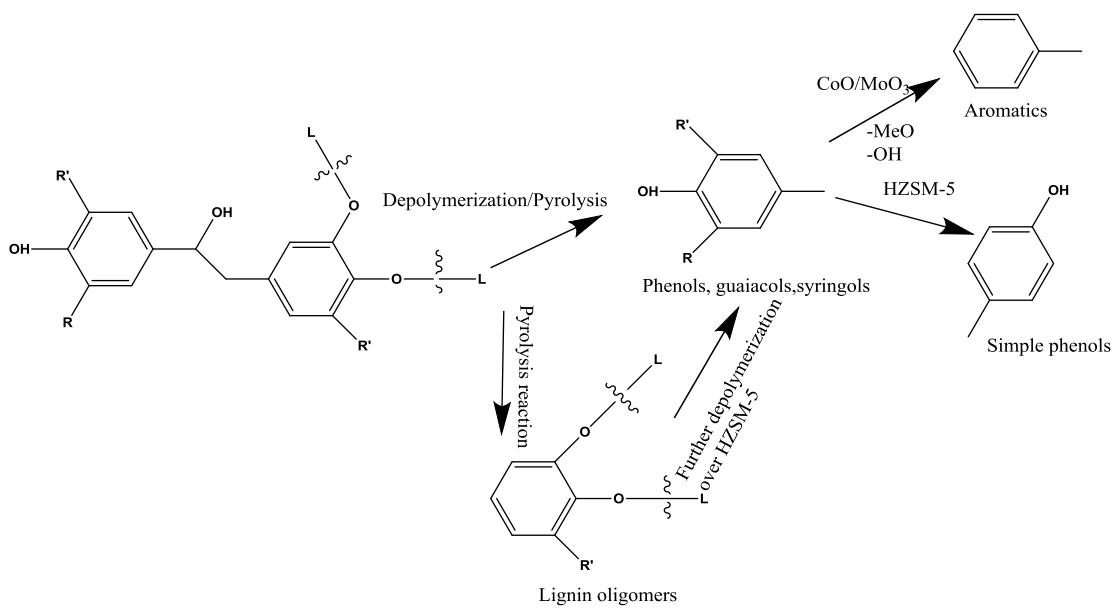
Figure 1.4 The conversion pathway of lignin catalytic fast pyrolysis. (Adapted with modification from [60])

$$\frac{H}{C_{eff}} = \frac{H - 2*O}{C}$$

The isotope technique was used to investigate the chemistry of co-pyrolysis of pine wood (^{12}C) and methanol (^{13}C) in this study. Results indicated that both feeds contributed to the production of aromatic compounds. The study also verified the assumption that co-feeding the biomass with cheap hydrogen donor [99] with high H/C_{eff} ratio (substitute of hydrogen gas) is effective in improving aromatics yield. However, a detailed economic assessment is still needed to provide information on how to minimize the production cost of aromatics through catalytic pyrolysis of biomass and alcohols. Patel et al [123] investigated catalytic pyrolysis of sugarcane bagasse using a supported molybdenum carbide (20 wt. % Mo_2C/Al_2O_3) catalyst. The results indicated that as the weight percent of catalyst in the bed materials increased from 0 to 50%, the pH of bio-oil changed slightly; however, the viscosity decreased from 2780 to 19.7 cP. Also, a significant decrease in sugars and increase in furanics and phenolics were observed. This improvement in bio-oil viscosity is of great importance for its further processing or transport.

To sum up, the major issues with bio-oil instability are due to its reactive oxygenated functional groups. Various methods have been researched to eliminate these oxygenated compounds but each has limitations. Esterification can only handle carboxylic acids and aldehydes. Mild HDO appear to be an effective and economic way to reduce oxygen content; however, aging of the treated oil has not been tested. Catalytic cracking and catalytic fast pyrolysis can reduce bio-oil polymerization; however, the catalysts can only enhance typical model reactions, while inhibitive effects of contaminates in real bio-oil is unproven. More research is needed on developing multifunctional catalysts and integrated catalysis.

1.5. Conclusions and Recommendations

Bio-oils produced from pyrolysis of lignocellulosic biomass have the potential to substitute fossil fuels in the future energy systems because bio-oil is a renewable fuel; raw materials are available abundantly, its use result in low pollutants emission; and it can directly substitute liquid transportation fuels. Bio-oil can also be used as a platform for production of high-value chemicals. However, the direct utilization of bio-oil is significantly challenged by its poor fuel quality associated with its undesirable attributes such as high water and oxygen content, acidity, and instability during storage and transportation.

Bio-oil contains large amounts of reactive functional groups (e.g., carbonyl, hydroxyl, phenol and unsaturated carbon-carbon bonds.) and free radicals, which are likely to initiate spontaneous reactions such as polymerization, condensation and esterification during storage. These reactions are responsible for the varying properties of bio-oil during storage. Evaluation of the bio-oil stability has primarily focused on thermal stability, and oxidative stability of bio-oil is vastly unexplored. Accelerated thermal aging test is the most commonly used approach for assessing the thermal stability of bio-oil. Several stability indicators, such as viscosity change, increase in average molecular weight, and change in carbonyl content are recommended to characterize the stability of bio-oil during storage. Different testing methods have been developed based on the change in these stability indicators. However, in order to achieve a long-term

success in commercialization of bio-oil, the testing methods for assessing the stability of bio-oil during storage and transportation must be standardized and normalized so that improvement in stabilizing bio-oil can be measured.

Approaches to improve stabilization of bio-oil can be categorized into physical and chemical methods. Physical methods include viscosity reduction and char removal, and chemical methods include removal of reactive functional groups. Briefly, physical methods, like solvents addition and emulsification with bio-diesel are both effective approaches of reducing viscosity and decreasing the viscosity changing rate of bio-oil during storage. Char removal techniques such as hot gas filtration and microfiltration are effective for trapping fine particles (<10 μm). Chemical methods focused on the removal of reactive oxygenated functional groups through various heterogeneous catalytic processes, such as esterification with alcohols, mild hydrodeoxygenation, catalytic cracking and catalytic fast pyrolysis. Through these processes, deoxygenated and less acidic liquids were produced, and hence the higher fuel stability is expected during storage.

For deployment of physical methods such as solvent addition and emulsification, further research on recovery of solvents and surfactants is critical. Among all the chemical methods, mild HDO appears to be a cost-effective technique to reduce bio-oil oxygen content, but its effect on aging is currently unknown. Catalytic fast pyrolysis is a promising method to produce liquid fuels that are expected to be more stable than traditional bio-oil. The resistance of catalysts towards deactivation is a major issue in use of catalysts during pyrolysis. In addition, multifunctional catalysts and integrated catalysis that are effective with multiple substrates are critically needed. Combinations of multiple approaches might be effective. Detailed economic analysis of each approach is also crucial for its successful commercialization. Understanding of reaction mechanisms in both thermal and oxidative aging processes would benefit the standardization of bio-oil stability test methods as well as the design of processes that produce high quality bio-oil.

CHAPTER II

PYROLYSIS OF EASTERN REDCEDAR: DISTRIBUTION AND CHARACTERISTICS OF

FAST AND SLOW PYROLYSIS PRODUCTS

This research paper was published as "Z. Yang, A. Kumar, R. Huhnke, M. Buser, S. Capareda,

Pyrolysis of eastern redcedar: Distribution and characteristics of fast and slow pyrolysis products,

Fuel, 166 (2016) 157-165."

Abstract: Eastern redcedar is a problematic plant in Oklahoma due to its extinguished environmental flexibility and rapid expansion. Pyrolysis, thermally converting solid biomass polymers into liquid fuel intermediate, solid char and gaseous products, is one promising approach to use redcedar for the production of sustainable fuels. The objective of this study was to investigate effects of eastern redcedar wood zones (heartwood and sapwood), pyrolysis temperature (450 and 500 °C) and pyrolysis types (slow at lab-scale and fast at micro-scale) on distribution and composition of pyrolysis products. In fast pyrolysis conditions, the products were dominated by anhydrous sugars, phenols and guaiacols. The total yield of lignin-derived compounds from heartwood was higher than sapwood at 500 °C but not significantly different at 450 °C. In slow pyrolysis conditions, acetic acid and furfural were the two most abundant species in bio-oil. Slow pyrolysis products consisted of significantly less branched compounds of phenols and guaiacols as compared to fast pyrolysis products. Cedar oil components (alpha/beta-cedrene) were only produced at slow pyrolysis conditions and its maximum yield (21.04 ± 1.08 area %) of was obtained from heartwood at 500 °C. Heartwood produced significantly more cedrenes than sapwood.

Keywords: Eastern redcedar; Pyrolysis; Cedar wood oil; Bio-oil

2.1. Introduction

Depletion of fossil fuels and increase in greenhouse gases emissions justifies the need to develop innovative energy technologies that are both alternative and sustainable. Biomass is considered as one of the potential energy resources that can maintain the energy and environmental sustainability mainly due to its abundance and CO_2 neutrality [124]. Biomass can be converted into fuels and energy through a number of different processes, among which thermochemical processes, namely gasification, pyrolysis and hydrothermal liquefaction, are promising technologies for production of renewable energies, fuels and chemicals [125, 126].

Pyrolysis converts biomass into multiple fuel products like solids (biochar), liquid fractions (bio-oil) and gaseous products (syngas) by thermally decomposing biomass under a medium temperature (~600˚C) in an inert atmosphere [127]. The operation conditions (e.g. temperature, heating rate, and residence time) can be adjusted to maximize the production of each product. Production of bio-oil has received great interest since the liquid is easier to store and transport than solid biomass feedstock to use as fuel. Bio-oil can be used in several applications, such as: direct boiler combustion for heat and power; transportation fuels that substitute traditional fossil fuels; or platforms for chemical production because it is composed of numerous organic species [14]. The properties of bio-oil are distinctly different from fossil based resources. Its undesirable qualities such as low heating value, high moisture content, acidity, viscosity and chemical instability towards temperature cause significant challenges to the application of bio-oil as a fuel [22, 128]. To obtain bio-oil with high yield and quality, considerable research [11, 129-134] has been focused on designing and optimizing the pyrolysis conditions, such as increasing heating rates, using fine particle size feedstocks and decreasing residence time for heating and quenching. In addition, various reactor configurations and liquid collection systems have been developed and researched to improve the quality of bio-oil [129, 135-137].

During pyrolysis, cellulose, hemicellulose and lignin follow different decomposition pathways, leading to different products. The cellulose and hemicellulose primarily degrade into

anhydrosugars and then convert into furan compounds through dehydration and rearrangement reactions [138]. Lignin primarily depolymerizes into phenols and methoxyphenols, such as guaiacols and syringols. Methoxyphenols can be further converted into simple phenols through demethoxylation and cracking[112]. Pyrolysis performance and end-product quality were dependent on the biomass properties that can vary because of crop variety, production practices, and climate. Even in the same species of woody biomass, the chemical compositions of sapwood (SW) and heartwood (HW) zones are significantly different. HW is the outer part of wood with a darker color and older cambial age than SW. A radial decrease in lignin content with cambial age is usually observed in individual tree species, e.g. the lignin contents in teak HW and SW are 37.3 and 35.4 wt. %, respectively [139]. In addition, the lignin compositions, such as *H*-lignin (p-hydroxyphenyl subunits), *G*-lignin (guaiacyl subunits) and *S*-lignin (syringyl subunits) vary in different wood zones, e.g. the content of S-lignin is higher in HW than SW of teakwood [139]. The extractive content of HW is usually higher than that of SW [140], e.g. the total extractives in the HW of Acacia melanoxylon was about twice of that in the SW [141]. The extractives decrease pulp yield and increase the consumption of pulping chemicals in paper industry [142]. Thus, understanding the effect of chemical compositional diversity of wood zones on pyrolysis products is important for optimizing conditions that enhance effective utilization of both sapwood and heartwood fractions for bio-oil production through pyrolysis.

Eastern redcedar is native to the Eastern United States [143, 144]. More than seven million acres of Oklahoma is occupied by eastern redcedar [145]. The continued spread of eastern redcedar has created severe negative impacts on the local ecosystems, such as loss of native plants and birds, reduction of forage production and livestock handling, impacts on soil hydraulic properties, and increased severity of wildfires [146-148].

Current utilization of eastern redcedar has mainly focused on cedar wood oil extraction, which is used in the production of fragrances, essential oils, insecticides and antifungals [145, 149]. Several techniques have been used to recover cedar wood oil, including steam distillation,

36

solvent extraction and super critical fluid extraction. Oil yield depends primarily on the techniques used and the properties of the wood. On average, oil yield from eastern redcedar ranges from 1 to 4.6 wt. % [150]. These low oil recovering rates are a concern. Therefore, the development of alternative conversion techniques and processes with high efficiency, such as biomass pyrolysis, is critically needed. Multiple valuable products, such as fuels, chemicals, syngas and char, can be produced simultaneously from biomass pyrolysis process. The pyrolysis-derived bio-oil could either be upgraded to transportation fuel in biorefineries or used for chemical extraction. Biochar, a porous material, can be used as a source of carbon sequestration, soil amendment and contaminants adsorbents for water and soil [151]. Syngas could be burned for heat and power, or converted into chemicals through fermentation or Fischer-Tropsch synthesis [125]. Moreover, pyrolysis process is less energy intense as compared to steam distillation [145].

To date, there is limited information on pyrolysis of eastern redcedar for fuels production. The purpose of this study was to evaluate performance and properties of end-products obtained from pyrolysis of softwood and heartwood of eastern redcedar. Both analytical and lab-scale pyrolysis reactors were be used to perform fast and slow pyrolysis study, respectively.

2.2. Materials and Methods

2.2.1. Biomass characterization

Eastern redcedar SW and HW crumbles were obtained from Forest Concepts, LLC (Auburn, WA, USA). The SW and HW were ground separately using a Wiley Mill (Thomas Model 4 Wiley® Mill) in Biosystems and Agricultural Engineering Laboratory at Oklahoma State University, using a 0.5 mm screen size. The ground samples were stored in zip-lock bags at room temperature.

Compositional analysis of eastern redcedar SW and HW including extractives, carbohydrates and lignin content was conducted following National Renewable Energy Laboratory (NREL) protocols [152, 153]. Detailed procedures were previously reported [154,

37

155]. Moisture, volatile matter and ash contents of SW and HW were determined according to ASAE standard S358.2, ASTM D3175 and ASTM E1755-01, respectively. The fixed carbon content was calculated by dry basis weight percentage difference. The ultimate analysis was performed using an elemental analyzer (Exeter Analytical CE-440, Chelmsford, MA, USA) at Midwest Microlab following ASTM D3176. The higher heating value (HHV) was measured with a Parr 6200 Bomb Calorimeter (model 6200, Parr Instrument Co., Moline, Ill).

2.2.2. Experimental design

Pyrolysis runs were carried out in a factorial design with two treatments, redcedar wood zones and pyrolysis temperatures for both fast and slow pyrolysis. The two wood zones were sapwood and heartwood. Pyrolysis temperatures were 450 and 500 ℃. Fast pyrolysis runs were replicated three times and slow pyrolysis runs were replicated twice.

2.2.3. Fast pyrolysis: Py-GC/MS

A commercial pyroprobe (model 5200, CDS Analytics Inc.) attached to a gas chromatography/mass spectrometry (Agilent 7890GC/5975MS) system was used for fast pyrolysis of eastern redcedar wood. The probe had a computer-controlled heating element and held a sample in the middle of a quartz tube (25 mm length, 1.9 mm ID). The actual temperature difference between the filament and sample varies 50-125 ℃ depending on the filament temperature [156, 157]. The temperature difference between the filament and sample was not measured during the study and was assumed to be 100 ℃ based on the literature[156]. Prior to pyrolysis, the ground eastern redcedar sample was screen sieved, and material with a particle size less than 106 μm was oven dried for 24 hrs. About 0.5 mg of the dried sample was loaded into the quartz tube. The sample was then pyrolyzed to the set temperature with a heating rate of 1000 ℃/s and maintained for 20 s. The volatiles evolved from biomass pyrolysis were conveyed from the probe into an adsorbent (Tenax-TA™) trap using ultrapure helium (99.99 vol. %), and the trap temperature was maintained at 40 °C. The condensable bio-oil components were captured by the trap, and the permanent gases were purged from the trap using helium. The bio-oil

components were evaporated by heating the trap to a temperature of 300 ºC, and the gases were pumped into GC/MS through a heated transfer line for volatile component analysis.

The GC contained a DB-5 capillary column (30 mL×0.32 mm ID, 0.25 μm film thickness). The GC oven temperature was set to maintain 40 °C for 4 min, and then increased at a rate of 5 °C/min to 280 °C and held for 20 min. The injector temperature was held at 250 °C. The split ratio was set at 30:1. Helium (purity: 99.99 vol. %) was used as the carrier gas at a flow rate of 1 mL/min. Pyrolysis products were identified by comparing the mass spectrum with National Institute of Standards and Technology (NIST) mass spectral library.

2.2.4. Slow pyrolysis: Parr reactor

A commercial reactor (Series 4570 HP/HT, Parr Instrument Company, Moline, Illinois, USA) was used for slow pyrolysis study. The reactor vessel is made of 316 stainless steel with a volume of 0.5 L. The vessel was heated by a cylindrical ceramic fiber electrical heater using a controller (Series 4840, Parr Instrument Company, Moline, IL, USA). The temperature inside the vessel was monitored by a J-type thermocouple. A pressure transducer (0~5000 psi) was used to measure the pressure build-up inside the reactor.

Approximately 50 g of crumbled Eastern redcedar wood sample was loaded into the reactor vessel for each test run. Prior to pyrolysis, the reactor vessel was purged with ultra-high pure nitrogen gas (99.99 vol. %) at 10 psi for 20 min to create an inert atmosphere. The reactor was then heated to the set temperature (450 or 500 °C) at a constant heating rate of 6 °C/min. The pressure inside the reactor vessel was allowed to increase to 100 psi as the temperature and gas production increased. Pressure was maintained at 100 psi by opening the outlet gas valve manually by a quarter turn to release the producing gases. The reaction was maintained at the set temperature for 30 min. Then, the heater was turned off to allow the reactor to cool to room temperature.

The liquid product was collected from flasks under the condensers and weighed. The char collected in the reactor vessel was weighed. The yield of produced gases was measured by

difference of weight percent. Gas sample was collected using a 0.5 L Tedlar sampling bag, and the composition was measured using a gas chromatograph (model CP3800, Varian Inc., CA) with a packed column (HayeSep DB-100/120, Alltech Associates, Inc., Deefield, Ill.) and a thermal conductivity detector (TCD).

2.2.5. Pyrolysis product characterization

The bio-oil samples were kept in a refrigerator at 4 °C prior to analysis. The physical properties analyses, including moisture content, specific gravity, pH value and higher heating value were conducted according to ASTM standard (D 7544-12). The moisture content of bio-oil was determined by KF Titrino 701 (Metrohm USA Inc.) at Kansas State University following the ASTM D 1744 protocol using hydranal as titrant [132]. The specific gravity of the bio-oil was measured using a pycnometer (2 mL, ACE GLASS INC. Vineland, NJ) according to ASTM D891-09. The pH value of bio-oil sample was determined using a pH meter (Mettler Toledo) following ASTM D7544-12. The higher heating value (HHV) of bio-oil and bio-char was measured using a bomb calorimeter (model 6200, Parr Instrument Co., Moline, Ill.). Ultimate analysis of bio-oil and bio-char was performed using an Exeter Analytical CE-440 (Exter Analytical. Inc., Chelmsford, MA) at Midwest Microlab, LLC (Indianapolis, IN). All measurements were performed at room temperature, and each measurement was repeated twice, the average of which was recorded as the final value.

The main chemical components of bio-oil were analyzed by gas chromatography/mass spectrometry (GC/MS, Agilent 7890/5975). The analysis procedure was the same as used for the pyroprobe pyrolysis treatments. Bio-oil samples were prepared as 0.02 g/mL solutions in methanol, and were filtered through a 0.45 μm micro-filter to remove the particles prior to injection into 5975 series mass selective detector. The m/z values corresponding to the fragment ions of the compounds were recorded for each compound. Bio-oil samples were fully scanned over an m/z range of 30 ~500.

2.2.6. Carbon balance and energy yield calculation

Carbon balance was performed to investigate the carbon distribution in bio-oil, biochar and syngas using **Error! Reference source not found.**.

$$Total\ carbon = \left(C_{bio-oil} \times Y_{bio-oil} + C_{char} \times Y_{char} + C_{syngas} \times Y_{syngas}\right) \times 100$$

Equation 2.1

Where

$C_{bio-oil}$ = carbon content in bio-oil (wt. %),

C_{char} = carbon content in bio-char (wt. %),

C_{syngas} = carbon content in syngas (wt. %),

$Y_{bio-oil}$ = yield of bio-oil (wt. %),

Y_{char} = yield of bio-char (wt. %), and

Y_{syngas} = yield of syngas (wt. %).

Energy yield (%) was defined as the portion of energy that contained in the biomass feed recovered in the pyrolysis products (Equation **2.2**).

$$Energy\ yield(\%) = \frac{Product\ yield\ (wt\ \%) \times HHV_{product}}{HHV_{biomass}} \times 100$$

Equation 2.2

Where

$HHV_{product}$ = higher heating value of the pyrolysis products (MJ/kg), and

$HHV_{biomass}$ = higher heating value of the biomass (MJ/kg).

2.3. Results and Discussion

2.3.1. Characterization of eastern redcedar SW and HW

Physical properties and chemical constituents of eastern redcedar are listed in Table 2.1 [35]. Glucan, a polysaccharide of D-glucose, generally represents cellulose content. SW and HW had similar cellulose contents. Hemicellulose content was characterized by pentose (xylan and arabinan) and hexose (galactan and mannan). The total hemicellulose of SW was 19.2±0.7 wt. %. Total hemicellulose content of HW was similar to that of SW. The lignin content of HW was not significantly different from that of SW. Extractives of HW were higher than that of SW. This

discrepancy could be due to the transport of extractives from transition zone (between the SW

and HW) to the HW zone [158]. The ash content of HW was significantly higher than that of SW.

SW contained 1.5 wt. % higher fixed carbon content than HW.

Table 2.1 Chemical composition, proximate and ultimate analysis of SW and HW zones of eastern redcedar[a] [154].

	Chemical compositions (wt. %)	
	Sapwood	Heartwood
Glucan	34.7 ± 0.5	34.6 ± 0.0
Xylan(C_5)	8.9 ± 0.2	8.5 ± 0.0
Arabinan(C_5)	1.0 ± 0.0	0.7 ± 0.0
Galactan	2.6 ± 0.0	3.0 ± 0.1
Mannan	6.7 ± 0.4	7.4 ± 0.0
Lignin[b]	33.7 ± 0.4	34.3 ± 0.1
Extractives	4.0 ± 0.0	4.9 ± 0.2
	Proximate analysis (w.b. wt. %)	
	Sapwood	Heartwood
Moisture content	8.64 ± 0.25	9.42 ± 0.04
Volatile matter	72.13 ± 0.30	71.83 ± 0.30
Ash content	0.12 ± 0.06	1.14 ± 0.25
Fixed carbon	19.10 ± 0.24	18.28 ± 0.60

[a] Values listed above are means ± standard error of two subsamples.

[b] Acid soluble lignin and acid insoluble lignin are included in lignin content.

2.3.2. Fast pyrolysis

The compositions of bio-oil obtained from pyrolysis of eastern redcedar can be

categorized into eight groups: ketone, acid, anhydrous sugar, pyran, furan, phenol, guaiacol and

nitrogen containing compounds according to functional groups. The distribution (area %) of the

eight groups the two pyrolysis temperatures are shown in **Error! Reference source not found.**

(450 ºC) and Figure 2.2 (500 ºC). The major compounds obtained from the two wood zones and

two pyrolysis temperatures are provided in Table 2.2. All of the major bio-oil compounds found

in bio-oil obtained from SW also existed in bio-oils obtained from HW but their quantities

differed.
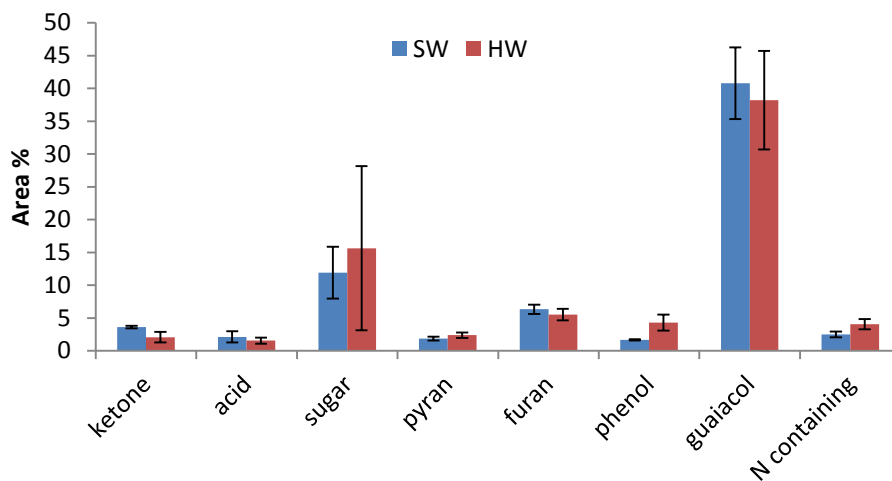
Figure 2.1 Fast pyrolysis products of eastern redcedar wood at 450 ºC (SW/HW= sapwood/heartwood, 450/500=pyrolyzed at 450/500 °C).
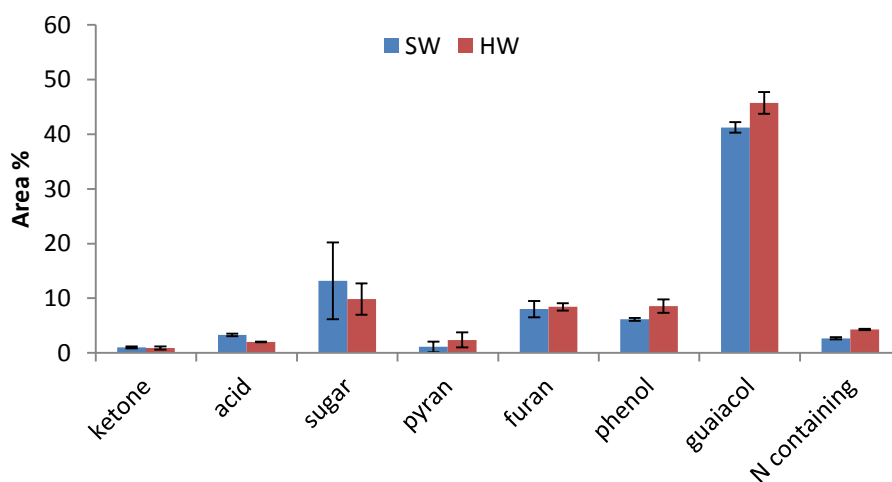
Figure 2.2 Fast pyrolysis products of eastern redcedar wood at 500 ºC (SW/HW= sapwood/heartwood, 450/500=pyrolyzed at 450/500 °C).

2.3.2.1. Fast pyrolysis: Effects of wood zone on bio-oil composition

Pyrolysis products obtained at 450 °C showed that anhydrous sugar (11.90 % for SW, and 15.63 % for HW) and guaiacol (40.80 % for SW, and 38.20 % for HW), primary products derived from depolymerization of cellulose and lignin structures, were the two most abundant species detected. This was consistent with the results of chemical composition analysis that glucan and lignin were the two dominant constituents in eastern redcedar wood. Levoglucosan

43

and D-Allose were the two dominant sugar compounds. These two sugar compounds had relatively large standard deviations, which might be due to the variation in biomass constituents, especially cellulose between the biomass samples used. As reported by others [156], this variation also explains significant changes in the anhydrous sugar yield in the repeated experiments. Anhydrous sugar yield obtained from SW was not significantly different from that obtained from HW at 450 ℃. Effect of wood zone on the total guaiacols yield was not significant but the wood zone significantly affected several guaiacol compounds. For example, 2-methoxy-4-propylphenol derived from HW (5.92±1.88 area %) was significantly higher than that derived from SW, and 2-methoxy-4-(1-propenyl)-phenol-(Z) derived from SW was significant higher than that derived from HW. There was no difference in total yield of furans from SW and HW. This can be attributed to the similar cellulose contents of both wood fractions (**Error! Reference source not ound.**). Furans are mainly derived from levoglucosan, the primary pyrolysis product from cellulose, via dehydration, decarboxylation and decarbonylation [159]. Among furans, 3, 5-dihydroxy-2-methyl-4H-pyran-4-one was the only pentose derived pyran that was identified. Acetic acid was the only acid compound detected in the pyrolysis product of SW and HW. Acid compounds were thought to be mainly derived from the elimination of the active O-acetyl groups linked to the xylan chain [160]. Ketones derived from SW and HW were significantly different. The total yield of phenols obtained from pyrolysis of HW was 4.30±1.22 area %, which was significantly higher than that of SW. Phenols and guaiacols, lignin originated groups, were 42.46±5.52 and 42.50±8.64 area % in SW and HW pyrolysis products, respectively. Syringols were not detected in the pyrolysis product indicating that eastern redcedar wood lignin was composed of Guaiacol-Hydroxyphenyl (G-H) structure. Suchithra et al. [156] also observed the absence of syringols in the pyrolysis products of pine wood. The absence of syringols was attributed to the lack of syringyl monomer in the pine lignin structures. Lignin structure in soft woods, such as pine wood and eastern redcedar were found to predominantly (over 95%)

composed of G-units [161]. 1, 4-dimethyl-3-pyrazolidinone (a heterocyclic oxygenated compound) was the only nitrogen containing compound.

2.3.2.2. Fast pyrolysis: Effects of temperature on bio-oil composition

Figure 2.2 shows the product distribution of eastern redcedar at 500 ℃. The total yield of lignin derived compounds from SW and HW increased to 47.38±0.74 and 54.28±2.61 area %, respectively. Phenols derived from both SW and HW increased significantly as the pyrolysis temperature increased from 450 to 500 ℃. Phenols were mainly the result of decomposition of lignin oligomers and guaiacols. Both processes are thermodynamically favorable, therefore leads to an increase in phenols. Guaiacols from both SW and HW were not significantly affected by the temperature increase. Guaiacols and phenols from HW were significantly higher than that from SW. Furans from both SW and HW increased significantly as the pyrolysis temperature increased from 450 to 500 ℃. The increase in temperature favored the degradation of levoglucosan and other anhydrous sugars.

Both HW and SW produced similar yields of lignin derived compounds at the low temperature (450 ℃). Increase in temperature facilitated the depolymerization of lignin and levoglucosan in both SW and HW, leading to increased phenols, guaiacols and furans. At the high pyrolysis temperature (500 ℃), lignin derived compounds from SW and HW were significantly different. As shown in Table 2.3, the interaction of temperature and wood zone was significant only on the yield of ketones. By comparing the ketone yield, it can be concluded that ketone yield was more sensitive to the variation in pyrolysis temperature than the variation in wood zone. The ketone yield was found to decrease with increase in temperature probably due to the increase in secondary pyrolysis reaction rates with increase in temperature, leading to formation of lighter gaseous compounds at 500 ℃ [162, 163].

Table 2.2 Pyrolysis products of eastern redcedar wood from Py-GC-MS[a] (SW/HW450/500= sapwood/heartwood pyrolyzed at 450/500 °C).

Chemicals	Group	SW450	HW450	SW500	HW500
		Cellulose/Hemicellulose derived compounds (Area %)			
Acetic acid	Acid	2.11±0.84	1.55±0.45	2.36±0.41	2.00±0.06
1,2-Cyclopentanedione	Ketone	2.58±0.07	1.29±0.41	-	-
2-Cyclopenten-1-one, 2-hydroxy-3-methyl-	Ketone[b]	1.18±0.15	-	1.01±0.16	-
4H-Pyran-4-one, 3,5-dihydroxy-2-methyl-	Pyran	1.87±0.29	2.38±0.40	1.66±0.21	2.38±0.37
2-Furanmethanol	Furan	1.03±0.11	-	1.25±0.67	-
Furfural	Furan	1.88±0.23	1.80±0.43	2.10±0.49	2.28±0.07
2-Furancarboxaldehyde, 5-methyl-	Furan	-	1.05±0.43	-	1.07±0.31
2(5H)-Furanone	Furan	1.77±0.14	-	1.88±1.01	1.10±0.08
2(3H)-Furanone, 5-methyl-	Furan	-	-	2.08±0.44	1.50±0.82
5-Hydroxymethylfurfural	Furan	1.64±0.28	1.87±0.41	1.83±0.21	2.46±0.03
Glutaraldehyde	Sugar	1.27±0.15	1.01±0.22	1.43±0.53	1.09±0.07
Levoglucosan	Sugar	5.43±2.84	3.68±1.57	6.56±5.00	1.19±0.73
D-Allose	Sugar	2.76±0.60	9.13±11.95	3.97±2.54	6.34±4.16
α-D-Glucopyranoside	Sugar	1.38±0.96	1.82±1.64	1.21±0.19	1.81±0.10
		Lignin derived compounds (Area %)			
P-cresol	Phenol	-	-	1.04±0.06	1.19±0.18
Catechol	Phenol	1.66±0.09	2.32±0.76	2.27±0.52	3.73±0.45
1,2-Benzenediol, 3-methyl-	Phenol	-	1.98±0.24	1.64±0.06	3.64±0.32
Phenol, 2-methoxy-	Guaiacol	4.24±0.87	3.44±0.81	3.74±0.04	4.17±0.10
Creosol	Guaiacol	5.94±1.35	6.56±1.50	5.64±1.16	9.21±1.58
2-Methoxy-4-vinylphenol	Guaiacol	6.91±1.03	6.39±1.51	6.46±1.05	7.87±0.88
2-Propanone,1-(4-hydroxy-3-methoxyphenyl)-	Guaiacol	2.81±1.83	2.45±1.64	2.19±1.12	1.62±0.30
Apocynin	Guaiacol	1.33±0.27	1.56±0.68	1.55±0.17	2.47±0.30
Vanillin	Guaiacol	2.11±0.30	1.94±0.68	2.42±0.32	2.57±0.32
Eugenol	Guaiacol	1.37±0.26	1.00±0.26	1.35±0.11	1.38±0.10
Homovanillic acid	Guaiacol	2.20±0.47	1.84±0.81	1.88±0.04	2.35±0.32
Phenol, 2-methoxy-4-propyl-	Guaiacol	2.08±0.72	5.92±1.88	2.31±0.41	5.63±1.03
Phenol, 4-ethyl-2-methoxy-	Guaiacol	1.65±0.70	1.96±0.93	1.32±0.31	2.54±0.44
Phenol, 2-methoxy-4-(1-propenyl)-, (Z)-	Guaiacol	5.69±1.22	1.67±2.30	5.04±1.06	4.55±0.41
Phenol,4-(3-hydroxy-1-propenyl)-2-methoxy-	Guaiacol	1.73±1.24	-	2.01±1.92	-
		Nitrogen containing compounds (Area %)			
3-Pyrazolidinone, 1,4-dimethyl	Nitrogen	2.47±0.44	4.06±0.78	2.65±0.21	4.31±0.11
Total		69.82	72.81	72.38	80.08

[a] "-"means the relative peak area percentage of the detected compound is less than 1 %.

[b] Values listed above are means ± standard deviation of three subsamples.

Table 2.3 Results of two-way ANOVA analysis (p-values): Effects on pyrolysis temperature and wood zone one yields of pyrolysis product groups.

Groups	Temperature	Wood Zone	Temperature*Wood Zone
Ketone	0.00	0.012	0.025
Acid	0.021	0.011	0.23
Sugar	0.61	0.96	0.44
Pyran	0.049	0.85	0.43
Furan	0.004	0.72	0.32
Phenol	0.00	0.001	0.84
Guaiacol	0.18	0.74	0.23
N containing Compound	0.45	0.00	0.90
Lignin derived Compound	0.024	0.28	0.28

2.3.3. Slow pyrolysis

2.3.3.1. Slow pyrolysis: Effects of temperature and wood zone on pyrolysis products distribution

The yields of bio-oil, biochar and syngas obtained from slow pyrolysis of HW and SW and at 450 and 500 °C (shown in Table 2.4) were not significantly different, except that biochar yield obtained from SW was significantly higher than that from HW at 500 °C. Biochar and total volatile (bio-oil + syngas) yields were comparable with those reported from slow pyrolysis of woody biomass, such as pine and fir wood [164-166]. Bio-oil yields from slow pyrolysis reported in this study and literature [167] are typically much lower than bio-oil yield (up to 60 wt %) from fast pyrolysis using auger and fluidized bed reactors at 500 °C [168, 169]. The high bio-oil yields of fast pyrolysis are due to its high heating rate and short gas residence time. In an auger reactor system, biomass moves continuously through the auger and heated via the thermal conduction between the reactor wall and biomass with a temperature gradient of 100-150 °C, with a residence time of approximately 8 s [169]. Owing to the fluidizing medium, high heating rate can be achieved in fluidized bed with short gas residence time (<2 s). High heating rate and short gas residence time are believed to enhance the rapid fragmentation of biomass and mitigate the

secondary cracking of tar [170], resulting in the high bio-oil yield. The Parr reactor system used

in this study for slow pyrolysis was operated at a low heating rate (6 °C/min). In addition, the

volatiles evolved from the reactor were in absence of any carrier gases.

Table 2.4 Distribution of products from slow pyrolysis of eastern redcedar woods (SW/HW450/500= sapwood/heartwood pyrolyzed at 450/500 °C).

Products (wt. %)	SW450	HW450	SW500	HW500
Bio-oil	[A]35.9±0.16[a]	[A]33.2±5.52	[A]33.4±3.11	[A]34.3±1.39
Biochar	[A]31.4±1.41	[A]32.6±2.62	[A]30.9±0.42	[B]29.3±0.14
Syngas	[A]32.7±1.34	[A]34.2±0.16	[B]35.7±0.89	[A]36.4±1.35

[a]Values listed above are means ± standard deviation of two subsamples.
[*]Means with the same letters under the same column are not significantly different at 5% level.

2.3.3.2. Slow pyrolysis: Effects of temperature and wood zone on bio-oil properties and composition

All bio-oil samples were brown in color and heterogeneous liquids with two phases, the

organic phase in the bottom and the aqueous phase on the top. The moisture contents of bio-oil

samples shown in Table 2.5 were higher (above 60%,) than those reported in the literature (20-40

wt. %) [171]. High moisture contents reduce bio-oil energy content and also lead to the phase

separation during the storage [3]. The carbon, hydrogen and oxygen contents of bio-oil samples

ranged from 52.69 to 57.81 wt. %, 7.51 to 8.75 wt. %, and 33.32 to 38.91 wt. %, respectively and

were comparable with the results previously reported [171, 172]. The low heating values of bio-

oil samples (shown in Table 2.5) were lower than those of bio-oil derived from forestry residue

(21 MJ/kg dry basis) reported in the literature [171]. The low bio-oil pH could cause corrosion

issues during the storage and transportation.

Table 2.5 Characteristics of bio-oil obtained from slow pyrolysis of eastern redcedar wood[b] (SW/HW450/500= sapwood/heartwood pyrolyzed at 450/500 °C).

Bio-oil sample	Moisture (wt. %)	C[a] (wt. %)	H[a] (wt. %)	N[a] (wt. %)	O[a] (wt. %)	Higher heating value[a] (MJ/kg)	pH	Specific gravity
SW450	[A]84.16±4.10	[A]68.98±14.91	[A]7.11±0.08	[A]0.21±0.14	[A]23.71±15.13	[A]31.00±5.24	[A]2.52±0.21	[A]1.01±0.001
HW450	[B]77.64±7.62	[A]53.27±19.58	[A]7.24±1.19	[B]0.11±0.01	[A]39.38±18.40	[B]17.42±7.96	[A]2.45±0.06	[A]1.02±0.01
SW500	[B]79.31±0.08	[A]52.69±2.34	[B]8.30±0.47	[B]0.10±0.00	[A]38.91±2.80	[B]14.19±6.69	[A]2.38±0.04	[A]1.00±0.02
HW500	[B]78.9±2.16	[A]57.81±3.86	[B]8.75±0.23	[B]0.12±0.05	[A]33.32±3.58	[B]17.29±7.07	[A]2.36±0.08	[A]1.02±0.01

[a] Values are converted to dry basis.

[b] Values listed above are means ± standard deviation of two subsamples.

[*] Means with the same letters under the same column are not significantly different at 95% level.

Bio-oils were mainly composed of carboxylic acids, ketones, furans, aromatics, phenols, guaiacols and olefins, as shown in Table 2.6. Acetic acid and furfural were the most abundant species identified in the bio-oil compounds. For example, acetic acid and furfural accounted for approximately 18 and 22 area %, respectively, for all bio-oil compounds identified from SW at pyrolysis temperature of 450 °C. Similar findings have also been observed in beech wood derived bio-oils [173]. Acetic acid was expected to form by primary decomposition of monosaccharides derived from hemicellulose [174]. The substantial quantity of acetic acid was responsible for the high bio-oil acidity as shown in Table 2.5. Ketones detected in bio-oils were 1-hydroxy-2-butanone, cylcopentanone and 2-methyl-2-cyclopenten-1-one, which confirm findings in the literature [10, 175]. Furan derivatives were dominated by furfural; derived from ring-open and rearrangement of monosaccharides in hemicellulose [174]. The observation of aromatic hydrocarbons was the major qualitative difference between the identified compounds from the fast and slow pyrolysis. The reaction mechanisms of aromatics production from lignocellulosic biomass has been well documented [91, 112, 159, 176]. Aromatics are derived from a series of reactions such as decarbonylation and oligomerization associated with furan compounds [159]. Lignin is a minor contributor to the production of aromatics even though its chemical structure is built on aromatic phenols blocks. Noticeable compositional differences on lignin derived products were observed between the fast (Table 2) and slow pyrolysis runs (Table 2.6). Guaiacols, especially those derived directly from degradation of lignin monomers (e.g. 2-Methoxy-4-vinylphenol, Vanillin, 2-methoxy-4-(1-propenyl)- phenol(Z)-, etc.), were the dominant lignin derived groups detected from fast pyrolysis runs, while simple phenols were the major chemical group for the slow pyrolysis runs. The qualitative difference could be due to the additional cracking of primary lignin derived products when exposed to the thermal environment. Alpha/beta-cedrenes were two hydrocarbon isomers sharing the formula $C_{15}H_{24}$, which were commonly identified in essential oils [177] as well as cedar wood oil [145]. Significant quantitative differences between alpha and beta-cedrene were observed between the bio-oils

produced in the slow pyrolysis runs. Also, HW produced significantly more total cedrenes than SW, suggesting that HW is more suitable than SW for extraction of this value-added chemical. It should be noted that these two species were not detected in the fast pyrolysis runs. These results indicated that slow pyrolysis were more favorable for the extraction of alpha/beta-cedrenes than fast pyrolysis, one of the main components of cedar wood oil.

Table 2.6 Composition of bio-oil from slow pyrolysis of eastern redcedar woods[a] (SW/HW450/500= sapwood/heartwood pyrolyzed at 450/500 °C).

Chemicals	Group	SW450	HW450	SW500	HW500
		Cellulose/Hemicellulose derived compounds			
(Area %)					
acetic acid	Acid	18.18±1.45	11.25±1.52	18.15±0.16	9.75±1.84
propanic acid	Acid	2.42±3.17	2.42±0.36	3.42±0.62	2.32±0.85
1-hydroxy-2-butanone	Ketone[b]	2.54±0.31	1.49±0.28	2.09±0.66	1.21±0.26
Cylcopentanone	Ketone	2.92±0.28	1.79	3.58	1.54±0.13
2-Cyclopenten-1-one, 2-methyl-	Ketone	4.42±0.46	1.56±0.56	2.58±0.91	1.51±0.25
Furfural	Furan	22.69±0.40	26.20±2.16	20.10±3.39	21.80±3.23
2-Furanmethanol	Furan	3.61±1.54	-	1.47±0.26	-
Ethanone, 1-(2-furanyl)-	Furan	0.99±0.15	-	-	-
2-Furancarboxaldehyde, 5-methyl-	Furan	3.16±0.57	4.46±0.97	2.94±0.21	4.43±0.38
		Lignin derived compounds (Area %)			
Toluene	Aromatic	1.97±1.02	-	-	-
p-Xylene	Aromatic	1.90±0.14	1.65±0.59	1.54±0.51	1.77±0.67
Phenol	Phenol	4.27±2.08	3.04±0.12	3.25±1.24	3.55±1.30
Phenol, 2-methyl-	Phenol	2.43±0.79	2.54±0.19	1.83±0.39	2.71±2.07
p-Cresol	Phenol	1.31±0.68	1.67±0.63	-	-
Phenol, 2-methoxy-	Guaiacol	10.34±1.63	7.98±0.67	10.13±1.82	5.22±0.03
Creosol	Guaiacol	4.28±0.02	5.71±0.33	4.24±0.14	4.34±0.61
		Cedar oil compounds (Area %)			
(-)-alpha-cedrene	Olefin	8.39±1.12	12.97±1.08	8.65±1.46	18.15±0.74
(+)-beta-cedrene	Olefin	2.27±0.32	1.93±0.93	1.81±0.10	2.89±0.34

[a] "-"means the relative peak area percentage of the detected compound is less than 0.5 %.

[b] Values listed above are means ± standard deviation of two subsamples.

2.3.3.3. Slow pyrolysis: Effects of temperature and wood zone on properties of biochar and syngas

Table 2.7 summarizes the elemental analysis and energy content for both unprocessed and biochar eastern redcedar SW and HW. Comparing the unprocessed components, HW had

51

higher carbon content than SW. The C/H and O/C molar ratios for HW were 0.74 and 0.71,

repectively, while these ratios were 0.73 and 0.77, respectively, for SW. The energy content of

unprocessed HW was significantly higher than that of unprocessed SW. Pyrolysis led to a

significant increase of carbon content and a significant decrease of hydrogen and oxygen content

in the biochar compared with the unprocessed sample, as indicated in Table 2.7. The C/H ratios

of biochar obtained at 450 °C were 2.34 and 2.7 for SW and HW, respectively, which were

comparable to wood waste results reported in literature [171]. The carbon and oxygen content

variation that resulted from pyrolysis also contributed to the significant increase in the biochar

heating value, e.g., the heating value of SW biochar obtained at 450 °C increased 58% compared

with that of unprocessed SW.

Table 2.7 Characterization of bio-char from slow pyrolysis of eastern redcedar woods (SW/HW450/500= sapwood/heartwood pyrolyzed at 450/500 °C).

Bio-char sample	C (d.b. wt. %)[a]	H (d.b. wt. %)	O (d.b. wt. %)	N (d.b. wt. %)	S (d.b. wt. %)	Higher heating value (MJ/kg)
Unprocessed SW	46.45	5.33	47.64	0.19	0.16	[A]19.84±0.077
Unprocessed HW	48.23	5.44	45.96	0.21	0.15	[A]20.22±0.13
SW450	[*A]84.35±2.19	[B]3±0.14[b]	[A]11.45±2.48	[A]0.45±0.07	[A]0.4±0.15	[B]31.36±0.40
HW450	[B]87.4±0.28	[A]2.7±0.3	[B]8.95±0.21	[A]0.4±0.1	[A]0.4±0.1	[B]33.77±2.19
SW500	[*A]85.8±2.97	[A]2.4±0.2	[A]10.85±2.90	[B]0.35±0.07	[B]0.35±0.07	[C]29.98±2.50
HW500	[B]88.88±0.45	[A]2.6±0.15	[B]7.75±0.07	[B]0.35±0.07	[A]0.4±0.1	[D]32.95±0.17

[a] Values are dry base ash free.

[b] Values listed above are means ± standard deviation of two subsamples.

[*]Means with the same letters under the same column are not significantly different at 95% level.

A statistical analysis (unpaired t-test) was performed to evaluate the effects of SW and HW on the derived biochar compositions. The results showed that biochar obtained from HW contained significantly higher carbon and lower oxygen contents than that obtained from SW for both temperatures investigated. Comparing the carbon, hydrogen and oxygen content of SW and HW before and after pyrolysis, it was determined that the extent of variation (increase/decrease in percent) was similar, indicating that biochar composition differences between SW and HW could be attributed to the unprocessed sample chemical composition.

Syngas obtained from pyrolysis of eastern redcedar contained four major species, H_2, CO, CH_4 and CO_2 (Table 2.8). The gross calorific value of the syngas was estimated using the individual gas component higher heating values given in literature [178]. The syngas obtained from HW had a significantly higher gross calorific value (GCV) than that from SW. This could be due to the high yields of CO and CH_4 and low yield of CO_2 in the syngas obtained from HW pyrolysis. Phan et al. [166] reported that syngas obtained from waste wood composition at 650 °C pyrolysis temperature contained 30.5 vol. % CO, 44.7 vol. % CO_2, 7.0 vol. % H_2, and 14.7 vol. % CH_4 with a GCV of 12.6 MJ/Nm^3, which was comparable to the GCV of syngas obtained from HW at 500 °C in this study. Researchers also observed CO and CO_2 maximize at temperature of 500 °C, whereas hydrogen continue to increase with pyrolysis temperature.

Table 2.8 Composition of syngas obtained from slow pyrolysis of eastern redcedar woods (SW/HW450/500= sapwood/heartwood pyrolyzed at 450/500 °C).

Sample	H_2 (vol. %)	CO (vol. %)	CH_4 (vol. %)	CO_2 (vol. %)	Gross calorific value (MJ/Nm^3)
SW450	[*][A]3.09±1.04[a]	[A]34.65±1.33	[A]11.16±1.13	[A]51.11±0.83	[A]9.21±0.75
HW450	[*][A]3.01±1.05	[B]37.27±0.89	[B]14.51±1.77	[B]44.56±4.62	[B]10.87±0.95
SW500	[B]3.92±0.73	[A]34.70±0.97	[B]14.31±1.22	[C]47.07±0.99	[B]10.58±0.70
HW500	[A]3.14±0.09	[C]40.42±1.34	[C]16.41±2.60	[D]40.03±4.04	[C]12.04±1.22

[a] Values listed above are means ± standard deviation of two subsamples.
[*] Means with the same letters under the same column are not significantly different at 5% level.

2.3.3.4. Slow pyrolysis: Carbon and energy balances

The percentages of carbon transferred from biomass into bio-oil, biochar and syngas during the pyrolysis process was estimated using **Error! Reference source not found.**, and the esults are shown in Table 2.9. Over 90 wt. % of carbon transfer was achieved in the pyrolysis products, with most being retained in the biochar. The secondary tar cracking instigated by the slow pyrolysis condition could have promoted the production of syngas and reduced the production of liquid, hence low carbon transfer into bio-oil was expected. Figure 2.3 shows the distribution of energy transferred to the pyrolysis products of eastern redcedar wood. Much of the energy (up to 50%) was retained in the biochar after pyrolysis. Less than 10 % of the energy transferred to bio-oil.
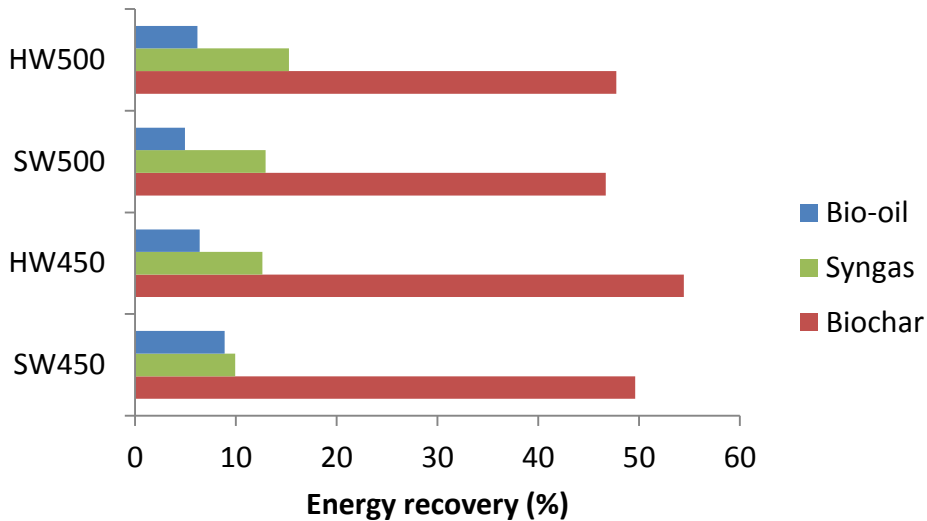
Figure 2.3 Energy recovery for pyrolysis of eastern redcedar wood in slow pyrolysis runs (SW/HW450/500= sapwood/heartwood pyrolyzed at 450/500 °C).

Table 2.9 Carbon balance of the products obtained from slow pyrolysis of eastern redcedar woods (S/HW450/500= sapwood/heartwood pyrolyzed at 450/500 °C).

Sample	Carbon in bio-oil (wt. %)	Carbon in biochar (wt. %)	Carbon in syngas (wt. %)	Total (wt. %)
SW500	7.84	57.08	27.00	91.92
HW500	8.82	54.00	27.73	90.54

2.4. Conclusions

This study investigated the pyrolytic behavior of eastern redcedar heartwood (HW) and sapwood (SW) in two process conditions (fast at micro-scale and slow pyrolysis at lab-scale) and at two temperatures (450 and 500 °C). Eastern redcedar wood was characterized by a G-H type lignin because of lack of S-lignin units in bio-oil. In fast pyrolysis conditions, bio-oils produced were dominated by primary products, such as anhydrous sugars, phenols and guaiacols. At 450 °C, ketones in bio-oils obtained from SW produced were significantly higher than that obtained from HW. There was no significant difference on the total yield of lignin-derived products from SW and HW; however, SW yielded fewer phenols and more guaiacols than HW. When temperature increased to 500 °C, HW yielded more lignin-derived products than SW.

Bio-oils produced from slow pyrolysis were dominated by small molecules, such as acetic acid, furfural and simple phenols that are derived from the decomposition of primary products. Cedar oil components (alpha/beta-cedrene) were only produced at slow pyrolysis conditions, indicating that slow pyrolysis could be used as an alternative way to extract cedar oil. The maximum yield (21.04±1.08 area %) of alpha/beta-cedrene was obtained from heartwood at 500 °C. Heartwood produced significantly more alpha/beta-cedrene than sapwood.

CHAPTER III

EFFECTS OF TORREFACTION AND DENSIFICATION ON SWITCHGRASS

PYROLYSIS PRODUCTS

This research paper was published as a research paper in the journal of Bioresource Technology

"Z. Yang, M. Sarkar, A. Kumar, J.S. Tumuluru, R.L. Huhnke, Effects of torrefaction and

densification on switchgrass pyrolysis products, Bioresource Technology, 174 (2014) 266-273.".

Abstract: The pyrolysis behaviors of four types of pretreated switchgrass (torrefied at 230 and 270 °C, densification, and torrefied at 270 °C followed by densification) were studied at three temperatures (500, 600, 700 °C) using a pyroprobe attached to a gas chromatogram mass spectroscopy (Py-GC/MS). Torrefied switchgrass had improved hydrogen to carbon ratio and energy content compared with raw switchgrass. Contents of anhydrous sugars and phenols in pyrolysis products of torrefied switchgrass were higher than those in pyrolysis products of raw switchgrass. As the torrefaction temperature increased from 230 to 270 °C, the contents of anhydrous sugars and phenols in pyrolysis products increased whereas content of guaiacols decreased. High pyrolysis temperatures (600 and 700 °C as compared to 500 °C) enhanced decomposition of lignin and anhydrous sugars, leading to increase in phenols, aromatics and furans. Densification enhanced depolymerization of cellulose and hemicellulose during pyrolysis.

Keywords: Torrefaction; Densification; Switchgras; Pyrolysis; Py-GC/MS

3.1. Introduction

Alternative energy sources can play an important role in reducing the dependence on fossil fuels and meeting the future energy demands [156, 179]. Biomass has been identified as an alternative, clean and carbon dioxide (CO_2) neutral energy source to produce liquid transportation fuels or biofuels and other forms of energy [180]. Switchgrass, a perennial, warm-season grass native to the prairies of North America, has emerged as an ideal biomass to produce biofuels because of its high yields of about 15 Mg ha^{-1} [181, 182], environmental benefits such as a 95% reduction in soil erosion and 90% reduction in pesticide and fertilizer usage and the ability to tolerate diverse growing conditions[183] . However, similar to other biomass, properties of switchgrass such as low energy and bulk densities, and high moisture content create challenges for storage, transportation and conversion into final fuels, chemicals and power [184].

Pretreatments such as torrefaction and densification can be used to improve properties of switchgrass because pretreating biomass results in the breakage of its lignin structure and decomposition of cellulose and hemicellulose structure rendering the biomass more accessible to be pyrolyzed [157, 185]. Torrefaction is a thermochemical process which occurs at temperatures between 200 and 300°C in an inert atmosphere resulting in a hydrophobic product with improved physical and chemical properties and an increased energy density [186]. Densification increases bulk density of the biomass by converting loose biomass into pellets and briquettes having more uniformity and higher bulk density [184, 187]. A combination of torrefaction and densification may provide additional benefits by increasing both the bulk and energy densities while making biomass hydrophobic.

Biomass is converted into biofuels via two processes namely biochemical and thermochemical conversion processes. Pyrolysis is one of the thermochemical conversion methods to produce liquid fuels and chemicals. In this process biomass is rapidly heated to 450-550°C in an inert atmosphere with a short residence time resulting in char, vapors and aerosols (bio-oil), and gas [171, 188]. The bio-oil produced is a dark brown liquid and a complex mixture

of water (20-25 wt.%) and polar organics (75-80 wt.%) [2]. Bio-oil can be used in several applications such as boilers, furnaces, turbines and internal combustion engines for heat, power or electricity generation [14]. However its adverse characteristics such as instability, low heating value, high density, viscosity, acidity, water and oxygen create challenges in its utilization [179, 188].

Few studies have been performed on pyrolysis of torrefied and densified biomass [157, 189, 190]. However, there has been no published report on effects of pretreatments on the bio-oil components obtained from pyrolysis of switchgrass. Hence, the objective of this study was to investigate the effects of torrefaction and densification pretreatments and pyrolysis temperatures on the bio-oil components obtained from pyrolysis of switchgrass.

3.2. Materials and methods

3.2.1. Biomass characterization

Kanlow Switchgrass (Panicum Virgatum) grown at the Plant and Soil Sciences department at Oklahoma State University was selected as the biomass feedstock. Bales of Kanlow switchgrass were chopped using a Haybuster tub grinder (H1000, Duratech Industries International Inc. Jamestown, N.D) with a screen size of 25 mm. The chopped switchgrass was then ground using a hammer mill (Bliss Industries, Ponca City, Oklahoma) with a mesh size of 4 mm and sent to Idaho National Laboratory (INL, Idaho Falls) for pretreatments. Four types of pretreatment included torrefaction at 230°C and 270°C for 30 min residence time, densification, and combined torrefaction and densification (torrefaction at 270°C for 30 min followed by densification). More details on the operation conditions of pretreatments can be found in our previous study [191]. The mass loss during torrefaction pretreatment at 230 and 270 °C was 25.01 wt % and 36.70 wt %, respectively. The loss could be due to the releasing of moisture, condensable and non-condensable volatiles.

Proximate analysis (contents of moisture, volatile, ash and fixed carbon) of biomass sample was determined using a furnace (model 3-550A, Dentsply Prosthetics, PA). The moisture,

60

volatile and ash contents were determined following ASAE standard S358.2 (ASABE Standards, 2006), ASTM D3175 and ASTM E1755-01, respectively. The fixed carbon content was determined by subtracting the volatile and ash contents from the total biomass on dry basis. The ultimate analysis of biomass was measured using an elemental analyzer (PerkinElmer 2400 Series II CHNS/O Elemental Analyzer, Shelton, CT).

The Higher Heating Value (HHV) of biomass was measured using an adiabatic Parr 6200 Bomb Calorimeter (model A1290DDEB, Parr Instrument Co., Moline, Ill). 0.5 g of biomass sample was pelletized using a pellet press and the pellet was kept in a nickel crucible and burned inside a bomb calorimeter surrounded by a water jacket. The sample was ignited by a 10 cm length aluminum wire in presence of oxygen. The wire was placed in such a way that only the tip touched the pellet. Upon ignition, the released heat transferred to the water jacket causing temperature to rise. The increase in temperature was used to calculate HHV of the sample. The HHV measurements were done three times and the average value was reported.

3.2.2. Py-GC experiments

Pyrolysis experiments were performed in a commercialized pyrolyzer (model no. 5200, CDS Analytics Inc.). The probe had a computer-controlled heating element which held a sample in a quartz tube (25 mm long, 1.9 mm i.d.). Pyrolysis experiments were conducted at three temperatures (500, 600 and 700 °C) at a constant heating rate of 1000 °C/s. About 1 mg of biomass sample was loaded for pyrolysis experiment using helium gas as the inert gas. The volatiles evolved from biomass pyrolysis were carried from the probe into an adsorbent (Tenax-TA™) trap, which was maintained at 40 °C. The condensable bio-oil components were captured by the trap, and the permanent gases were purged out with helium. Then, the bio-oil components were evaporated by heating the trap to 300 °C, and then were directed into a gas chromatography/mass spectrometry (Agilent 7890GC/5975MS) through a heated transfer line for analysis of bio-oil compounds.

The GC column was equipped with a DB-5 capillary column (30 mL×0.32mm I.D., 0.25 µm film thickness). The GC oven temperature was set to maintain at 40 °C for 4 min, and then the temperature was programmed at a rate of 5 °C/min to 280 °C and maintained for 20 min. The injector temperature was 250 °C, and the split ratio was set to 30:1. Helium (purity: 99.99%) was used as the carrier gas at a flow rate of 1mL/min.

3.2.3. Experiment design

A full factorial experimental design was used with two factors namely switchgrass pretreatment and pyrolysis temperatures. Five levels of switchgrass pretreatment were a) no pretreatment (raw switchgrass), b) torrefaction at 230°C, c) torrefaction at 270°C, d) densification, e) combined torrefaction and densification (torrefaction at 270°C followed by densification). Three levels of pyroprobe (pyrolysis) temperatures were 500, 600 and 700°C.

3.3. Results and discussions

3.3.1. Effects of pretreatment on switchgrass properties

The results of proximate and ultimate analysis of raw and pretreated switchgrass were indicated in Table 3.1[191]. It can be seen that moisture contents of switchgrass decreased after pretreatment with torrefaction at 230 and 270 ºC. However, moisture content of pellets (switchgrass with densification and combined pretreatments) was not compared with others because pellets were further dried after densification to allow storing those safely. The volatile content decreased after pretreating with torrefaction at 230 °C and continued to decrease as the torrefaction temperature increased to 270 ºC due to the partial decomposition of biomass polymers (cellulose, hemicellulose and lignin) and release of light volatiles[192]. On the other hand, densification did not show significant effect on switchgrass volatile content. However, the combined pretreatment of torrefaction and densification resulted in the least volatile content (62.63 wt. %). Ash content of switchgrass was significantly affected only by the high temperature torrefaction and combined torrefaction and densification pretreatments, which can be due to the

high loss of volatile content. Fixed carbon content was significantly affected at all pretreatment conditions except densification. The highest fixed carbon content was observed when switchgrass was pretreated with combined torrefaction and densification (31.45 wt. %) and followed by pretreated with torrefaction at 270 and 230 °C, respectively. The ultimate analysis results indicated that the carbon content increased significantly by torrefaction and combined pretreatments with torrefaction and densification. In addition, the carbon content increased significantly as the torrefaction temperature increased from 230 to 270 °C. Inverse trend was observed for both hydrogen and oxygen content in both raw and pretreated switchgrass. Densification has no significant effects on the carbon and oxygen contents according to statistical analysis using Duncan multiple range tests. The HHV of switchgrass was increased at all pretreatment conditions except densification. The increase in HHV could be due to decreased oxygen to carbon (O/C) and hydrogen to carbon (H/C) ratios in the switchgrass pretreated with torrefaction compared with raw switchgrass. This fact can be also seen in the Van Krevelen diagram shown by Sarkar et al [191].

Table 3.1Proximate and ultimate analysis and HHV of pretreated switchgrass (adapted from Sarkar et al., 2014).(SG=switchgrass, T230=switchgrass torrefied at 230 °C, T270=switchgrass torrefied at 270 °C, DEN=densified switchgrass, T270+DEN=Switchgrass pretreated by combined torrefaction and densification, same in Table 3.2 ~Table 3.4.)

	Proximate analysis (w.b. wt. %)				
	Raw SG	T230	T270	DEN	T270+DEN
Moisture content	$9.80\pm0.65^{*}$	2.39 ± 0.61	2.05 ± 1.04	5.05 ± 0.78	7.44 ± 0.15
Volatile matter	80.63 ± 0.18	78.99 ± 0.54	67.52 ± 0.93	80.23 ± 0.54	62.63 ± 0.23
Ash content	3.50 ± 0.44	3.63 ± 0.15	4.98 ± 0.50	3.62 ± 0.14	5.91 ± 0.16
Fixed carbon	15.87 ± 0.42	17.38 ± 0.45	27.51 ± 1.38	16.15 ± 0.67	31.45 ± 0.38
	Ultimate analysis (d.b. wt. %)				
	Raw SG	T230	T270	DEN	T270+DEN
Carbon	47.37 ± 0.03	52.79 ± 0.16	59.16 ± 0.45	47.11 ± 0.29	52.09 ± 0.34
Hydrogen	6.61 ± 0.18	5.77 ± 0.27	4.67 ± 0.28	5.93 ± 0.12	5.13 ± 0.11
Oxygen	43.97 ± 0.35	39.58 ± 0.59	34.53 ± 1.00	45.44 ± 0.37	41.34 ± 0.15
Nitrogen	0.62 ± 0.01	0.32 ± 0.08	0.44 ± 0.18	0.29 ± 0.01	0.39 ± 0.01
Sulfur	1.43 ± 0.13	1.54 ± 0.08	1.20 ± 0.08	1.24 ± 0.04	1.05 ± 0.06
HHV (MJ/kg)	20.60 ± 0.69	23.53 ± 0.19	27.11 ± 0.27	19.14 ± 0.25	22.27 ± 0.32

*Values listed above are means ± standard deviation of three samples.

3.3.2. Characterization of pyrolysis products

The chemical compositions of pyrolysis products of raw and pretreated switchgrass obtained at three temperatures (500, 600 and 700 ℃) are classified into different families as shown in Figure 3.1~Figure 3.3 in terms of relevant peak areas. More than 100 compounds were identified by comparing the spectrum with the MS library. The pyrolysis products can be classified into various families according to their functional groups, such as ketones, anhydrous sugars, furans, phenols, guaiacols, syringols, aromatics and carboxylic acids, and this result is comparable with literature [156, 189]. Among these groups, ketones, anhydrous sugars, furans and carboxylic acids are derived from decomposition of cellulose and hemicellulose, and the remaining groups are derived from decomposition of lignin derived oligomers. Table 3.2,

Table 3.3 and Table 3.4 list the major compounds (with relative peak area >=1 %) and their relative area percentages obtained from the pyrolysis of raw and pretreated switchgrass at 500, 600 and 700 °C, respectively. All the listed chemical compounds were sorted according to their chemical families and the source they derived from. It can be seen that majority of the

compounds are oxygenated polar species. Although most of the compounds in pyrolysis products obtained from both raw and pretreated switchgrass were similar, their quantity (and hence yield) differed.
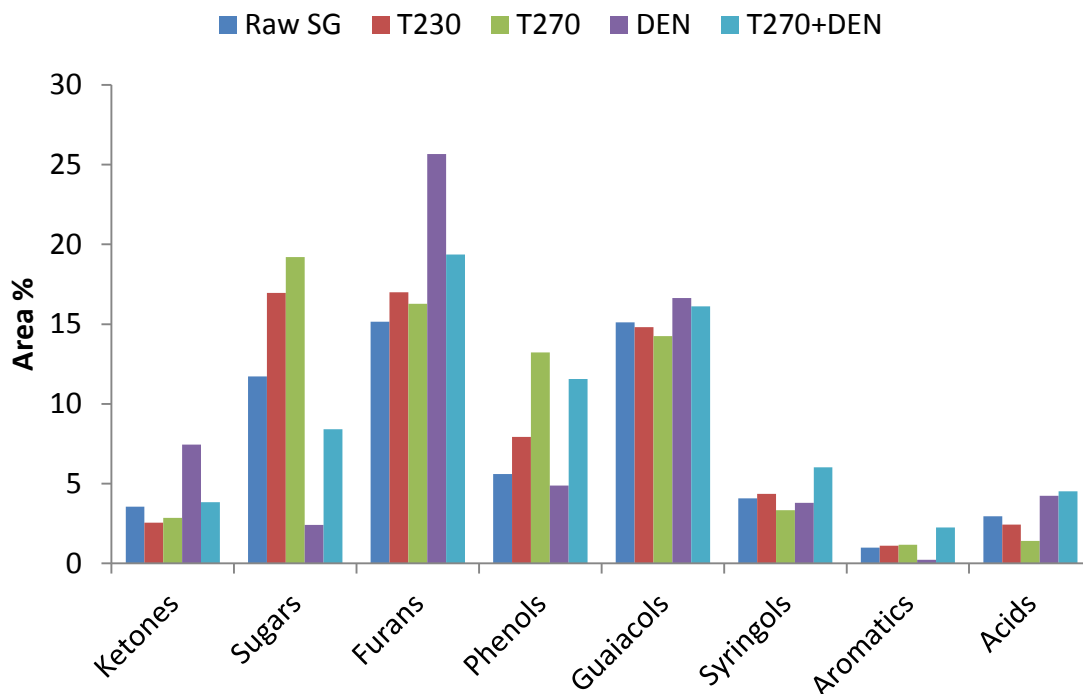
Figure 3.1 Product distribution of raw and pretreated switchgrass pyrolyzed at 500 °C (SG=switchgrass, T230=switchgrass torrefied at 230 °C, T270=switchgrass torrefied at 270 °C, DEN=densified switchgrass, T270+DEN=Switchgrass pretreated by combined torrefaction and densification, same in Figure 3.2 and Figure 3.3).

Table 3.2 Pyrolysis products of raw and torrefied switchgrass obtained at 500 °Cª. (SG=switchgrass, T230=switchgrass torrefied at 230 °C, T270=switchgrass torrefied at 270 °C, DEN=densified switchgrass, T270+DEN=Switchgrass pretreated by combined torrefaction and densification, same in

Table 3.3 and Table 3.4.)

Chemicals	Group	Raw SG	T230	T270	DEN	T270+DEN
		Cellulose/Hemicellulose derived compounds (Area %)				
Benzofuran, 2,3-dihydro-	Furans	6.36	4.14	2.30	9.45	4.14
Furfural	Furans	3.08	2.25	1.78	4.25	-
Furan, 2-methyl-	Furans	1.44	1.65	1.63	3.09	2.49
2-Furancarboxaldehyde, 5-methyl-	Furans	1.28	1.35	1.53	1.31	2.02
2(3H)-Furanone, 5-methyl-	Furans	-	2.08	1.87	-	1.85
5-Hydroxymethylfurfural	Furans	-	1.18	1.07	1.02	-
Acetic acid	Acid	2.95	1.40	-	4.24	1.66
3,4-Altrosan	Sugars	3.08	3.42	-	-	-
.beta.-D-Glucopyranose, 1,6-anhydro-	Sugars	5.96	7.27	13.36	-	5.90
D-Allose	Sugars	2.40	5.15	5.14	-	1.66
1,2-Cyclopentanedione	Ketones	2.07	-	-	1.46	-
1,2-Cyclopentanedione, 3-methyl-	Ketones	1.12	-	1.53	-	-
2-Cyclopenten-1-one, 2-hydroxy-3-methyl-	Ketones	-	1.26	-	1.77	1.76
		Lignin derived compounds (Area %)				
Phenol	Phenols	-	1.17	1.61	-	1.64
p-Cresol	Phenols	1.02	1.47	2.31	-	2.18
Catechol	Phenols	1.55	1.89	3.00	1.62	2.58
Phenol, 4-ethyl-	Phenols	-	-	1.04	-	1.21
2-Methoxy-4-vinylphenol	Guaiacols	5.79	4.22	2.66	7.00	4.14
1,2-Benzenediol, 3-methoxy-	Guaiacols	-	-	1.73	-	1.64
Phenol, 4-ethyl-2-methoxy-	Guaiacols	-	-	1.77	-	1.70
Creosol	Guaiacols	2.11	-	3.87	2.24	3.26
Phenol, 2-methoxy-	Guaiacols	1.98	2.19	-	1.89	2.30
Benzoic acid, 4-hydroxy-3-methoxy-	Guaiacols	1.76	-	1.85	-	1.08
3,5,-dimethoxyacetophenone	Syringols	2.44	-	-	1.27	1.51
Phenol, 2,6-dimethoxy-4-(2-propenyl)-	Syringols	1.32	1.25	-	1.46	1.63
Phenol, 2,6-dimethoxy-	Syringols	1.55	2.56	2.19	2.08	2.53
Toluene	Aromatics	-	1.10	1.16	1.45	1.50

[a] "-"means the peak area percentage of the detected compound is less than 1 %.

3.3.2.1. Effects of torrefaction

Significant compositional variation can be found between the pyrolysis products of raw and torrefied switchgrass. As shown in Figure 3.1, anhydrous sugars, furans, phenols and

guaiacols are the four most abundant groups identified in the pyrolysis product of both raw and torrefied switchgrass. At 500 ℃ pyrolysis temperature, anhydrous sugar content increased from 11.71 area % of raw switchgrass to 16.96 area % of switchgrass torrefied at 230 ℃, to 19.19 area % of switchgrass torrefied at 270 ℃. However, increase in the anhydrous sugars content due to torrefaction was not consistent when pyrolysis temperature increased to 600 and 700 °C, as shown in Figure 3.2 and Figure 3.3.One of the major anhydrous sugars listed in Table 3.2 (at pyrolysis temperature of 500 °C), 1 was 6-anhydro-β-D-Glucopyranose (also known as levoglucosan). Levoglucosan was found to increase from 5.96 area % of raw switchgrass to 7.27 area % of switchgrass torrefied at 230 ℃, and then to 13.36 area % of switchgrass torrefied at 270 ℃. The furans content increased slightly from 15.14 area % of raw switchgrass to 16.99 area % of switchgrass torrefied at 230 ℃, however, no significant variation was observed in switchgrass torrefied at 270 ℃ and 230 °C. Among the furans listed Table 3.2, both 2, 3-dihydro-benzofuran and furfural decreased dramatically after torrefaction initially, and continued to decrease as the torrefaction temperature increased from 230 to 270 °C. However, no consistent trend was observed for other furans identified and listed as the major compounds. Few earlier studies on pyrolysis of torrefied biomass reported that furans content decreased by torrefaction when pyrolysis temperature was ranging from 480 to 650 °C [157, 189, 193]. Interestingly, in this study, the decreasing trend for furans was noticeable when pyrolysis temperature increased to 600 and 700 °C, as shown in Figure 3.2 and Figure 3.3.
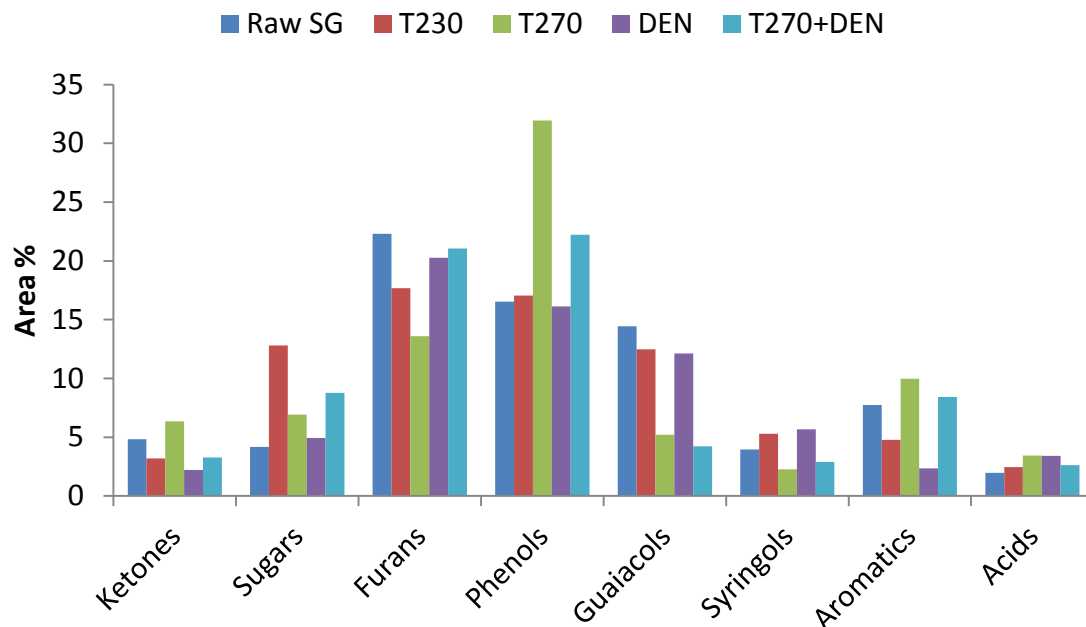
Figure 3.2 Product distribution of raw and pretreated switchgrass pyrolyzed at 600 °C.

Table 3.3 Pyrolysis products of raw and torrefied switchgrass obtained at 600 ºCª.

Chemicals	Group	Raw SG	T230	T270	DEN	T270+DEN
		Cellulose/Hemicellulose derived compounds (Area %)				
Benzofuran, 2,3-dihydro-	Furans	9.33	5.80	2.99	9.11	5.085
Furfural	Furans	4.84	2.96	1.78	3.24	2.88
Furan, 2-methyl-	Furans	-	2.86	-	-	2.15
2-Furancarboxaldehyde, 5-methyl-	Furans	1.94	1.55	1.84	1.42	2.49
2(3H)-Furanone, 5-methyl-	Furans	1.44	1.97	-	2.35	2.54

5-Hydroxymethylfurfural	Furans	-	1.34	1.23	1.21	1.32
2-Furanmethanol	Furans	1.20	1.10	1.04	1.22	1.27
2(5H)-Furanone	Furans	1.59	1.10	-	-	1.13
Acetic acid	Acid	1.49	2.09	-	3.40	1.42
3,4-Altrosan	Sugars	1.13	1.64	-	-	-
.beta.-D-Glucopyranose, 1,6-anhydro-	Sugars	2.38	4.93	-	4.40	-
D-Allose	Sugars	-	5.59	3.74	-	1.11
2-Cyclopenten-1-one, 2-hydroxy-3-methyl-	Ketones	1.33	1.61	1.93	1.38	1.91
Lignin derived compounds (Area %)						
Phenol	Phenols	1.47	2.33	3.20	1.62	3.69
p-Cresol	Phenols	2.22	-	5.10	-	4.13
Catechol	Phenols	3.08	3.70	5.49	3.08	5.22
4-Ethylcatechol	Phenols	-	-	1.26	-	1.15
Phenol, 2-methyl-	Phenols	1.03	-	2.22	-	2.18
Phenol, 4-ethyl-	Phenols	1.27	1.35	1.95	1.03	1.76
1,2-Benzenediol, 3-methyl-	Phenols	1.51	-	2.50	1.72	2.01
1,2-Benzenediol, 4-methyl-	Phenols	1.68	2.07	3.81	2.04	2.82
2-Methoxy-4-vinylphenol	Guaiacols	6.46	4.52	1.75	5.95	2.43
Creosol	Guaiacols	2.29	2.17	1.11	1.69	1.02
Phenol, 2-methoxy-	Guaiacols	1.44	1.51	1.33	1.30	1.12
Phenol, 2,6-dimethoxy-4-(2-propenyl)-	Syringols	1.29	-	-	1.29	-
Phenol, 2,6-dimethoxy-	Syringols	1.82	1.95	1.67	1.78	1.66
Toluene	Aromatics	2.11	2.15	2.63	2.09	2.97
Benzene	Aromatics	3.87	-	1.43	-	1.27
p/o-Xylene	Aromatics	-	1.02	-	-	1.31
Benzene, 1,3-dimethyl-	Aromatics	1.00	-	1.44	-	-

[a] "-"means the relative peak area percentage of the detected compound is less than 1 %.

As for lignin-derived compounds, at 500 °C pyrolysis temperature, the phenols in pyrolysis products of two torrefied switchgrass were 7.92 and 13.23 area %, which was significantly higher than that in pyrolysis products of raw switchgrass (5.59 area %). Similar increasing trend was also noticeable for pyrolysis at 600 and 700 °C, as shown in Figure 3.2 and Figure 3.3.Consistently, significant increasing trend was also observed for typical phenol compounds (listed in Table 3.2) i.e. phenols, p-cresol and catechol that increased from less than 1, 1.02 and 1.55 to 1.61, 2.31 and 3.00 area %, respectively. Guaiacols, the main oxygenates derived from lignin oligomers slightly decreased on torrefaction (14.80 area % of switchgrass torrefied at 230 to 15.10 area % of raw switchgrass). 2-Methoxy-4-vinylphenol, one of the dominant guaiacols decreased significantly from 5.79 to 2.66 area %. The guaiacols content decreased more

69

significantly as the severity of torrefaction increased at 600 °C pyrolysis temperature, i.e. the total area % of guaiacols obtained in raw switchgrass decreased from 14.43 to 5.20 compared to that obtained from switchgrass torrefied at 270 °C. However, for 700 °C pyrolysis, the content of guaiacols increased slightly from 8.73 to 9.80 area % after torrefaction at 230 °C, but no significant change was observed between switchgrass torrefied at 230 and 270 °C.

The above analysis of pyrolysis products obtained from raw and torrefied switchgrass indicate that torrefaction promotes the production of anhydrous sugars and phenols. Hence, torrefaction can promote pyrolysis-based biorefinery by producing multiple high-value chemicals in only few conversion steps. Toluene was the only aromatic compound identified in the pyrolysis products of both raw and torrefied switchgrass at 500 °C with small increase in the toluene content after torrefaction. Similar results were reported in the literature [156]. Aromatics larger than toluene could have condensed in the trap or be in low concentration. Other simple oxygenates such as ketones and carboxylic acids were also detectable. Ketones were dominated by cycloketones with five carbon rings that are derived from deploymerization of levoglucosan or conversion of 5-hydroxymethylfurfural [156]. Acetic acid was the primary carboxylic acid in the pyrolysis products of raw and torrefied switchgrass, the content of which decreased from 2.95 to less than 1 area % after torrefaction at 270 °C. This finding is consistent with results reported in the literature [189, 193].

The variation in the composition of pyrolysis product obtained from raw and torrefied switchgrass was due to partial decomposition of cellulose and hemicellulose during torrefaction [189]. Thermal stability, decomposition rates and decomposition products of the three biomass components (cellulose, hemicellulose and lignin) differ. Hemicellulose is considered as the most thermally unstable component, whose decomposition mainly occurs at 220-315 °C, whereas lignin is the most stable one, whose degradation occurs at a broader temperature range at 160-900 °C [194, 195]. In addition, the pyrolysis products from these three components are also extremely different. The pyrolysis of hemicellulose mainly produces small molecules such as ketones, acetic

acids and furfural. Cellulose is the dominant source for the production of anhydrous sugars and furans and lignin produces most of the phenols and phenol derivatives. Previous studies also found strong interaction effects of hemicellulos- cellulose and cellulose-lignin[196, 197] during pyrolysis. On one hand, hemicellulose is believed to decompose prior to cellulose and form a liquid film wrapping around the surface of cellulose which inhibits the decomposition of cellulose, thus leads to a decrease in the production of anhydrous sugars. On the other hand, the cellulose derived volatiles act as an H-donor that stabilizes the lignin derived compounds (e.g. guaiacols and syringols), which act as an H-acceptor via O-CH_3 homolysis to produce phenols and methane[198]. The interaction of hemicellulose-cellulose could be mitigated or eliminated and the interaction of cellulose-lignin could be promoted by torrefaction pretreatment which removes most hemicellulose from the raw biomass[199] and concentrates cellulose and lignin as a result. This may explain the increase of anhydrous sugars and phenols in the pyrolysis product of switchgrass pretreated by torrefaction. By analyzing the volatile products of biomass torrefaction, previous studies [192, 199] have shown that hemicellulose and cellulose derived compounds such as acetic acids, hydroxyl ketones, furans and levoglucosan are the dominant while lignin derived compounds such as phenols, guaiacol and vanillin were negligible in the volatile product. Our finding further confirmed that chemical transformation during torrefaction process affects composition of pyrolysis products obtained from the torrefied biomass.

3.3.2.2. Effects of pyrolysis temperature

The composition of pyrolysis products obtained from both raw and torrefied switchgrass at elevated temperature (600 and 700 °C) were different from those obtained at pyrolysis temperature of 500 °C. The four most abundant groups (anhydrous sugars, furans, phenols and guaiacols) obtained at 500 °C pyrolysis were still dominant in the pyrolysis products at 600 and 700 °C. However, the content of aromatic compounds obtained at 500 °C pyrolysis temperature was lower than that obtained at the elevated pyrolysis temperatures (600 and 700 °C). As shown in Figure 3.2, the aromatics contents of raw switchgrass, switchgrass torrefied at 230 and 270°C

were 7.74, 4.77 and 9.98 area %, respectively at 600 °C, and then increased to 12.18 and 8.25

area at 700 °C, respectively. In addition, aromatics other than toluene such as benzene, xylenes,

and styrene were also detected (as shown in

Table 3.3 and Table 3.4). Other polymeric aromatic compounds such as naphthalenes

were also detected but in low concentration. The aromatics were mainly derived from

decomposition of lignin-derived oligomers such as guaiacols and syringols [156], and the

decomposition rate increased with increase in pyrolysis temperature. The guaiacols content for

raw switchgrass, switchgrass torrefied at 230 and 270 °C decreased from 15.10, 14.80, and 14.25

area % at 500 °C to 14.43, 12.48 and 5.20 area % at 600 °C, and further decreased to 8.73 and

9.80 area % at 700 °C. Similar decreasing trend was also observed for syringols. On the contrary,

the phenols in switchgrass pyrolysis products of raw and torrefied at 230 °C increased from 5.59

and 7.92 area % at 500 °C to 16.54 and 17.06 area % at 600 °C and further increased to 17.32 and

21.34 area % at 700 °C, respectively. The conversion path way of lignin during pyrolysis includes

three processes[112, 157]: depolymerization of lignin, conversion of lignin monomers into

guaiacols or syringols, conversion of guaiacols or syringols into simple phenols and aromatic compounds (Figure 3.4). Phenols are derived from either depolymerization of lignin or decomposition of lignin oligomers such as guaiacols [112], and these reactions are highly enhanced at elevated temperature.
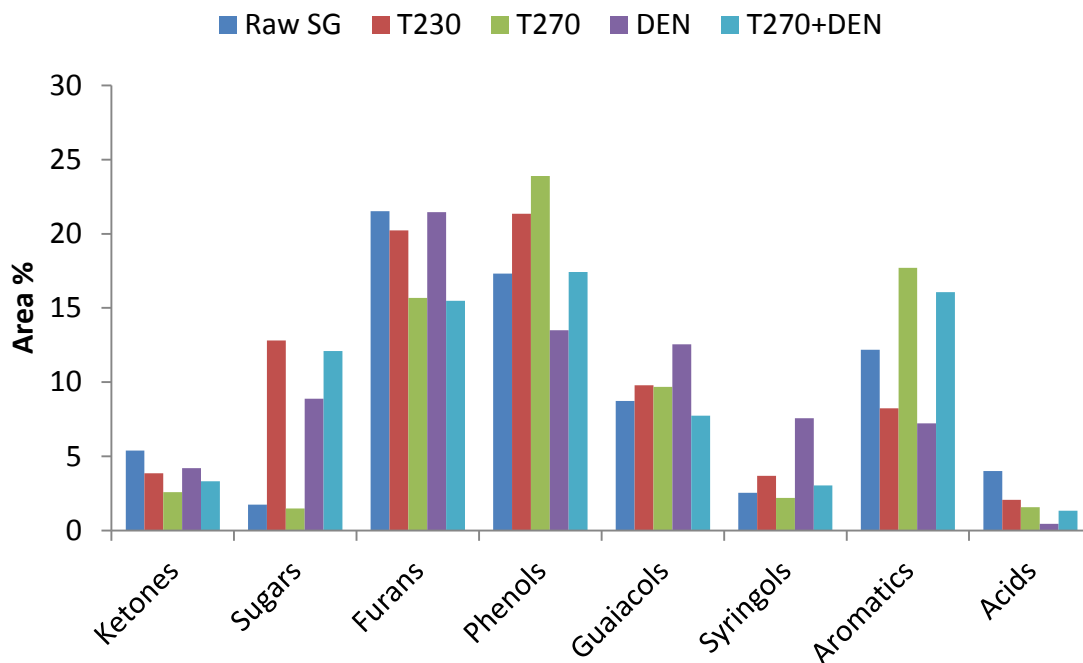
Figure 3.3 Product distribution of raw and pretreated switchgrass pyrolyzed at 700 °C.

Table 3.4 Pyrolysis products of raw and torrefied switchgrass obtained at 700 ºC[a].

Chemicals	Group	Raw SG	T230	T270	DEN	T270+DEN
		Cellulose/Hemicellulose derived compounds (Area %)				
Benzofuran, 2,3-dihydro-	Furans	10.71	6.30	3.13	9.69	3.81
Furfural	Furans	3.82	2.94	-	3.17	-
Furan, 2-methyl-	Furans	-	-	2.80	-	2.41
Furan, 2,5-dimethyl-	Furans	-	-	2.23	-	2.12
2-Furancarboxaldehyde, 5-methyl-	Furans	1.71	1.63	1.06	1.17	1.61
2(3H)-Furanone, 5-methyl-	Furans	-	2.46	1.78	1.59	-
5-Hydroxymethylfurfural	Furans	-	1.39	1.21	-	-
2-Furanmethanol	Furans	-	1.22	-	1.33	-
Acetic acid	Acid	4.01	2.07	1.58	-	1.33
D-Allose	Sugars	-	5.78	-	2.82	3.61
.beta.-D-Glucopyranose, 1,6-anhydro-	Sugars	1.05	6.62	-	4.94	3.55
2-Cyclopenten-1-one, 2-hydroxy-3-methyl-	Ketones	1.08	-	1.30	1.13	1.00

1,2-Cyclopentanedione	Ketones	1.97	1.36	-	-	1.69
	Lignin derived compounds (Area %)					
Phenol	Phenols	2.99	2.83	5.01	2.03	3.52
p-Cresol	Phenols	2.95	-	-	-	3.72
Catechol	Phenols	3.90	4.44	3.20	2.80	2.58
Phenol, 2-methyl-	Phenols	1.24	1.02	2.05	2.01	1.43
Phenol, 4-ethyl-	Phenols	1.44	1.46	1.40	-	1.10
Phenol, 2,4-dimethyl-	Phenols	1.19	1.17	1.72	-	1.40
1,2-Benzenediol, 3-methyl-	Phenols	1.64	1.89	-	-	-
1,2-Benzenediol, 4-methyl-	Phenols	2.29	2.76	1.39	1.50	-
2-Methoxy-4-vinylphenol	Guaiacols	4.45	3.79	2.25	6.37	2.35
Creosol	Guaiacols	-	2.57	1.89	1.81	1.08
Phenol, 2-methoxy-	Guaiacols	-	1.47	1.78	1.44	1.28
Phenol, 2,6-dimethoxy-	Syringols	1.37	2.07	1.72	2.04	1.18
Toluene	Aromatics	3.80	3.15	4.30	2.97	3.86
Benzene	Aromatics	2.55	1.61	3.49	-	3.07
Xylene	Aromatics	1.24	1.16	1.42	-	-
Styrene	Aromatics	1.28	-	1.78	-	1.22

[a] "-" means the relative peak area percentage of the detected compound is less than 1 %.

The content of anhydrous sugars in pyrolysis products of raw switchgrass, switchgrass torrefied at 230 and 270 °C obtained at 600 °C and 700 °C decreased significantly compared to those obtained at 500 °C. In detail, the content of dominant anhydrous sugar compound, levoglucosan obtained from pyrolysis of raw SG dropped from 5.96 to 2.38 and then to 1.05 area % when pyrolysis temperature increased from 500 to 700 °C. On the contrary, furans, increased with increase in pyrolysis temperature. This was also noticeable when comparing the content of typical furan compound, such as 1, 3-dihydro-benzofuran at the three pyrolysis temperatures. Numerous efforts have been done to investigate the mechanism of cellulose pyrolysis [160, 174, 200, 201]. Basically, cellulose first decomposes into oligosaccharides [202], known as active cellulose and then further degrades into anhydrous monosaccharides such as levoglucosan and D-Allose, and these monosaccharides can further transform by dehydration, decarboxylation or decarbonylation to form furans or fragment to form simpler linear carbonyl compound such as hydroxyacetaldehyde. Levoglucosan is considered an important pyrolytic product, which can be either utilized in organic synthesis or hydrolyzed into glucose for bioethanol production [203]. The maximum yield of levoglucosan reported in the literature was 40 wt % using pure cellulose

as the substrate [204], however, yield from pyrolysis of lignocellulosic biomass is expected to be much lower due to the catalytic effect of inorganic metals [203].
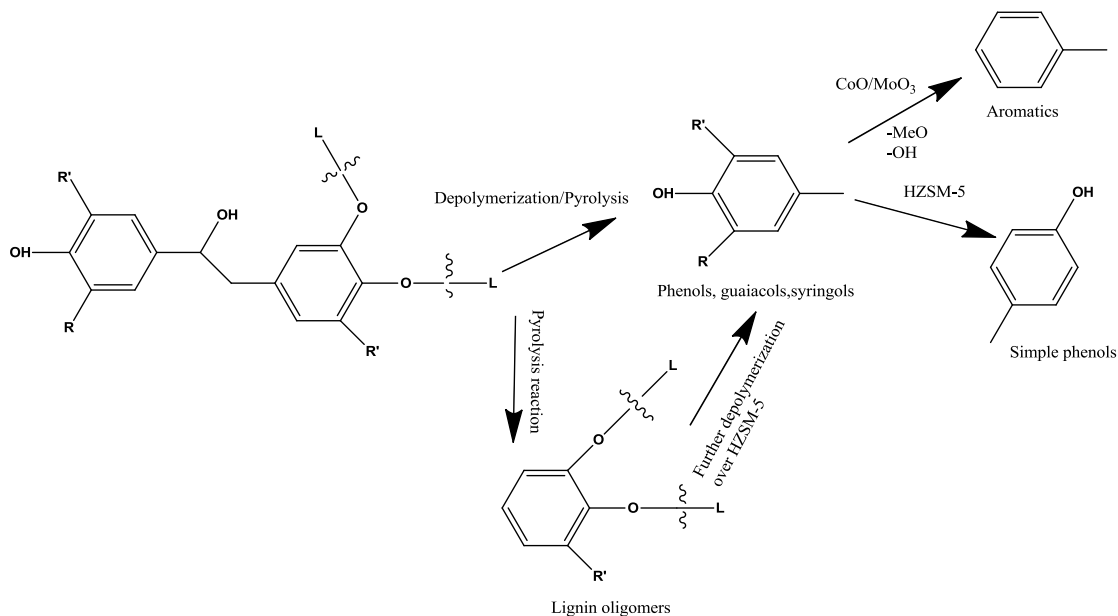
Figure 3.4 The conversion pathway of lignin catalytic fast pyrolysis. Adapted with modification from [27]

3.3.2.3. Effect of densification

By comparing compositions of pyrolysis products obtained from raw switchgrass, densified switchgrass, switchgrass torrefied at 270 °C and switchgrass pretreated by combined torrefaction and densification at 500 ℃ pyrolysis, it can be seen that the yield of anhydrous sugars decreased significantly due to densification, i.e. the anhydrous sugars obtained from densified switchgrass dropped from 11.71 to 2.41 area % compared to those obtained from raw switchgrass. However, the sugar content increased after densification at 600 and 700 °C pyrolysis. On the other hand, furans content of densified and torrefied-densified switchgrass increased to 25.66 and 19.37 area % compared to those from non-densified samples which were observed at 15.14 and 16.28 area %. It should also be noticed that acetic acid content of densified and torrefied-densified switchgrass were 4.24 and 4.51 area %, respectively, which increased by 1.5 and 2 folds of that from non-densified switchgrass. In addition, cycloketones content also increased significanty due to densification. These results indicate that densification promoted the

depolymerization of hemicellulose and cellulose resulting in production of furans, cycloketones and ring-scission products such as acetic acids. Densification also mildly promoted production of lignin-derived compounds such as guaiacols and lowered yield of phenols. As can be observed from Figure 3.1, phenols content of densified and torrefied-densified switchgrass dropped to 4.88 and 11.56 area % from 5.59 and 13.23 area %, respectively. The guaiacols obtained from densified and torrefied-densified switchgrass increased to 16.63 and 16.11 area %, respectively, compared to that from non-densified switchgrass. The proximate and ultimate analysis indicated that densified swichgrass was insignificantly different to raw switchgrass. In addition, previous study [205] confirmed that densification process had no significantly impact on the chemical composition (cellulose, hemicellulose and lignin content) of raw switchgrass. The morphological analysis of pretreated switchgrass in our previous study[191] confirmed that the destruction of fibrous structure by shear force during the extrusion process led to the exposure of the interior structure. This variation may affect micro-scale heat and mass transfer during the pyrolysis, e.g. the decomposition may initiate from interior material rather than propagate from outer surface of the particles, thereby leading to the variation in the pyrolysis products.

The effect of pyrolysis temperature on the pyrolysis product obtained from densified switchgrass was very different from that obtained from torrefaction. As seen in Figure 3.1~Figure 3.3, the anhydrous sugars contents of densified switchgrass and switchgrass pretreated by combined torrefaction and densification increased significantly from 2.41, 8.40 to 8.89 and 12.10 area %, respectively, as the pyrolysis temperature increased from 500 to 700 °C. However, anhydrous sugars obtained from both pyrolysis of switchgrass torrefied at 230 and 270 ℃ decreased significantly as the pyrolysis temperature increased from 500 to 700 ℃, i.e. the anhydrous obtained from pyrolysis of switchgrass torrefied at 270 ℃ decreased from 19.19 to 6.92 and then further to 1.49 area %. Furans of densified switchgrass decreased from 25.66 to 20.25 area % when pyrolysis temperature increased from 500 to 600 °C, followed by a slight increase to 21.46 area % at 700 °C pyrolysis. Compared to densification, the furans obtained from

76

switchgrass torrefied at 230 ℃ increased consistently from 16.99 to 20.23 area % as the pyrolysis temperature increased from 500 to 700 °C. Phenols of densified switchgrass increased from 4.88 to 16.12 area % first as the pyrolysis temperature increased from 500 to 600 °C, followed by a decrease to 13.50 area %. As comparison to densification, the phenols obtained from pyrolysis of switchgrass torrefied at 230 °C increased consistently from 7.92 to 21.34 area % as the pyrolysis temperature increased from 500 to 700 °C. Guaiacols compound of densified switchgrass decreased from 16.63 to 12.13 area % as the pyrolysis temperature increased from 500 to 600 °C, and no significant variation was observed at 700 °C. By contrast, the guaiacols obtained from pyrolysis of switchgrass torrefied at 230 °C decreased consistently from 14.80 to 9.80 area % as the pyrolysis temperature increased from 500 to 700 °C. The aromatic compounds increased consistently as the pyrolysis temperature increased for switchgrass pretreated by either torrefaction or densification. For both densified switchgrass and switchgrass pretreated by torrefaction and densification, aromatics increased from 0.22 and 2.25 to 7.22 and 16.07, respectively. The highest aromatics yield was 17.70 area % derived from 700 ℃ pyrolysis of switchgrass torrefied at 270 °C.

3.4. Conclusions

The effects of torrefaction and densification on pyrolysis products of switchgrass were investigated. Torrefied switchgrass produced a higher quantity of anhydrous sugars and phenols than raw switchgrass. The content of anhydrous sugars and phenols also increased as the temperature of torrefaction increased. Densification enhanced the depolymerization of cellulose and hemicellulose thus promoted the production of small molecules such as furans, ketones and acids. Higher pyrolysis temperature favored decomposition of lignin and anhydrous sugars, resulting in increased yields of phenols, aromatics and furans.

CHAPTER IV

INTEGRATION OF BIOMASS CATALYTIC PYROLYSIS AND METHANE

AROMATIZATION OVER MO/HZSM-5 CATALYST

Abstract: The development of an effective process to convert bio-oil into intermediate platforms that are compatible with the existing refinery infrastructure is highly needed. To overcome the high cost of hydrogen consumption in conventional bio-oil upgrading processes, this paper reports a novel process that converts three major biomass constituents (cellulose, hemicellulose and lignin) directly into liquid fuels via pyrolysis in the presence of methane over molybdenum impregnated HZSM-5 catalysts. The carbon yield of total aromatics from lignin increased from 12.80 to 15.13 % when pyrolysis atmosphere switched from helium to methane in presence of HZSM-5 support. However, methane was not effective in improving the aromatics yield from cellulose and hemicellulose in presence of Mo-modified HZSM-5 catalysts. The molybdenum impregnated catalyst was found to promote deoxygenation of lignin-derived phenols. The carbon yield of polyaromatics from lignin was 5.47 % in presence of HZSM-5 support under methane, compared to 2.61 % that obtained in presence of $Mo_2C/HZSM-5$.

4.1. Introduction

Lignocellulose biomass is the only carbon-based renewable resource that has the potential to alleviate our dependence on fossil fuels and mitigate global warming and other environmental issues associated with the use of fossil fuels [206]. Fast pyrolysis has been considered to be a promising and sustainable route to convert solid biomass into liquid fuel. In pyrolysis, biomass is rapidly decomposed into vapors, aerosols and solid char thermochemically under an inert atmosphere in a mild temperature range (400~600 ℃), followed by a rapid condensation to recover a liquid product, which is 60-75 wt % of the biomass feed [171, 207, 208]. Bio-oil can be combusted as a fuel in a burner for power generation, or used in engines or turbines [14]. Bio-oil can also be further upgraded to transportation fuels and chemicals that are currently produced by petroleum refineries [3, 14]. However, bio-oil suffers from several negative attributes associated with its high oxygen content, such as low energy content, high viscosity, corrosiveness, thermal instability, and immiscibility with petroleum fuels. These negative attributes of bio-oil pose significant challenges to the facilities in refineries and end users for effectively utilizing bio-oil in existing infrastructure [22, 31]. Therefore, there is a critical need for developing methods to enhance bio-oil properties.

One of the most common bio-oil upgrading techniques is deoxygenation. Most deoxygenation methods require heterogeneous catalysts to initiate reactions such as dehydration, decarboxylation, decarbonylation and hydrodeoxygenation, that convert the raw bio-oil into a deoxygenated product [209]. However, these upgrading processes typically require high pressure of hydrogen and consist of multiple steps that increase process complexity and cost. Therefore, catalytic fast pyrolysis (CFP), which combines biomass pyrolysis and catalytic upgrading in a single reactor system, has emerged as a more efficient and economical process [3, 210]. Extensive studies have been conducted to improve the yield of targeted petroleum chemicals (e.g. benzene, toluene, ethylbenzene and xylenes, collectively known as BTEX) using zeolite catalysts [90, 211-216]. The selectivity of these petrochemicals during CFP increased with increasing feed

H/C$_{eff}$ ratio, which is defined in   Equation **4.1**, where H, C, and O

are the mole percentages of hydrogen, carbon and oxygen, respectively, in the feed [209, 210,

217]. In addition, catalyst deactivation rate decreased with increasing H/C$_{eff}$ ratio [210].

$$\frac{H}{C_{eff}} = \frac{H - 2O}{C}$$ Equation 4.1

The H/C$_{eff}$ ratio of biomass varies from 0 to 0.3 making it not suitable for production of

petrochemicals due to rapid deactivation of zeolites [210]. To correct for the low H/C$_{eff}$, a

hydrogen-rich donor can be co-fed into the reactor with the biomass to increase the overall H/C$_{eff}$

ratio of the feed. A number of studies [210, 218, 219] have demonstrated that co-feeding alcohols

such as methanol and propanol can significantly improve the petrochemicals yields due to a

synergistic effect of alcohols and pyrolysis vapors.

Methane, the major component of natural gas, can be an ideal hydrogen donor for CFP of

biomass for petrochemicals production due to its low cost and high H/C$_{eff}$ of 4. Typically,

conversion of methane into higher hydrocarbons requires multiple steps: first, methane is

converted into synthesis gases (H$_2$ and CO) via steam reforming or partial oxidation, and then

further converted into hydrocarbon fuels and chemicals via Fischer-Tropsch (FT) synthesis. This

reaction route is highly energy intensive due to the need for high reaction temperature and

pressures. Furthermore, FT products have wide chain lengths that require further cracking and

aromatization [220]. Therefore, one-step methane dehydroaromatization methodologies that

utilize metal modified HZSM-5 catalysts for the production of selected aromatic hydrocarbons

have been the focus of recent studies [220-223]. The reaction mechanism for methane

aromatization with metal zeolites is believed to occur in two steps as indicated in Figure 4.1.

Initially, methane reacts to form intermediate radicals such as CH$_x$ (x<4), H·, C$_2$H$_y^+$ (y=3, 5) on

metal sites, and then these radicals oligomerize into olefins or aromatics on the acidic sites of the

zeolite [220, 224]. Thermodynamic analysis [220] showed an increasing trend for coke deposition

as the methane conversion increases. Hence, deposition of carbon on the catalyst is thought to be

a key challenge in methane aromatization. To overcome catalyst deactivation due to the carbon deposition, oxygenates (e.g. CO, CO_2, O_2, and NO) were co-fed during the methane aromatization process [225-227]. Several studies also investigated the impacts of co-feeding oxygenates and coals in methane aromatization. By co-feeding methane with CO_2, acetic acid and formic acid mixtures onto a Mo/HZSM-5 catalyst, Bedard et al. [228] and concluded that methane dehydroaromatization was highly dependent on thermodynamic equilibrium, while the addition of oxygenates had no effect on the net rate of benzene synthesis. Jin et al. [229] conducted coal pyrolysis over Mo/HZSM-5 catalyst under methane and hydrogen atmosphere, and found that the total liquid yield under methane atmosphere was significantly higher than that under hydrogen atmosphere. Liu and Wang et al. [230, 231] found that by integrating coal pyrolysis with CO_2 reforming of methane, the liquid yield increased by 60 and 80 wt. % as compared to the liquid yield obtained by coal pyrolysis under nitrogen and hydrogen, respectively. Additionally, by using deuterated methane CD_4, they concluded that the free radicals released from coal cracking were stabilized by the intermediates, such as CH_x (x<4), H· and $C_2H_y^+$ (y=3, 5) produced from CO_2 reforming of methane.
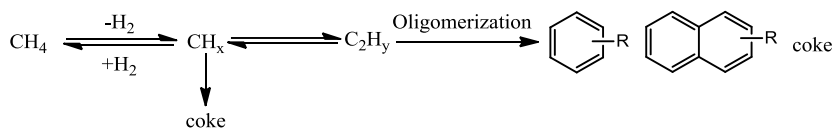
Figure 4.1 Reaction mechanisms for methane aromatization [220].

The hypothesis of this study was that catalytic deoxygenation of biomass-derived vapors and methane aromatization can be combined to maximize the yield of hydrocarbons. However, before studying reaction mechanisms of aromatics production through co-pyrolysis of biomass and methane over HZSM-5 catalyst, it was imperative to understand the behavior of the three major biomass components (i.e. cellulose, hemicellulose and lignin) and their individual contributions to the targeted hydrocarbons. The reaction pathways for each of these components during CFP have been well studied [156, 212, 214, 232]. Carlson et al. [212] developed a four-

step reaction pathway for conversion of cellulose into aromatics over HZSM-5 catalysts. In the first step, cellulose thermally decomposes into anhydrous sugars and other oxygenates. Second step involves dehydration of the anhydrous sugars to form furans in presence of catalyst. In the third step, furans convert into olefins inside the acid pores of zeolite through a series of decarboxylation, dehydration and decarbonylation reactions. Finally, the olefins oligomerize into aromatics. A similar reaction mechanism [157] was proposed for hemicellulose, and furans were thought to be the common intermediates derived from thermal degradation of hemicellulose and cellulose. Mullen et al. [214] hypothesized that lignin depolymerizes into small olefins that can repolymerize into aromatics over HZSM-5 catalysts. Phenol was found to be the end product of deoxygenation of lignin-derived monomers, and could not be further reduced into oxygen-free aromatics because of rapid catalyst coking due to diffusion into catalyst channels. However, the impacts of methane on the pyrolysis reaction pathways of cellulose, hemicellulose and lignin are not available in literature.

The objective of this study was to investigate pyrolysis of cellulose, hemicellulose and lignin (major biomass constituents) over two Mo-modified HZSM-5 catalysts (MoO_3/HZSM-5 and Mo_2C/HZSM-5) in methane atmosphere. MoO_3 and Mo_2C were selected as the Mo species because they have shown difference in reactivity towards methane activation [233].

4.2. Materials and methods

4.2.1. Biomass model components

Avicel PH 105 Cellulose (FMC Biopolymer, Philadelphia), beech wood xylan (Sigma Aldrich, St. Louis) and Kraft lignin (Sigma Aldrich, St. Louis) were used as models of cellulose, hemicellulose and lignin, respectively. All the biomass models were used as received without any further treatment. Results of elemental analysis of the feedstock are listed in Table 4.1.

Table 4.1 Elemental analysis of the feedstock as received basis.

Feedstock	Elemental analysis (wt. %)			
	C	H	N	O
Cellulose	42.09	6.32	0.18	51.51
Hemicellulose	39.79	6.09	0.22	51.32
Lignin	61.59	5.63	0.89	30.7

4.2.2. Catalysts preparation

ZSM-5 zeolites (Si to Al molar ratio of 30 and nominal surface area of 425 m^2/g) in the

ammonium (Alfa Aesar Company, VA 20191, USA) were calcined in air at 550 ºC for 4 h to

make protonated form of HZSM-5. The precursor for Mo was $(NH_4)_6Mo_7O_{24} \cdot 4H_2O$ (Sigma

Aldrich, St. Louis, USA), and was purified by recrystallization from water. The Mo species were

impregnated on the HZSM-5 support using wet impregnation method. 1 g of HZSM-5 support

was degassed under vacuum for 24 h and then was impregnated with a solution containing

ammonium heptamolybdate (3.5 wt %) and ammonia (1.4 wt %) for 16 h at room temperature.

Ammonia was added to prevent the ammonium heptamolybdate from precipitating within the

HZSM-5 to form molybdic acid. After 16 h, the mixture was centrifuged to separate the solid.

The supernatant liquid was then decanted and the centrifuge tubes were placed in a -25˚C freezer

for 5 h to freeze the liquid within the pores of the zeolite. The samples were then freeze-dried on

a lyophilizer for 24 h. The resulting powder was then calcined in air at 550 ºC for 4 h to yield

MoO_3/HZSM-5. The synthesis of Mo_2C/HZSM-5 catalyst followed the same procedure as

MoO_3/HZSM-5 but used a different precursor solution as described by Wang et al [234]. This

precursor solution contained the same concentrations of ammonia heptamolybdate and ammonia

but also contained 3.8 % by weight of hexamethylenetetramine (HMT). Unlike the MoO_3/HZSM-

5, the Mo_2C/HZSM-5 was calcined at 700 °C for 2 h in a flow of helium.

4.2.3. Catalysts characterization

Powder X-ray diffraction (XRD, Bruker D8-A25-ADVANCE diffractometer) was used

to characterize the crystallinity of the metal impregnated catalysts. The test was performed using

Cu Kα radiation at 40 kV and 100 mA at a continuous scanning at step size of 0.02º, 0.5 s per step over a scanning range from 5° to 70° (2θ). Data analysis was carried out with MDI Jade 6.5 software (Materials Data Inc., Livermore, CA, USA).

The pore structures of metal impregnated catalysts were determined by isothermal nitrogen adsorption at 77 K using a surface area analyzer (Autosorb-1C, Quantachrome, Boynton Beach, FL, USA). Prior to the analysis, catalysts were degased at 300 ºC for 12 hrs. The surface area was calculated according to Brunauer-Emmett-Teller (BET) theory. External surface area, micropore area, and pore volume were derived using a t-plot method [235]. The amount of Mo in the catalysts was measured using inductively coupled plasma-atomic emission spectroscopy (ICP-AES; ThermoScientific, Waltham, MA, USA).

The surface morphology was characterized by scanning electron microscope (SEM; FEI Quanta 600, Hillsboro, OR, USA). To measure the metal dispersion on the catalysts, energy dispersive X-ray spectroscope (EDS; Evex EDS, Belle Mead, NJ, USA) with X-ray dot mapping was used.

4.2.4. Pyrolysis-GC-MS

Catalytic pyrolysis experiments were carried out in a commercial micro pyrolyzer (Pyroprobe model 5200, CDS Analytical Inc., Oxford, PA). The detailed experimental procedure has been described in a previous study [236]. About 0.3 mg of feedstock and 3 mg of catalysts were loaded into a quartz tube and separated into two layers with quartz wool as shown in Figure 4.2. The samples were heated to 700 ºC at a filament heating rate of 1000 °C/s and then held at 700 °C for 90 s. The volatiles produced were analyzed using a gas chromatography/mass spectrometry (Agilent 7890GC/5975MS) system connected to the pyroprobe by a transfer line. The chromatographic separation was performed using a DB-5 capillary column (30 mL×0.32mm I.D., 0.25 μm film thickness). The GC oven was held at 40 °C for 4 min, and then increased to 280 °C at a ramping rate of 5 °C/min and held for 20 min. The injector temperature was kept at

85

250 °C, and the split ratio was set to 30:1. Helium (purity: 99.99%) was used as the carrier gas at a flow rate of 1 mL/min.
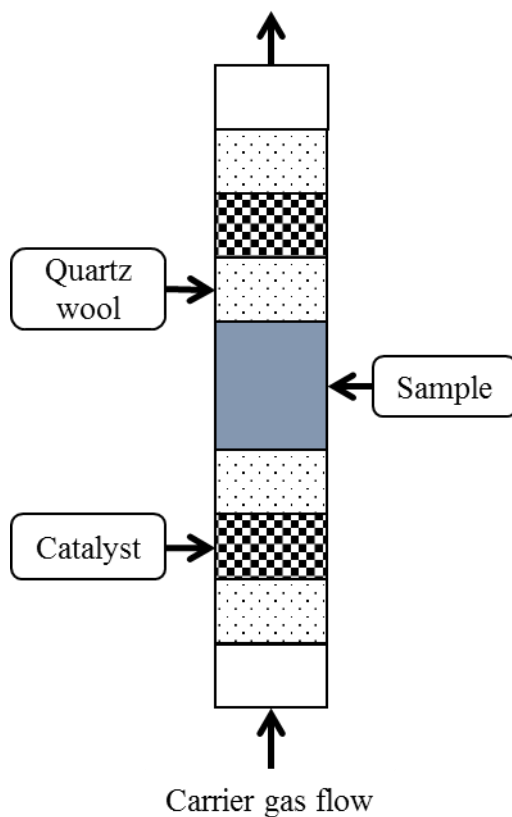
Figure 4.2 Schematic diagram of sample loading.

The compounds were identified by comparing the peaks with National Institute of Standards and Technology (NIST) mass spectral library. Quantification of targeted compounds was performed by calibrating with known concentrations of working standards into GC/MS. The carbon yield and aromatics selectivity was calculated using   Equation **4.2** and Equation 4.3.

$$Carbon\ yield = \frac{Moles\ of\ carbon\ in\ specific\ species}{Moles\ of\ carbon\ in\ biomass\ models} \qquad \text{Equation 4.2}$$

$$Aromatics\ selectivity = \frac{Moles\ of\ carbon\ in\ specific\ aromatic\ species}{Moles\ of\ carbon\ in\ all\ quantified\ aromatic\ species} \qquad \text{Equation 4.3}$$

4.2.5. Experimental design

A full factorial experimental design was used with three independent parameters: two pyrolysis atmospheres (helium and methane), three biomass components (cellulose, hemicellulose and lignin) and three impregnated metal precursors (None, MoO_3 and Mo_2C). All the experiments were run in triplicate. The average and standard deviation were used to compare carbon yields and selectivity.

4.3. Results and discussion

4.3.1. Catalysts characterization

The phases present in HZSM-5 and Mo modified HZSM-5 catalysts were determined by XRD technique as shown in Figure 4.3. The main diffraction peaks of HZSM-5 were present at $2\theta=7.96°$ (011), 8.87° (200), 23.11° (051), 23.96° (033), and 24.43° (313) and matched those reported in typical zeolite structure [237, 238]. The XRD patterns of MoO_3/HZSM-5 and Mo_2C/HZSM-5 were similar to that of HZSM-5 indicating that the crystal structure of HZSM-5 was retained after impregnating with Mo species. However, no Mo-containing crystalline phases were observed in the patterns of the metal modified catalysts. This may be attributed to either low loading of Mo, as shown in the ICP (Table 4.3), or formation of amorphous or highly nanocrystalline phase. The relative degree of crystallinity of the catalysts, the ratio of integrated peak areas of the samples over that of reference sample in the range of $2\theta=22.5$ to 25°, was calculated according to ASTM standard D5758-01 [239]. For this study, three major diffraction peaks at the positions of 23.11° (051), 23.96° (033), and 24.43° (313) were used to determine the degree of crystallinity. HZSM-5 support was used as the reference sample, since it exhibited the highest intensities at these positions. Table 4.2 summarizes the crystallinity and the average crystallite size obtained from the major diffraction peaks of all three catalysts. Crystallinities of

both Mo-modified catalysts were lower than that of the HZSM-5 support. The decrease of crystallinity was due to the dispersion of Mo species in the support.

The catalysts porous structure, BET surface area, pore volume and average pore size as determined from nitrogen isothermal adsorption at 77 K are shown in Table 4.3 and Figure 4.4. All the catalysts showed a rapid increase of adsorbed volume of nitrogen at low relative pressure (less than 10^{-3}) followed by a slow increase, indicating that adsorption occurred mainly on micropores. The nitrogen isotherms of HZSM-5 support and MoO_3/HZSM-5 were type IV in the Brunauer classification, corresponding to the narrow hysteresis loop at $P/P_0=0.5\sim0.9$ (shown on the isotherm plot, Figure 4.4). However, the Mo_2C/HZSM-5 exhibited a type I isotherm with no observable hysteresis loop in its adsorption isotherm. BET surface area (480 m^2/g) of HZSM-5 support was higher than the nominal specific surface area (425 m^2/g) provided by the manufacturer (Table 4.3), which is due to calcination. Micropore area accounted for up to 70 % of total surface area in both the HZSM-5 support and the Mo-modified catalysts, and this further confirmed the dominance of micropores in all of the catalysts. The incorporation of Mo species led to a slight decrease in the BET surface area and micropore volume of MoO_3/HZSM-5 and Mo_2C/HZSM-5. The decrease in BET area and micropore volume can be attributed to deposition of the Mo species within the channels of the HZSM-5 support.
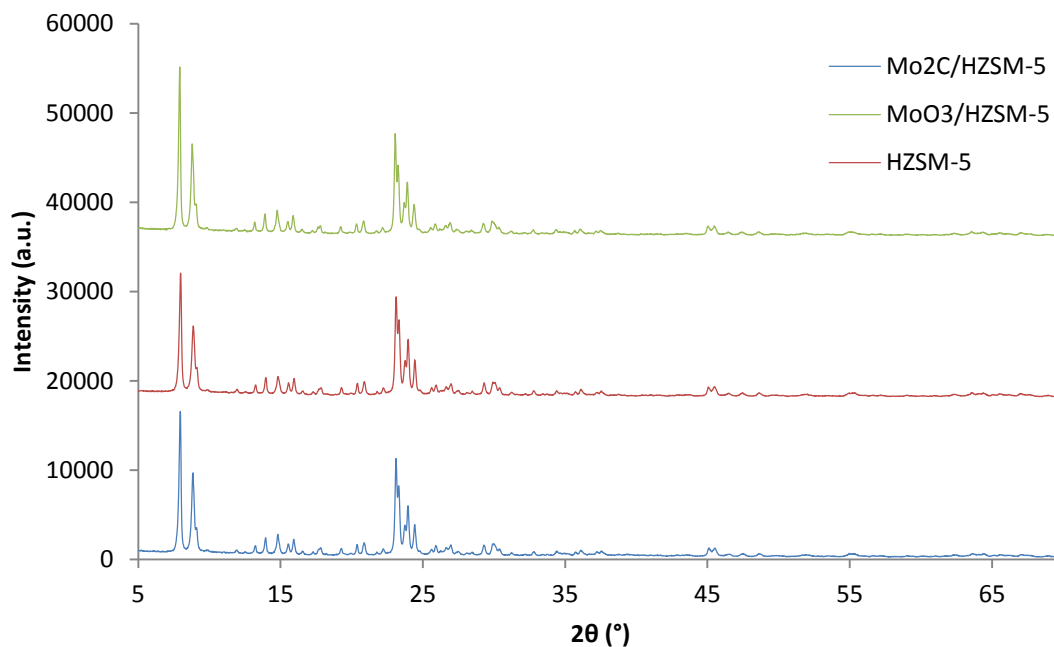
Figure 4.3 XRD patterns of catalysts.

Table 4.2 Relative crystallinity and crystallite sizes of catalysts.

Catalysts	Crystallinity (%)	[a]Average crystallite size (nm)
HZSM-5	100	[b]52.7±0.6
MoO₃/HZSM-5	92.45	59.9±0.9
Mo₂C/HZSM-5	92.74	58.2±0.8

[a]Average crystallite size estimated from the major diffraction peaks at position of 7.96° (011), 8.87° (200), 23.11° (051), 23.96° (033), and 24.43° (313).
[b]Value reported as the mean ± estimated standard deviation.
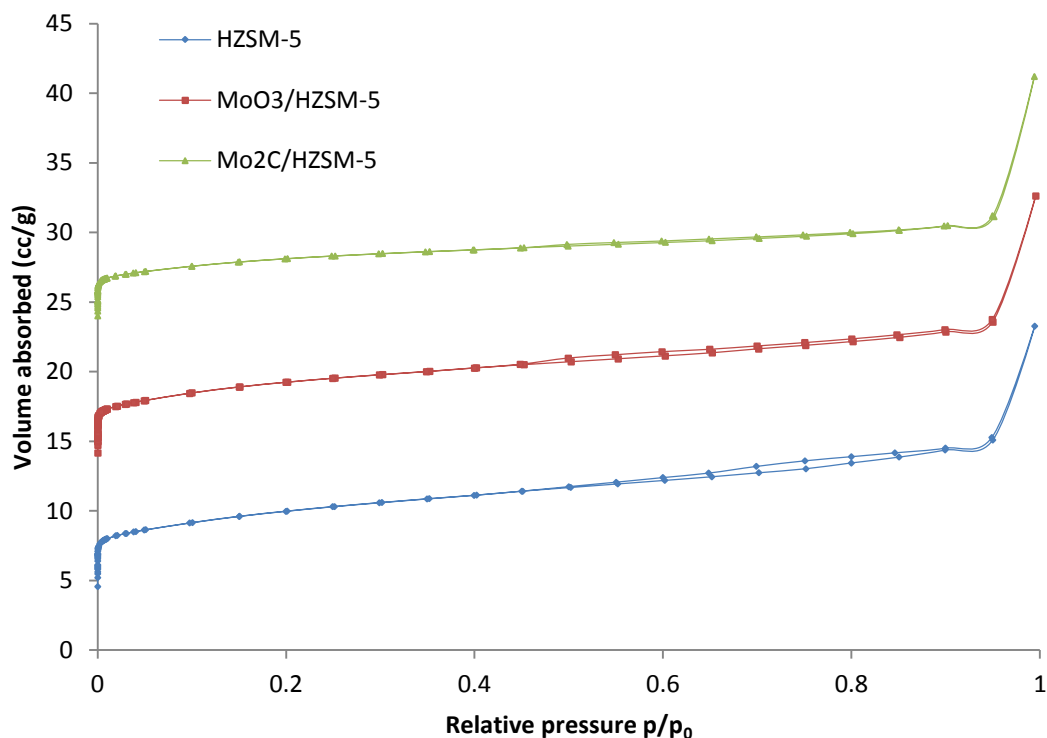
Figure 4.4 N_2 isothermal adsorption plot of catalysts.

Table 4.3 BET surface area, pore volume, pore size, and Mo content of the catalysts.

Catalysts	BET surface area (m^2/g)	Micropore area (m^2/g)	External surface area (m^2/g)	Micropore volume (cc/g)	Total volume (cc/g)	Average pore size (nm)	Mo content by ICP (wt %)
$Mo_2C/HZSM-5$	467	344	122	0.115	0.468	4.03	2.50
$MoO_3/HZSM-5$	457	334	122	0.113	0.439	3.92	2.43
HZSM-5	479	345	134	0.119	0.448	3.69	N/A

The morphologies of HZSM-5 support and the Mo-modified catalysts are shown in Fig. 4. The HZSM-5 support was an agglomeration of cubic or spherical particles within sizes ranging from 38.3 to 185.2 nm (Figure 4.5 (a, d)). The standard cubic or spherical crystals that were clearly observed in HZSM-5 are difficult to identify in the microstructure of $MoO_3/HZSM-5$ (Figure 4.5 (b)) and $Mo_2C/HZSM-5$ (Figure 4.5 (c)). Both of these catalysts exhibited compact clusters that were made up of crystals with irregular geometrical profile. The images obtained

from X-ray mapping (Figure 4.6) show that the major elements, such as Mo, Si, and Al in the

Mo-modified catalysts were dispersed uniformly throughout the imaged microstructures. The

EDS results (Table 4.4) indicate that both MoO_3/HZSM-5 and Mo_2C/HZSM-5 had similar Mo

content.

(a)

(b)

(c)

(d)
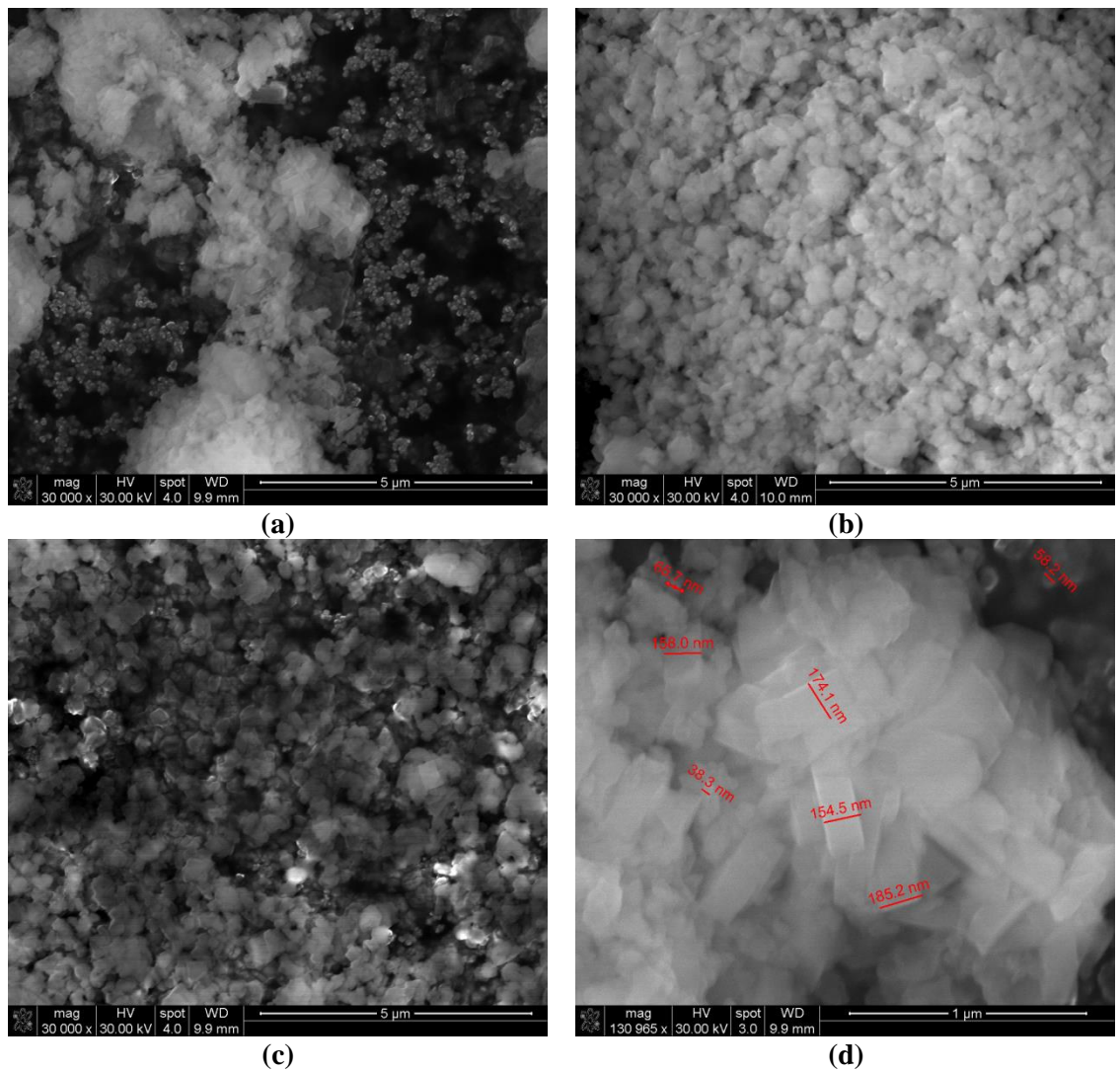
Figure 4.5 SEM images of catalysts: (a) HZSM-5, (b) MoO₃/HZSM-5, (c) Mo₂C/HZSM-5, (d) particle size of HZSM-5.

(a-1)

(b-1)

(a-2)

(b-2)

(a-3)

(b-3)

(a-4)   (b-4)
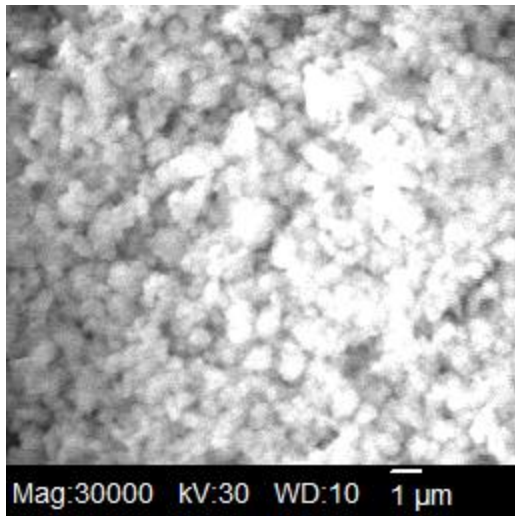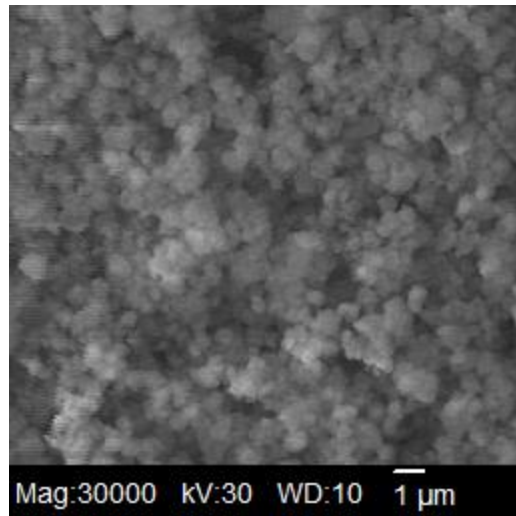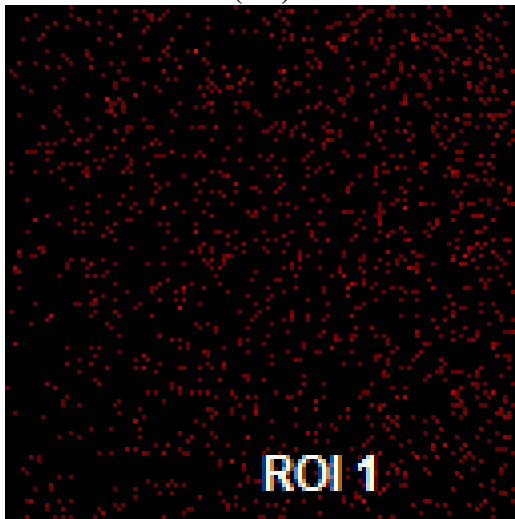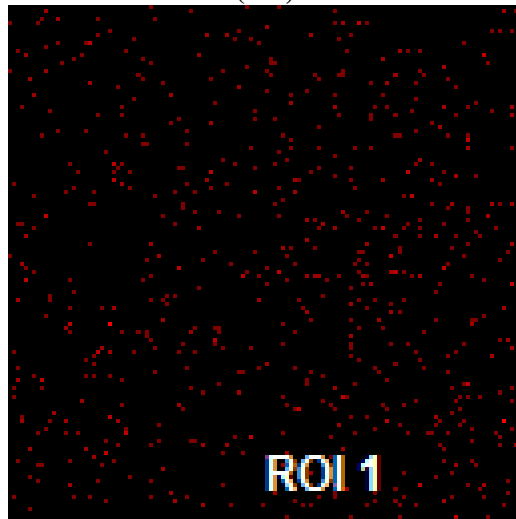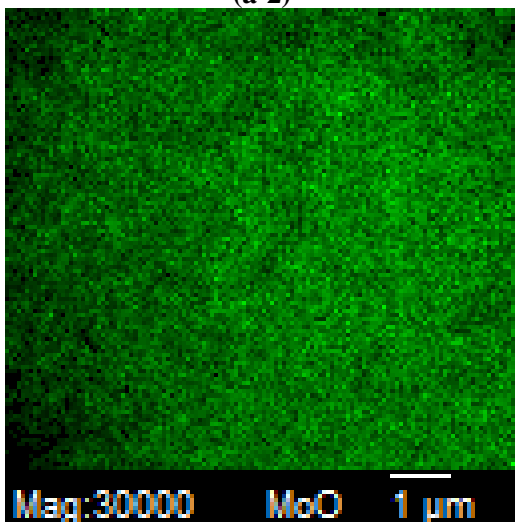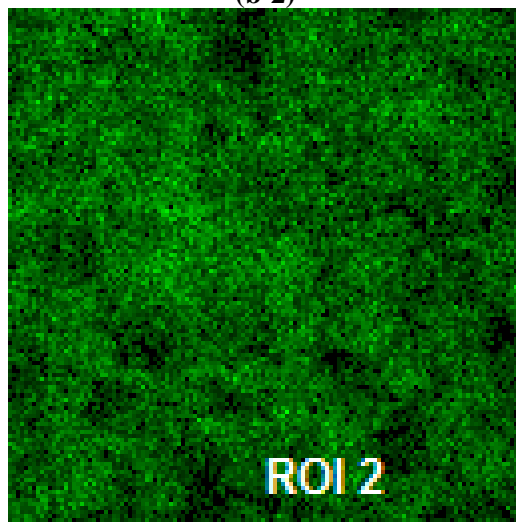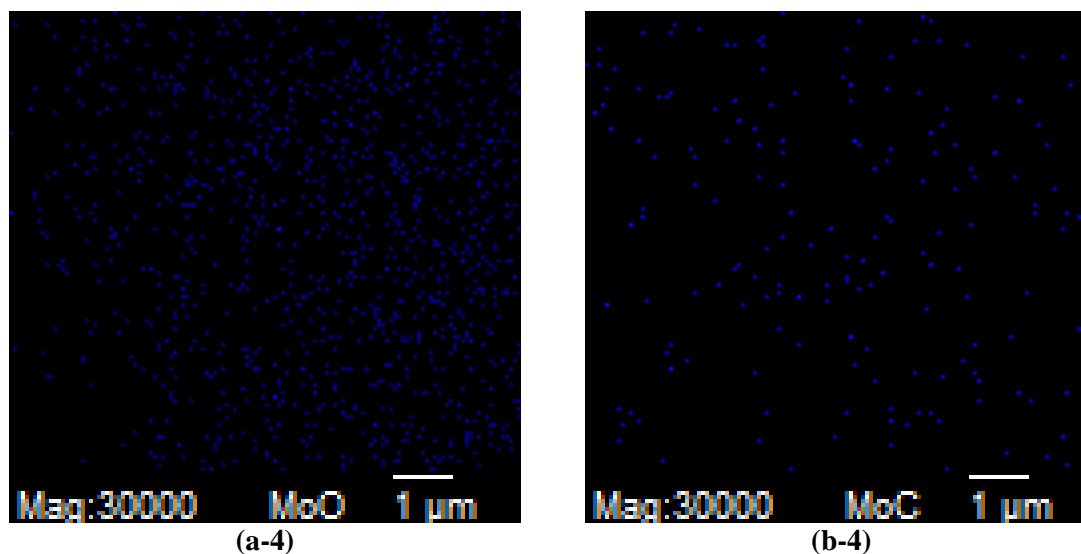
Figure 4.6 X-ray mapping of elemental composition within the selected microstructure of (a) MoO₃/HZSM-5 and (b) Mo₂C/HZSM-5, Red: Mo; Green: Si; Blue: Al.

Table 4.4 Relative contents of Mo, Si and Al within selected microstructure in Figure 4.6.

Catalysts	Mo (wt. %)	Si (wt. %)	Al (wt. %)
MoO₃/HZSM-5	23.56	72.84	3.60
Mo₂C/HZSM-5	24.05	71.33	4.63

4.3.2. Catalyst activity tests

The products from catalytic pyrolysis of cellulose, hemicellulose and lignin in the presence of HZSM-5 supported catalysts were mostly aromatic hydrocarbons (all products listed in Table 4.5). These products were grouped into (a) simple aromatics, such as BTEX, (b) benzene derivatives, such as alkybenzene, indanes and indenes, and (c) polyaromatics, such as naphthalenes and phenanthrene and (d) oxygenates, such as phenols and methoxyphenols. There was no difference in the compounds from cellulose and hemicellulose since they were both polysaccharides. Simple phenols were the only oxygenates detectable in the products of cellulose and hemicellulose. Methoxyphenols (e.g. 2-methylphenol, creosol, etc.) and catechol were only identified in the products derived from lignin. The reaction atmosphere (helium or methane) did not affect the compounds produced during catalytic pyrolysis but changes in their relative concentrations were observed.

Table 4.5 List of compounds identified from catalytic pyrolysis products (CE=Cellulose, HC=Hemicellulose, LN=Lignin, same for other parts of this paper).

Compound	Category	CE	HC	LN
Benzene	BTEX	[a]*	*	*
Toluene	BTEX	*	*	*
Ethylbenzene	BTEX	*	*	*
Styrene	BTEX	*	*	*
p-Xylene	BTEX	*	*	*
o-Xylene	BTEX	*	*	*
Phenol	Oxygenates	*	*	*
Benzene, 1,2,3-trimethyl-	Benzene derivatives	*	*	*
Indane	Benzene derivatives	*	*	*
Indene	Benzene derivatives	*	*	*
Phenol, 2-methyl-	Oxygenates	*	*	*
p-Cresol	Oxygenates	*	*	*
Phenol, 2-methoxy-	Oxygenates			*
2-Methylindene	Benzene derivatives	*	*	*
1H-indene, 1-methyl-	Benzene derivatives	*	*	*
Naphthalene	Polyaromatics	*	*	*
Creosol	Oxygenates			*
Catechol	Oxygenates			*
Phenol, 4-ethyl-2-methoxy-	Oxygenates			*
Methylnaphthalene	Polyaromatics	*	*	*
2-Methoxy-4-vinylphenol	Oxygenates			*
Dimethylnaphthalene	Polyaromatics	*	*	*
Fluorene	Polyaromatics	*	*	*
Phenanthrene	Polyaromatics	*	*	*
Anthracene, 1-methyl-	Polyaromatics	*	*	*

[a]Compounds detected in the catalytic pyrolysis products of individual biomass constituent.

4.3.2.1. Catalytic pyrolysis of cellulose

Aromatic hydrocarbons were found to be the major products derived from cellulose, whereas the oxygenates were trivial (Table 4.6). The total carbon yield of aromatics varied across different HZSM-5 supported catalysts, with a low of 16.63±2.09% for MoO_3/HZSM-5 under inert atmosphere and a maximum of 35.00±4.37% for HZSM-5 under inert atmosphere (Table 4.6). Tukey`s multiple comparison showed that pyrolysis atmosphere (helium and methane) had no significant effect on the yield of individual aromatic groups and total aromatic hydrocarbons. ANOVA analysis revealed that the performance of the three HZSM-5 supported catalysts was different. MoO_3/HZSM-5 yielded the lowest amount of aromatic hydrocarbons, whereas HZSM-5 support yielded the highest amount of aromatics. However, the difference between HZSM-5 support and Mo_2C/HZSM-5 was not significant.

94

The tornado plot in Figure 4.7 shows the aromatics selectivity of products, namely benzene, toluene, ethylbenzene, *p/o*-Xylene, benzene derivatives and polyaromatics from cellulose under helium and methane atmospheres. It can be seen that all HZSM-5 supported catalysts have high selectivity (up to 70%) towards BTEX. Among all the aromatics, the selectivity for toluene was the highest for all of the catalysts, with a maximum of 32.87% with MoO_3/HZSM-5 under helium. The pyrolysis environment did not have significant impact on the selectivity for aromatic. However, the impacts of Mo impregnation on aromatics selectivity were noticeable. With MoO_3/HZSM-5, the selectivity for polyaromatics significantly decreased, whereas selectivities for the benzene and toluene increased significantly as compared for the other two HZSM-5 supported catalysts. Polyaromatics are commonly viewed as indicators for coke formation that may lead to catalyst deactivation during catalytic fast pyrolysis. By comparing aromatics yield and selectivity, it can be concluded that HZSM-5 deactivated during impregnation with MoO_3. Generally, there are three common reasons to account for catalyst deactivation: (1) poisoning of active sites by catalyst coking; (2) blockage of pores by catalyst coking; (3) reduction in number/strength of active sites [233]. In this case, MoO_3/HZSM-5 showed the lowest selectivity towards polyaromatics, indicating low tendency towards coking. Therefore, the low catalytic reactivity of MoO_3/HZSM-5 could be attributed to the reduction in acidity of HZSM-5 support during impregnation. To verify this assumption, the MoO_3/HZSM-5 catalyst was treated with a solution of nitric acid followed by calcination. After acidification, the catalytic reactivity was restored (data not shown).

Table 4.6 Carbon yield from catalytic pyrolysis of cellulose (wt. %) (He=Helium, Me=Methane,)[a].

| Trial | Aromatics | | | Total Aromatic HCs | Oxygenates |
	BTEX	Benzene derivatives	Polyaromatics		
He, HZSM-5	23.67±3.19[a]	4.29±0.43[a]	7.03±1.28[a]	35.00±4.37[a]	0.78±0.11[b]
Me, HZSM-5	23.70±3.40[a]	3.72±0.30[a,b]	7.04±0.44[a]	34.47±3.98[a]	0.75±0.23[b]
He, MoO_3/HZSM-5	12.30±1.74[b]	2.15±0.27[c]	2.18±0.23[b]	16.63±2.09[b]	0.86±0.10[b]

Me, MoO₃/HZSM-5	13.33 ± 2.54^{b}	$2.48\pm0.76^{b,c}$	2.67 ± 0.49^{b}	18.47 ± 3.60^{b}	0.96 ± 0.36^{b}
He, Mo₂C/HZSM-5	20.41 ± 4.33^{a}	4.46 ± 1.02^{a}	5.80 ± 0.34^{a}	30.67 ± 5.67^{a}	1.60 ± 0.33^{a}
Me, Mo₂C/HZSM-5	$17.69\pm1.26^{a,b}$	$3.56\pm0.36^{a,b}$	6.20 ± 0.49^{a}	27.46 ± 1.79^{a}	$1.28\pm0.21^{a,b}$

[a]Means in the same column with no letter in common are significantly different ($p < 0.05$) from the Tukey's HSD test. The letters (a-c) superscripts refer to the highest estimates to the least.
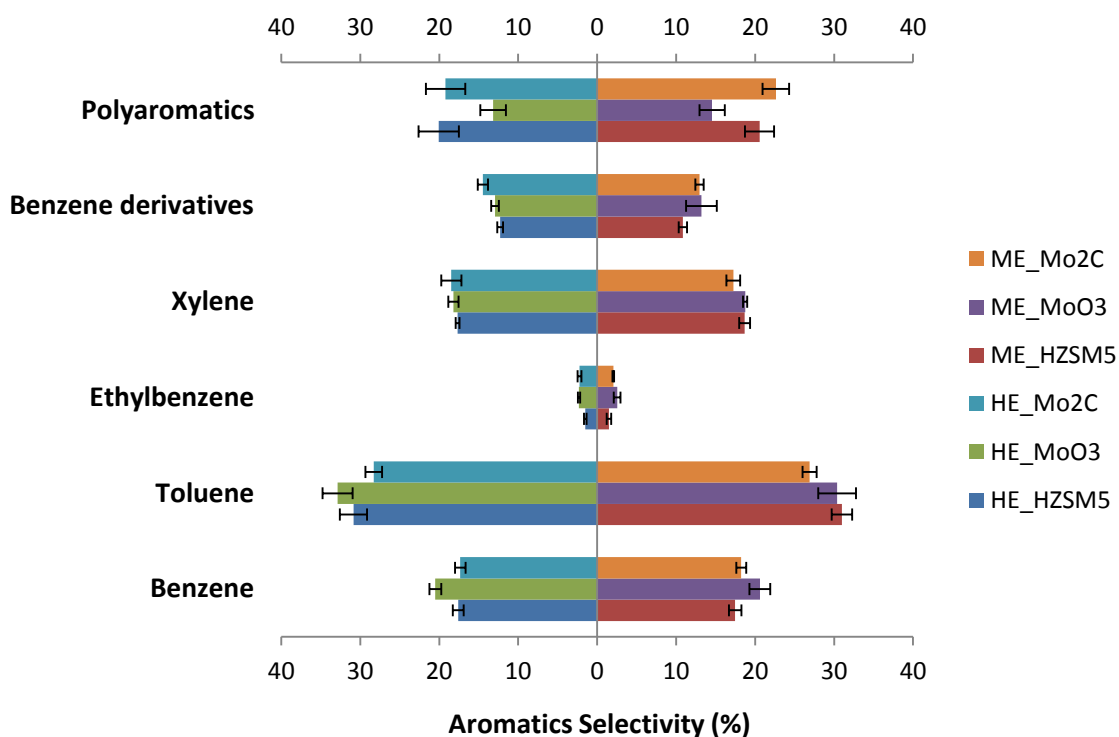
Figure 4.7 Aromatics selectivity of catalytic pyrolysis products of cellulose.

4.3.2.2. Catalytic pyrolysis of hemicellulose

The product yield from catalytic pyrolysis of hemicellulose is shown in Table 4.7. The total aromatics yield from hemicellulose was significantly lower than that from cellulose. For instance, the carbon yield of total aromatics from cellulose and hemicellulose in the presence of HZSM-5 under helium was 35.00 ± 4.37 and $19.48\pm1.26\%$, respectively. These values are in good agreement with those reported in the literature [240]. Although both cellulose and hemicellulose are carbohydrates, hemicellulose is thermally less stable than cellulose. Therefore, the cracking of hemicellulose in the presence of a zeolite is easier than that of cellulose. This is confirmed from the high yield of gaseous products from the catalytic pyrolysis of hemicellulose reported in other

studies [240, 241]. Similar to the results of cellulose, methane shows no significant effects in improving the yield of aromatics of hemicellulose.

The selectivity of aromatic products from catalytic pyrolysis of hemicellulose is shown in Figure 4.8. All of the HZSM-5 supported catalysts yielded product compositions with the selectivity of BTEX up to 70%. The maximum BTEX selectivity of 79.14% was achieved when MoO$_3$/HZSM-5 was used under methane environment. Cellulose and hemicellulose yielded similar selectivities for toluene, ethylbenzene and polyaromatics. Variations are noticeable in the yields of benzene, xylene and benzene derivatives from cellulose and hemicellulose. The selectivity of benzene and benzene derivatives was lower for hemicellulose than that for cellulose. However, the selectivity for xylene showed opposite trend. For example, benzene selectivity dropped from 17.58 to 14.41%, xylene selectivity increased from 17.67 to 23.01%, and benzene derivatives selectivity decreased from 12.29 to 11.36% when hemicellulose was used instead of cellulose. The introduction of methane had an impact on the formation of some of the aromatic compounds. As shown in Figure 4.8, the benzene selectivity under methane was slightly higher than that under helium, and this difference was significant ($p < 0.05$) with MoO$_3$/HZSM-5 and Mo$_2$C/HZMS-5 as the catalysts. In contrast, the selectivity of benzene derivatives under methane was slightly lower than that under helium, and the difference was significant with HZSM-5 and MoO$_3$/HZSM-5 catalysts. The impacts of impregnated Mo species on formation of aromatics for hemicellulose were similar to that observed for cellulose. No significant differences in aromatic yields were observed between HZSM-5 support and Mo$_2$C/HZSM-5. However, MoO$_3$/HZSM-5 did yield more toluene and benzene and less polyaromatics than the HZSM-5 and Mo$_2$C/HZSM-5 catalysts.

Table 4.7 Carbon yield from catalytic pyrolysis of hemicellulose (wt. %)[a].

Trial	BTEX	Aromatics Benzene derivatives	Polyaromatics	Total Aromatic HCs	Oxygenates
He, HZSM-5	12.99±0.96[a]	2.29±0.06[a]	4.20±0.32[a]	19.48±1.26[a]	0.31±0.02[a]
Me, HZSM-5	12.45±0.51[a]	1.45±0.08[a,b]	3.95±0.27[a]	17.84±0.77[a]	0.25±0.07[a]

He, MoO$_3$/HZSM-5	7.29±1.05[b]	1.11±0.30[a,b]	1.25±0.21[b]	9.65±1.56[b]	0.35±0.06[a]
Me, MoO$_3$/HZSM-5	7.47±0.79[b]	0.79±0.29[b]	1.22±0.26[b]	9.48±1.34[b]	0.24±0.07[a]
He, Mo$_2$C/HZSM-5	13.00±1.54[a]	2.21±0.99[a]	3.90±0.53[a]	19.10±2.96[a]	0.74±0.48[a]
Me, Mo$_2$C/HZSM-5	13.34±1.20[a]	1.47±0.48[a,b]	3.76±0.54[a]	18.57±1.82[a]	0.67±0.64[a]

[a]Means in the same column with no letter in common are significantly different ($p < 0.05$) by the Tukey's HSD test. The letters (a-b) superscripts refer to the highest estimates to the least.
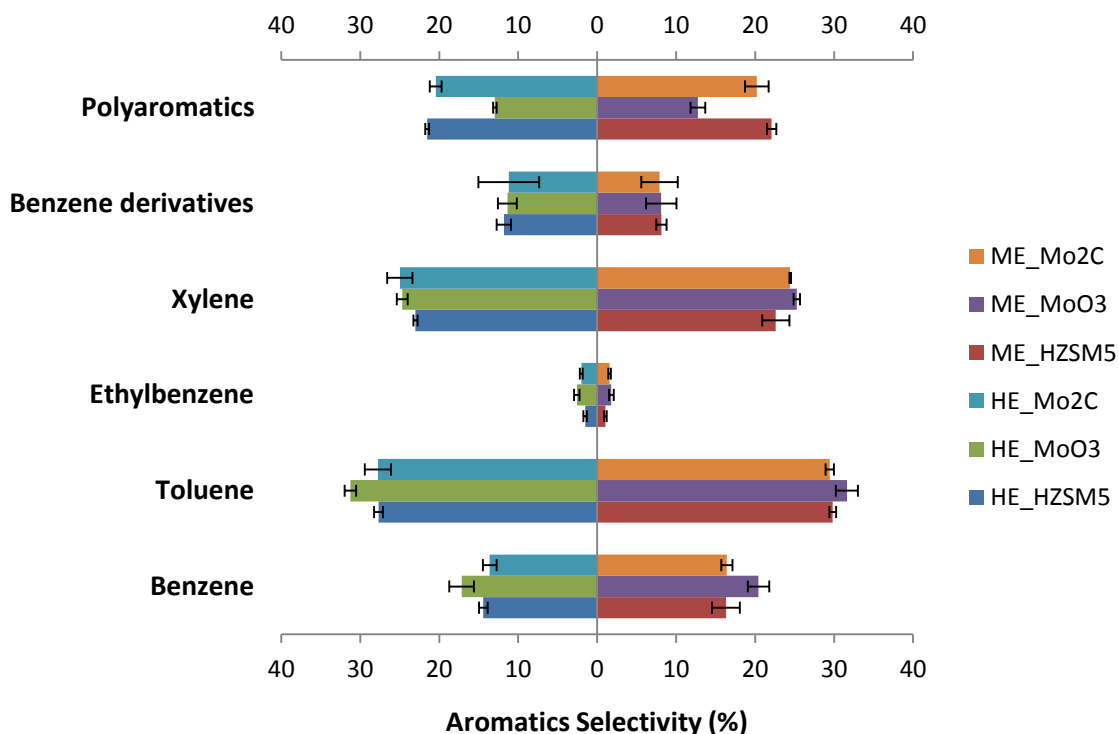
Figure 4.8 Aromatics selectivity of catalytic pyrolysis products of hemicellulose.

4.3.2.3. Catalytic pyrolysis of lignin

The carbon yields of catalytic pyrolysis products from lignin are shown in Table 4.8. The total carbon yields of lignin were even lower than those of hemicellulose. Therefore, the rank order of three biomass constituents in terms of yielding aromatics was cellulose > hemicellulose > lignin, which is consistent with other results reported [240, 241]. Also, it should be noted that the oxygenate yield from lignin was significantly higher than that from either cellulose or hemicellulose. Lignin is primarily depolymerized into phenolic compounds during pyrolysis. The low reactivity of these phenols in HZMS-5 is responsible for the high yield of oxygenates from

lignin [214, 240]. Methane slightly increased the yield of BTEX, polyaromatics and total aromatics but the change was not statistically significant. MoO_3/HZSM-5 had the lowest aromatics yield among all three catalysts. This is likely due to deactivation during catalyst impregnation as discussed above.

The tornado plot in Figure 4.9 shows the aromatic selectivity of products from lignin. The selectivity of polyaromatics from lignin was the highest among biomass components. The maximum polyaromatics selectivity from lignin reached up to 36% in the presence of HZMS-5, while the selectivity was only 20% from cellulose and hemicellulose. This variation could also be attributed to the conversion of the lignin-derived phenols into polyaromatics and coke through polycondensation in the channel of HZSM-5 [240]. Effect of methane was only significant on the selectivity of benzene and benzene derivatives with HZSM-5. However, the carbon yields of lignin-derived BTEX and polyaromatics under methane were higher (but not significant) than those under Helium. Also, impregnation with the Mo species significantly changed the selectivity of aromatics (Figure 4.9). In general, the presence of Mo increased selectivity of BTEX and decreased selectivity of polyaromatics. Transition metals such as Ni, Co, and Mo have shown to catalyze deoxygenation of phenolic compounds to form aromatics leading to their widespread use in hydrodeoxygenation (HDO) of bio-oil compounds [209, 242, 243]. Rather than ending up as polyaromatics and coke in the channels of HZSM-5, lignin-derived phenolic compounds may have incorporated into the active sites of the Mo species, where hydroxy and methoxy groups, possibly, directly stripped from the aromatic rings. Zheng et al. [244] demonstrated that Mo_2N/Al_2O_3 exhibited a high selectivity of monocyclic aromatics and an extremely low selectivity of polyaromatics (2.2%) from lignin. In the current study, Mo impregnated HZSM-5 acted as a bifunctional catalyst: Mo species provided active sites for deoxygenation and the Lewis and Bronsted acid sites in HZSM-5 were responsible for the aromatization of lignin-derived olefins. The increase in BTEX selectivity and decrease in polyaromatics is the synergistic result of these two mechanisms.

Table 4.8 Carbon yield from catalytic pyrolysis of lignin (wt. %)[a].

| Trial | Aromatics | | | | |
	BTEX	Benzene derivatives	Polyaromatics	Total Aromatic HCs	Oxygenates
He, HZSM-5	$6.73\pm0.56^{a,b}$	1.38 ± 0.17^{a}	4.70 ± 0.90^{a}	$12.80\pm1.59^{a,b}$	1.40 ± 0.41^{a}
Me, HZSM-5	8.41 ± 0.39^{a}	1.26 ± 0.03^{a}	5.47 ± 0.17^{a}	15.13 ± 0.45^{a}	1.40 ± 0.43^{a}
He, MoO$_3$/HZSM-5	3.34 ± 1.26^{c}	0.49 ± 0.34^{a}	0.67 ± 0.58^{d}	4.50 ± 1.99^{d}	1.19 ± 0.77^{a}
Me, MoO$_3$/HZSM-5	$4.60\pm0.65^{b,c}$	0.48 ± 0.17^{a}	$1.09\pm0.21^{c,d}$	$6.17\pm1.03^{c,d}$	1.35 ± 0.65^{a}
He, Mo$_2$C/HZSM-5	$6.31\pm0.58^{a,b}$	1.30 ± 0.54^{a}	$2.30\pm0.16^{b,c}$	$9.90\pm1.20^{b,c}$	1.70 ± 0.37^{a}
Me, Mo$_2$C/HZSM-5	7.03 ± 1.08^{a}	1.21 ± 0.94^{a}	2.61 ± 0.63^{b}	$10.85\pm2.62^{a,b}$	1.45 ± 0.74^{a}

[a]Means in the same column with no letter in common are significantly different ($p < 0.05$) by the Tukey's HSD test. The letters (a-d) superscripts refer to the highest estimates to the least.
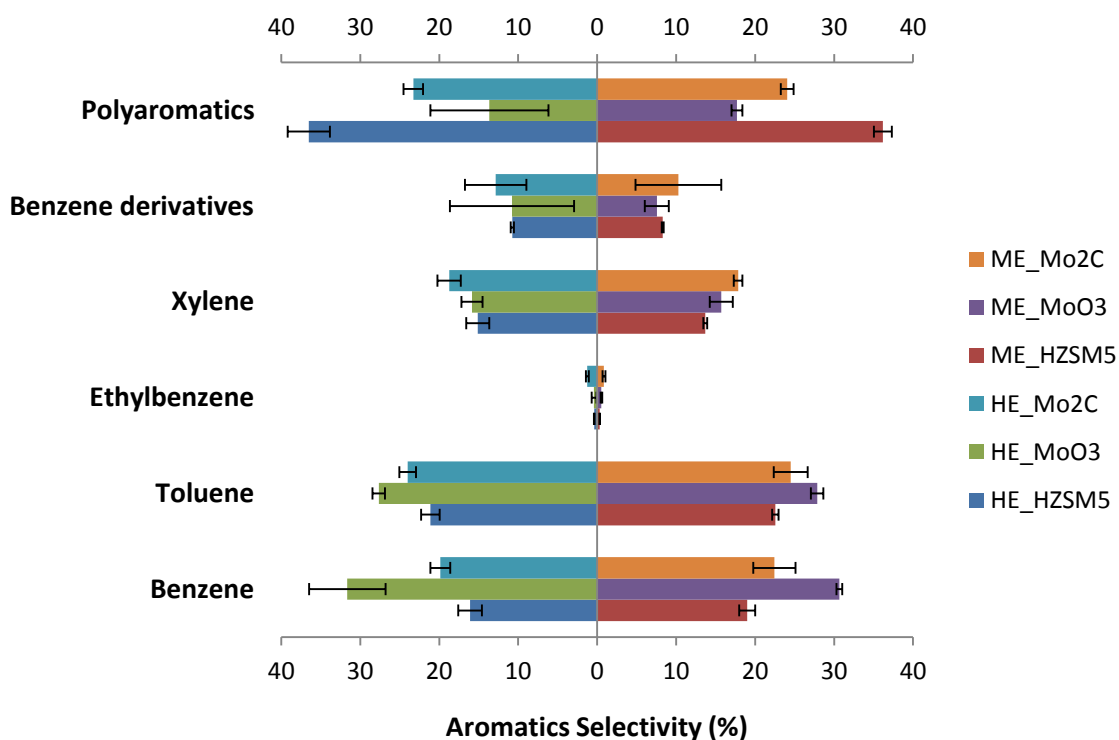
Figure 4.9 Aromatics selectivity of catalytic pyrolysis products of lignin.

4.3.2.4. Role of methane and reaction network

As discussed above, methane significantly increased aromatic hydrocarbon yield from lignin but did not significant effect the aromatic hydrocarbon yield from cellulose and hemicellulose. Even with only HZSM-5 support, the carbon yield of aromatics obtained with methane was higher than that obtained under helium (Table 4.8). These results imply that

methane can incorporate into lignin derived phenols directly and form aromatics through HDO without being activated on the active sites on Mo species. Lignin-derived intermediates, such as guaiacols and phenols can be converted into aromatics through a series of reactions like dehydration, demethylation and transalkylation that occur in the HDO process [157]. These reactions are promoted under a hydrogen-rich environment, possibly provided by reforming of methane with water that evolved from lignin degradation. The reaction pathway on conversion of lignin over HZSM-5 supported catalysts under methane is summarized in Figure 4.10. However, to validate this reaction pathway and further understand the reaction mechanisms, an isotope labeling study using deuterated methane (CD_4) or ^{13}C containing biomass model compound as the feed is needed. The fact that the yield of aromatic compound from carbohydrates was not very sensitive to reaction atmosphere, suggest that the Mo-based catalysts might not have activated methane efficiently.
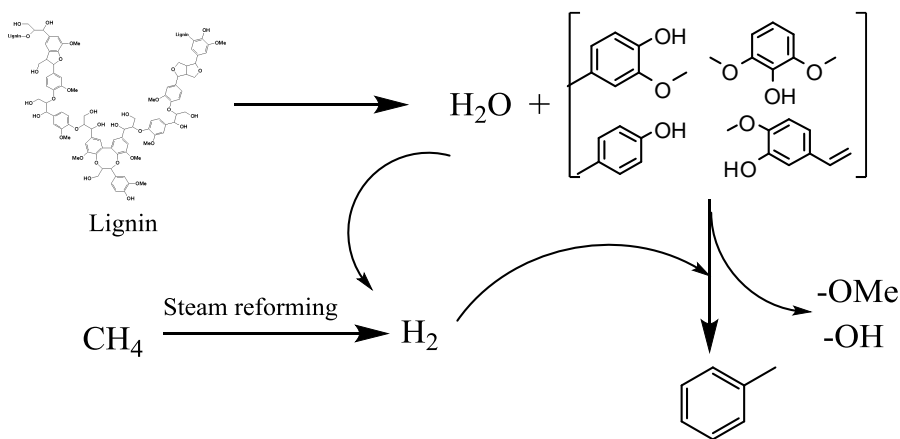
Figure 4.10 Conversion pathways of lignin with methane.

4.4. Conclusions

This study investigated catalytic pyrolysis of three biomass constituents (cellulose, hemicellulose and lignin) under both helium and methane atmospheres in the presence of HZSM-5 and HZSM-5 supported molybdenum-based catalysts. Cellulose contributed most to the production of aromatic hydrocarbons followed by hemicellulose and lignin. The introduction of

methane enhanced hydrodeoxygenation of lignin-derived phenols leading to increased aromatics yield in presence of HZSM-5 zeolites. The carbon yield of total aromatics from lignin increased from 12.8 to 15.13 % when pyrolysis atmosphere changed from helium to methane in presence of HZSM-5 support. However, in contrast to our expectation, methane was not effective in improving the aromatics yield from cellulose and hemicellulose. The active sites provided by Mo species facilitated the deoxygenation of lignin-derived phenols and thus inhibited the production of polyaromatics and coke.

CHAPTER IV

CO-PYROLYSIS OF TORREFIED BIOMASS AND METHANE OVER MOLYBDENUM

MODIFIED BIMETALLIC HZSM-5 CATALYST FOR HYDROCARBONS PRODUCTION

Abstract: Catalysis of torrefied switchgrass under methane atmosphere was performed over molybdenum modified bimetallic catalysts. Compared with other molybdenum-only catalysts (MoO_3/HZSM-5 and Mo_2C/HZSM-5), bimetallic catalysts demonstrated a higher reactivity towards methane activation. Higher reaction temperatures favored the yield of aromatics under both helium and methane atmospheres. The maximum aromatic yield of 39.31 % was achieved from co-catalysis of raw switchgrass and methane over MoZn/HZSM-5 at 700 °C. Torrefaction had no effect on the aromatics yield. Aromatics yield of switchgrass torrefied at 270 °C was lower than that torrefied at 230 °C. The reduction of aromatics from torrefied switchgrass is due to the loss of cellulose and concentration of lignin during torrefaction.

5.1. Introduction

Alternative energy resources, such as hydroelectric, solar, geothermal, wind power and biomass have played important roles in ensuring the national energy security and mitigating environmental impacts that associated with the utilization of fossil fuels. Biomass is even more attractive and important than other alternative energy resources listed above because other than meeting energy demands, biomass is the only sustainable source of organic carbon capable of producing petroleum like products and chemicals, ranging from plastic products to oils that are used in vehicles [115, 245]. Various methods of producing biofuels and biobased products from biomass have been under development, and these methods can be generally categorized as either biochemical or thermochemical processes. Fast pyrolysis is a promising thermochemical process due to its high yield of liquid product known as bio-oil, which is reported up to 90 wt. % depending on the feedstock and process conditions [6]. Bio-oil can be either burned as a fuel in various applications such as boilers, gas turbines and diesel engines, or served as a platform for synthesis of chemicals such as levoglucosan, acetic acid, phenol compounds and aromatic hydrocarbons [14, 246]. However, the final application of bio-oil to end users is greatly limited due to its negative attributes such as high water and oxygen content, high viscosity and acidity, low heating value and instability during storage. Moreover, these attributes, especially the high oxygen content (up to 40 wt. %) [6] make bio-oil incompatible with crude oil, thus resulting in more challenges and cost to modify the existing refining infrastructures. Fuel products can be evaluated by their O/C and H/C ratios, and the ones with lower O/C and higher H/C ratios result in higher quality fuels [209]. Hence, reducing the oxygen content of bio-oil prior to its final application or refinery is critical. A number of methods have been used to upgrade the properties of bio-oil chemically, which can be broadly classified as hydrodeoxygenation, catalytic cracking and catalytic fast pyrolysis [3, 13, 102]. In addition to these bio-oil upgrading techniques, a thermal pretreatment (torrefaction) appears promising since the oxygen in raw biomass can be partially removed before biomass is introduced into the pyrolysis reactor.

Torrefaction is a slow pyrolysis process that occurs in a temperature range of 200-300 ℃ [186]. During torrefaction, biomass partially decomposes and releases most of the moisture and part of volatiles, resulting in a hydrophobic solid product with improved grindability and increased energy density [247] . Torrefied switchgrass showed higher H/C and lower O/C as compared to raw switchgrass [191]. The three major biomass constituents (cellulose, hemicellulose and lignin) behaved differently under thermal pretreatment due to their different thermal stabilities. Typically, hemicellulose is the least stable under thermal pretreatment, whereas lignin is the most stable [195]. Zheng et al. [199] found that hemicellulose was the major component that decomposed during torrefaction (at 240-320 ℃), and cellulose began to decompose at 280 ℃, while lignin concentrated as the temperature of torrefaction increased.

Several studies concluded that torrefaction increased deoxygenated compounds, such as simple phenols and sugars, but decreased oxygenated derived phenols such as guaiacols and small oxygenated compounds including furans and acids [248-250]. Recently, several studies [251-253] suggest that torrefaction could be an effective thermal pretreatment to improve the selectivity of aromatic hydrocarbons over HZSM-5 catalysts during pyrolysis. Zheng et al. [253] found that high torrefaction temperatures (270 to 300 ℃) significantly decreased aromatic compounds and increased coke yield. Adhikari et al. [254, 255] found that high acidity of the HZSM-5 resulted in higher aromatics yield from both torrefied cellulose and lignin. A reaction pathway for torrefied cellulose catalytic pyrolysis was also proposed. The glycosidic bonds connecting monomers of cellulose were partially cleaved due to torrefaction, leading to an open chain structure that can be further converted into aromatics [254].

Large reserves of natural gas have motivated the development of methods to convert methane, the major component of natural gas to higher value chemical and hydrocarbon fuels [221]. Methane can be converted to hydrocarbons through both indirect and direct approaches. Two indirect conversion approaches have been extensively studied, one of which is based on the steam/CO_2 reforming of methane into synthesis gas (CO and H_2) followed by Fischer-Tropsch

synthesis, and the other one involves the partial oxidation of methane into methanol and dimethyl ether (DME) which can be further converted to gasoline [222, 256]. Also, there are two direct (oxidative and non-oxidative) approaches for methane conversions into higher hydrocarbons. In the early 1980s, Keller and Bhasin pioneered the research on oxidative coupling of methane (OCM), a high temperature exothermic process (~1200 K) that converts methane into ethylene and ethane under oxygen atmosphere [257, 258]. However, low C_2 yields (less than 30 % in theory) due to further oxidation of these products into CO/CO_2 and engineering difficulties resulting from the heat of reaction become the major challenges for the further development of OCM process [222].

Recently, an increasing interest has been focused on the non-oxidative direct methane aromatization (DMA) process, which selectively converts methane into aromatic hydrocarbons, especially benzene, toluene, ethylbenzene and xylenes (BTEX) in presence of bifunctional zeolite catalysts [223, 233, 259]. Transition metal based catalysts like tungsten (W) and molybdenum (Mo) are considered as the most promising components for DMA [260-262]. The metal components are responsible for the hydro/dehydrogenation and the acid sites provided by zeolites are responsible for the aromatization [259]. During the DMA process, there is an initial stage that is crucial for the activation of methane, also known as "the introduction period" during which molybdenum oxides are reduced to more active components like molybdenum carbide (Mo_2C) or Molybdenum oxycarbide (MoC_xO_y) [220]. Molybdenum carbide species, formed through the partial reduction of molybdenum oxide are believed to be involved with the cleavage of C-H bonds, resulting in methyl radicals, which can undergo oliomerization and cyclization reactions on acid sites of zeolites to form aromatics [260, 262, 263].

Addition of oxygenates (CO, CO_2, NO) have also significantly improved the efficiency of the catalysts by mitigating the carbon deposition issues [220, 228]. Several studies [229-231] found the coupling effects of coal-derived volatiles and methane when co-processed in the presence of Mo/HZSM-5 catalysts to further improve the aromatics yield at a temperature range

of 600~900 °C. A mechanism was proposed [229, 230] that the intermediate radicals, such as CH_x (x<4), H· and $C_2H_y^+$ (y=3, 5) degraded from methane, combined with free radicals, released from thermal cracking of coals, and formed aromatics on the acid site of HZSM-5 catalysts via dehydration, decarboxylation and oglimerization. Besides, methane conversion has been proven to increase significantly in the presence of higher hydrocarbons, especially unsaturated hydrocarbons, at a low temperature (400~600 °C) and atmospheric pressure over HZSM-5 catalyst loaded with Zn or Ag [264-267]. These previous results inspired our novel process for production of hydrocarbons from biomass through coupling biomass pyrolysis and methane dehydroaromatization. It is hypothesized that biomass pyrolysis can offer various motivators, such as light alkane/alkenes and oxygenates that promote methane DMA process, thus maximizing the hydrocarbon yields. To date, limited information on this integrated process for biomass and natural gas is available in the literature.

In this study, we combined torrefaction pretreatment and co-pyrolysis with methane to improve the aromatics yields through biomass catalytic fast pyrolysis process using bimetallic catalysts. It is hypothesized that both torrefaction pretreatment and co-feeding of methane will improve the H/C_{eff} ratio of the reactant, which would result in high aromatics yield. The specific objective of this study was to investigate the co-pyrolysis of methane with raw and torrefied biomass feedstocks to selectively improve BTEX (benzene, toluene, ethylbenzene and xylenes) yield in presence of a molybdenum modified HZSM-5 catalyst. The effects of torrefaction, torrefaction temperature, pyrolysis temperature and reaction atmosphere on the aromatic hydrocarbon yields were investigated.

5.2. Materials and methods

5.2.1. Biomass characterization

Raw switchgrass, obtained from Plant and Soil Sciences Department at Oklahoma State University, was processed in a Wiley Mill (Thomas Model Wiley® Mill, USA) with a screen size of 0.5 mm for size reduction. The compositional analysis of the switchgrass, including cellulose,

hemicellulose, lignin and extractives was performed at Kansas State University according to the procedure provided by National Renewable Energy Laboratory (NREL) [268]. The results of proximate and ultimate analysis were reported in our previous paper [191].

5.2.2. Torrefaction

Grounded switchgrass was sent to Idaho National Laboratory (INL, Idaho Falls) for thermal pretreatment. The detailed description of torrefaction procedures were outlined previously [191]. Briefly, biomass samples were torrefied at 230 and 270 ℃ in a torrefaction reactor system for 30 min and then exited from the bottom of the reactor through a horizontal auger.

To eliminate the impacts of mineral contents, the feedstock was purified by washing with diluted acid and deionized water. Briefly, 5 g of feedstock was washed with 0.1 N HNO_3 under stirring for 3 hrs, and then the acid was filtered through a funnel, followed by 3~5 washes with deionized water until the solution reached to central. Then, the purified feedstock was dried overnight at 105 °C for use.

5.2.3. Catalyst preparation

ZSM-5 zeolites (Si/Al=30, surface area=425 m^2/g) were purchased in ammonium form (Alfa Aesar Company, VA, USA), and were calcined in the air at 550 ℃ for 4 hrs to make protonated HZSM-5. The synthesis of MoO_3/HZSM-5 and Mo_2C/HZSM-5 is provided in in Chapter 4. MoAg/HZSM-5 was synthesized by impregnating MoO_3/HZSM-5 with a solution of silver acetate (0.5 wt. %) for 24 h. The catalyst was separated by centrifugation and then freeze dried followed by calcination at 700 ℃. Figure 5.1 depicted the synthesis route of bimetallic MoZn/HZSM-5 catalyst. The detailed synthesis procedures were described elsewhere [269]. Then, the catalyst sample was freeze dried and calcined in a flow of helium at 700 °C for 2 h.

5.2.4. Catalysts characterization

Powder X-ray diffraction (XRD, Bruker D8-A25-ADVANCE diffractometer) was used to characterize the crystallinity of the metal impregnated catalysts. The test was performed using Cu Kα radiation at 40 kV and 100 mA at a continuous scanning at step size of 0.02º, 0.5s per step over a scanning range from 5° to 70° (2θ).

The pore structures of metal impregnated catalysts were determined by isothermal nitrogen adsorption at 77 K using a surface area analyzer (Autosorb-1C, Quantachrome, Boynton Beach, FL, USA). Prior to the analysis, catalysts samples were degased at 300 ºC for 12 hrs. The specific surface area was calculated according to Brunauer-Emmett-Teller (BET) theory. External surface area, micropore area, and pore volume were derived based on t-plot method [235]. The quantity of molybdenum in catalysts was measured using inductively coupled plasma-atomic emission spectroscopy (ICP-AES; ThermoScientific, Waltham, MA, USA).

The catalyst morphology was characterized by transmission electron microscope (TEM; JEOL JEM-2100) coupled with an energy dispersive X-ray spectroscopy (EDS; Evex Nanoanalysis) operated at 200 kV. Prior to the test, the catalyst samples were suspended in isopropanol and then dispersed on a copper grid.
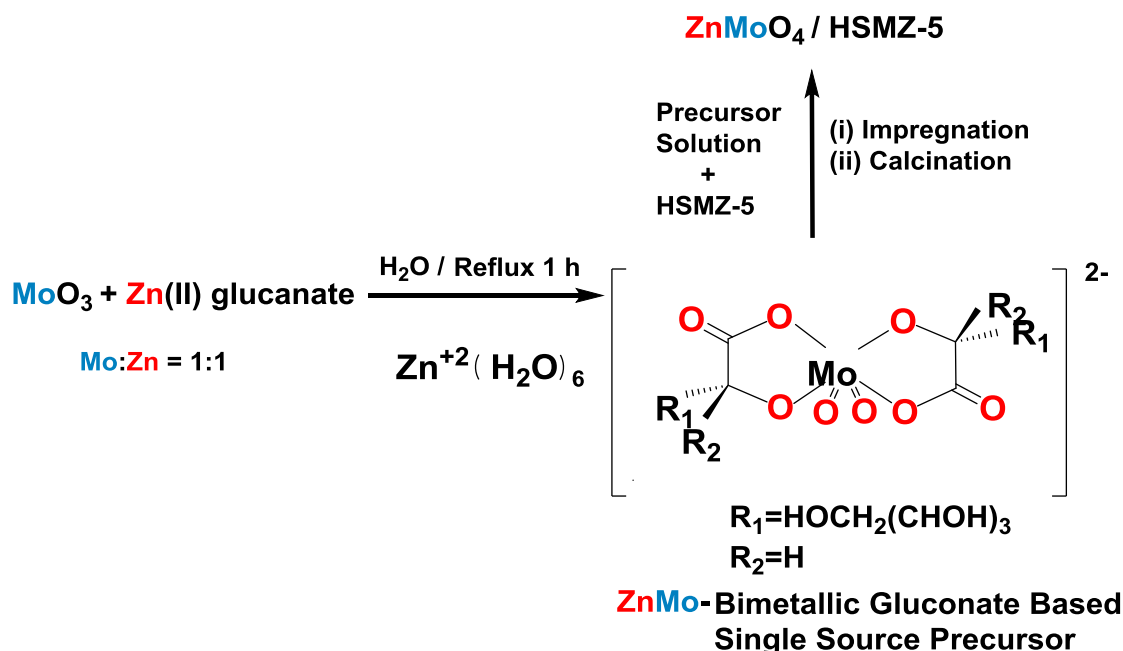
Figure 5.1 Synthesis of MoZn/HZSM-5 catalyst

5.2.5. Py-GC-MS experiments

Pyrolysis experiments were performed in a commercialized pyrolyzer (model no. 5200, CDS Analytics Inc.), which was connected to an Agilent gas chromatograph/mass spectrometer (7890GC/5975MS). A detailed description about the experimental procedures were stated elsewhere [248]. For the sample loading, biomass sample was sandwiched between two catalyst layers. The biomass sample and catalyst layers were separated by quartz wool so that only pyrolysis vapors of biomass sample would pass through the catalyst layers. The pyrolysis products were analyzed with an Agilent 7890GC/5975MS using a DB-5 capillary column (30 mL×0.32mm I.D., 0.25 µm film thickness). The GC/MS ramping method was similar as described in our previous paper [248].

The compounds were identified by comparing the peaks with National Institute of Standards and Technology (NIST) mass spectral library. Quantification of targeted compounds was performed after calibration by injecting different known concentrations of working standards

into GC/MS. The carbon yield and selectivity was calculated using   Equation 5.1 and

Equation 5.2.

$$Carbon\ yield = \frac{Moles\ of\ carbon\ in\ specific\ species}{Moles\ of\ carbon\ in\ biomass\ models} \qquad \text{Equation 5.1}$$

$$Carbon\ selectivity = \frac{Moles\ of\ carbon\ in\ specific\ species}{Moles\ of\ carbon\ in\ all\ quantified\ species} \qquad \text{Equation 5.2}$$

5.2.6. Experimental design

The effects of molybdenum modified HZSM-5 catalysts (HZSM-5, MoO_3/HZSM-5, Mo_2C/HZSM-5, MoAg/HZSM-5 and MoZn/HZSM-5), pyrolysis temperature (400, 500, 600, 700 and 800 °C) and torrefaction pretreatment (no torrefaction, torrefaction at 230 °C and torrefaction at 270 °C) were investigated individually using single factor design. The experiments were performed under helium and methane atmospheres. All experiments were replicated at least three times.

5.3. Results and discussion

The weight percentages of carbohydrates, lignin and ash in raw and torrefied switchgrass are shown in Table 5.1. Among these carbohydrates, glucan denotes cellulose and xylan and arabinan are the two compounds to characterize hemicellulose. In addition, the weight loss due to torrefaction pretreatment is also shown in the table. This weight loss includes moisture, condensable and non-condensable vapors that evolve during the process of torrefaction. It should be noted that the values of compositional analysis of torrefied switchgrass shown in Table 5.1 are normalized by weight loss during torrefaction so that the values are reported as a fraction of raw switchgrass. The major compositional changes of switchgrass torrefaction involve the decomposition of hemicellulose and partial decomposition of cellulose and lignin. As shown in Table 5.1, the composition of switchgrass was significantly affected by torrefaction. As the torrefaction temperature increased, the content of cellulose and hemicellulose decreased significantly. The degradation of cellulose was approximately correlated with torrefaction

112

temperature. However, the degradation of hemicellulose was drastic even at lower torrefaction, for example, the xylan content dropped from 26.34 to 7.58 wt. %. It is known that hemicellulose, the most unstable content in biomass, decomposes rapidly at the temperature range of 220-315 °C [195]. The lignin content increased steadily as the torrefaction temperature increased, showing that lignin is the most stable component during torrefaction, thus its content increases due to rapid loss of carbohydrates.

Table 5.1 Compositional analysis of raw and torrefied switchgrass (wt. %)[a]
(SG=switchgrass, T230=torrefied at 230 °C, T270=torrefied at 270 °C).

Sample	Glucan	Xylan	Arabinan	Lignin	Ash	Weight Loss
Raw SG	38.46±0.69[a]	26.34±0.54[a]	3.41±0.32[a]	21.40±0.24[c]	1.91±0.10[a]	NA
T230 SG	27.08±0.27[b]	7.58±0.12[b]	1.28±0.12[b]	23.48±0.08[b]	1.43±0.02[b]	25.01
T270 SG	17.09±0.16[c]	2.75±0.002[c]	0.96±0.07[b]	33.98±0.10[a]	1.98±0.04[a]	36.07

[a]Means in the same column with no letter in common are significantly different ($p < 0.05$) from the Tukey's HSD test. The letters (a-d) superscripts refer to the highest estimates to the least. NA: not applicable.

5.3.1. Catalysts characterization

The XRD patterns of HZSM-5 support, MoAg/HZSM-5 and MoZn/HZSM-5 were shown in Figure 5.2. No additional diffraction peaks were found after modified with metal impregnation, indicating that the framework of HZSM-5 was not affected during metal impregnation. Furthermore, the intensities of diffraction peaks at 7-10° increased whereas the intensities of diffraction peaks at 23-25° decreased after impregnation of metals, indicating a lattice distortion of the HZSM-5 support.

The morphologies of bimetallic molybdenum modified HZSM-5 catalysts were further characterized with transmission electron microscopy technique. As shown in Figure 5.3 (a), metal particles were highly dispersed on the surface of HZSM-5 support with a particle width ranged from 8 to 12 nm (data not shown). The EDS elemental analysis of MoAg/HZSM-5 indicated the existence of silver but not molybdenum. Thus, these metal particles could be only derived from

silver species. Metal particles were not visible on TEM image of MoZn/HZSM-5 (Figure 5.3 (b)), which might suggest that Zn species did not present in the form of ZnO crystals but incorporated into the structure of HZSM-5 as cations Zn^{2+}.
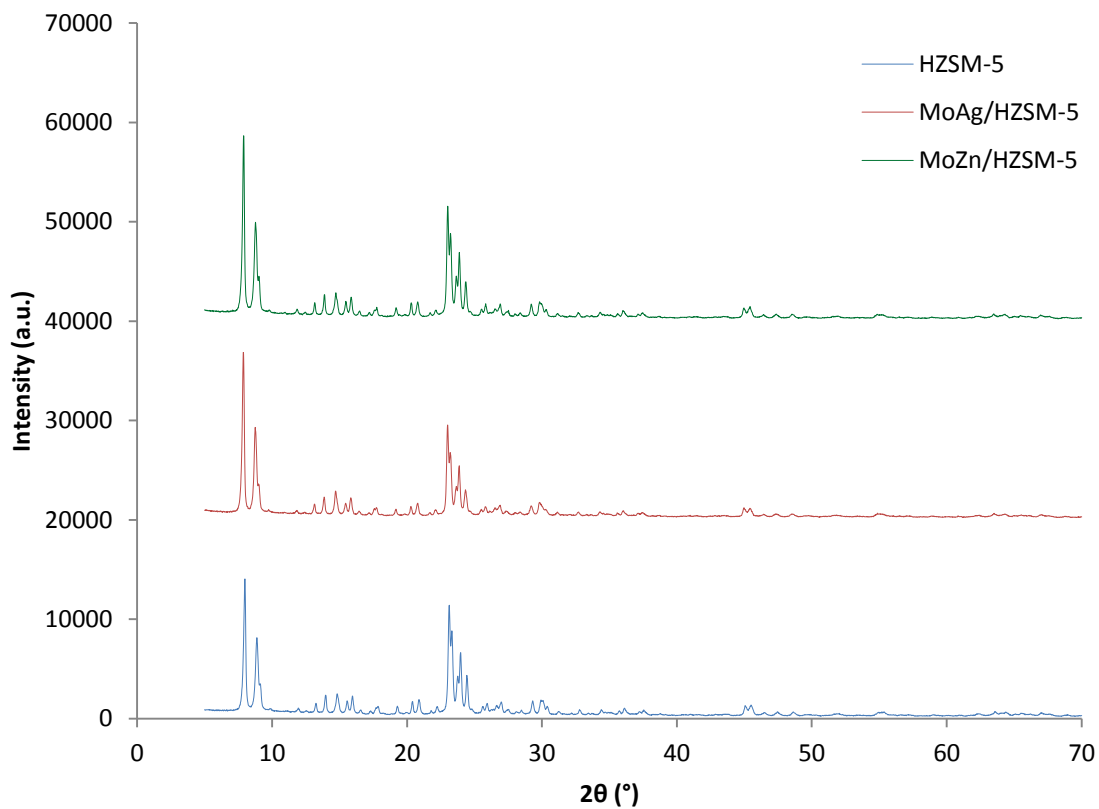
Figure 5.2. XRD patterns of HZSM-5, MoAg/HZSM-5 and MoZn/HZSM-5

| (a) | (b) |
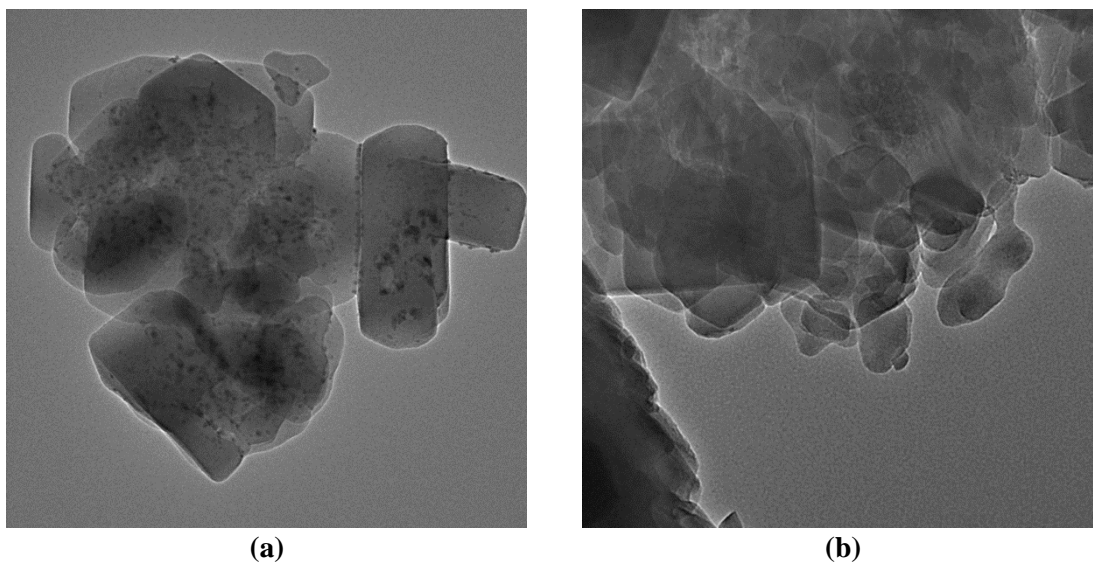
Figure 5.3 TEM images of MoAg/HZSM-5 (a) and MoZn/HZSM-5 (b), mag=40000x

114

5.3.2. Effects of molybdenum modified catalysts on co-catalysis of biomass and methane

Products of catalytic pyrolysis of raw switchgrass are mostly aromatic hydrocarbons, which can be grouped into BTEX, benzene derivatives (alkyl benzenes, indane and indenes) and polyaromatics (naphthalenes, fluorene and anthracene). Pyrolysis products of raw switchgrass obtained under different molybdenum modified catalysts are summarized in Table 5.2. The maximum carbon yields of BTEX (27.27 %) and total aromatics (39.31 %) were obtained using MoZn/HZSM-5 under methane atmosphere. The catalytic pyrolysis was also performed using only methane in presence of Mo-modified HZSM-5 zeolites (Figure 5.4). The results indicated that the higher aromatics yield from catalytic pyrolysis of switchgrass under methane was due to the synergistic effect of methane and biomass-derived vapors in presence of Mo-modified HZSM-5 zeolites. The reactivity of individual molybdenum catalyst towards co-catalysis of biomass and methane was revealed by comparing the pair of values associated with helium or methane. When methane is introduced in the feed, the carbon yield of aromatics increased in presence of HZSM-5, MoO_3/HZSM-5, MoAg/HZSM-5 and MoZn/HZSM-5 compared with the aromatics carbon yield obtained using the same catalyst under helium atmosphere. However, the results of Tukey`s multiple comparison indicated that the improvement in aromatics carbon yield due to methane is significant only with MoZn/HZSM-5, and in this case the aromatic carbon yield and BTEX carbon yield increased from 29.53 % and 20.06 % (without methane) to 39.31 % and 27.27 % (with methane), respectively. It is also worth noting that the impregnation of molybdenum species varied the reactivity of HZSM-5 catalyst. In general, the reactivity of catalysts with molybdenum loading (e.g. MoO_3/HZSM-5 and Mo_2C/HZSM-5) reduced compared with that of only support. However, when the support is loaded with bimetallic molybdenum species, such as MoAg/HZSM-5 and MoZn/HZSM-5, the catalytic reactivity recovered or even further improved. In detail, the carbon yields of BTEX obtained with MoAg/HZSM-5 under helium and methane were 17.01 and 20.27 %, respectively, which were similar to that obtained in presence of support only. And, the carbon yields of BTEX obtained in presence of MoZn/HZSM-

5 (helium: 20.06 %, methane: 27.27 %) were higher than that obtained in presence of HZSM-5 (helium: 17.24 %, methane: 21.22 %). The difference in catalytic reactivity of Mo-loading and bimetallic catalysts indicated that single Mo species did not effectively activate methane. Also, the carbon yield of polyaromatics obtained with both Mo-loaded and bimetallic HZSM-5 catalysts were lower than that obtained with the support only. Carbon yields of oxygenates, which include mainly phenolic compounds, were low (varying from 0.76 % with HZSM-5 to1.59 % with MoZn/HZSM-5).

Production of aromatic hydrocarbons from biomass involves a series of acid-catalyzed dehydration, decarboxylation, and decarbonylation, followed by oligomerization in the channel of zeolite [217]. As a result, the biomass oxygen is removed in the form of H_2O, CO_2 and CO. The maximum theoretical carbon yield of aromatic hydrocarbons can be achieved when only dehydration and decarboxylation occur [240]. The theoretical yield of aromatics, which is characterized as $CH_{1.2}$ [270] from switchgrass can be derived from   Equation 5.3:

$$nCH_{1.68}O_{0.697} \ (RSG) \xrightarrow{\Delta} 0.824n \ CH_{1.2} + 0.176n \ CO_2 + 0.345n \ H_2O \quad \text{Equation 5.3}$$
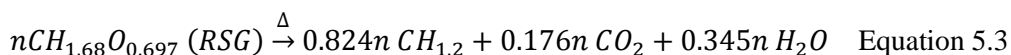
In this study, the maximum aromatics carbon yield obtained from switchgrass under helium was 29.53 %, which corresponds to 35.8 % of the theoretical carbon yield. When methane is introduced, the theoretical carbon aromatics yield increases because all carbon in the feedstocks (biomass and methane) can be theoretically converted into aromatic products, while oxygen is removed as H_2O (Equation 5.4).

$$nCH_{1.68}O_{0.697} \ (RSG) +0.32n \ CH_4 \xrightarrow{\Delta} 1.32n \ CH_{1.2} + 0.69n \ H_2O \quad \text{Equation 5.4}$$
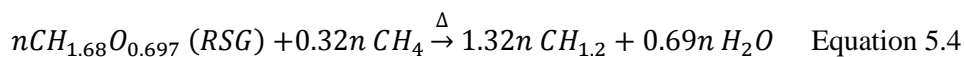
As shown in   Equation 5.4, the theoretical aromatics carbon yield obtained from switchgrass increases by approximately 60 % through intervention of methane. In this study, the maximum aromatics carbon yield obtained under methane was 39.31 %, which correspond to 29.78 % of the theoretical yield.

Table 5.2 Carbon yield from raw switchgrass in presence of HZSM-5 supported catalysts (C %)[a] (He=Helium, Me=Methane).

Trial	Aromatics			Total Aromatic HCs	Oxygenates
	BTEX	Benzene derivatives	Polyaromatics		
He, HZSM-5	$17.24\pm5.17^{b,c,d}$	$3.28\pm1.28^{a,b}$	$6.92\pm2.20^{a,b}$	$27.43\pm8.56^{b,c,d}$	0.77 ± 0.43^{b}
Me, HZSM-5	21.22 ± 1.94^{b}	3.14 ± 0.39^{b}	8.25 ± 0.57^{a}	$32.62\pm2.43^{a,b}$	0.76 ± 0.22^{b}
He, MoO₃/HZSM-5	13.42 ± 1.12^{d}	2.52 ± 0.47^{b}	3.07 ± 0.76^{d}	19.01 ± 2.32^{d}	$1.11\pm0.33^{a,b}$
Me, MoO₃/HZSM-5	$15.74\pm1.20^{b,c,d}$	2.68 ± 0.39^{b}	$3.46\pm0.61^{c,d}$	$21.87\pm2.19^{c,d}$	$1.11\pm0.17^{a,b}$
He, Mo₂C/HZSM-5	$16.50\pm0.56^{b,c,d}$	$3.42\pm0.19^{a,b}$	$5.09\pm0.46^{b,c,d}$	$25.02\pm1.19^{b,c,d}$	$1.19\pm0.10^{a,b}$
Me, Mo₂C/HZSM-5	$15.11\pm0.41^{c,d}$	2.71 ± 0.092^{b}	$4.81\pm0.48^{b,c,d}$	$22.63\pm0.96^{c,d}$	$0.95\pm0.13^{a,b}$
He, MoAg/HZSM-5	$17.01\pm0.79^{b,c,d}$	2.69 ± 0.33^{b}	$4.04\pm0.33^{c,d}$	$23.75\pm1.36^{b,c,d}$	0.78 ± 0.26^{b}
Me, MoAg/HZSM-5	$20.27\pm1.25^{b,c}$	2.97 ± 0.53^{b}	$4.91\pm0.42^{b,c,d}$	$28.15\pm1.90^{b,c,d}$	$1.01\pm0.27^{a,b}$
He, MoZn/HZSM-5	$20.06\pm1.13^{b,c}$	$3.71\pm0.30^{a,b}$	$5.76\pm0.11^{b,c}$	$29.53\pm1.31^{b,c}$	$1.35\pm0.17^{a,b}$
Me, MoZn/HZSM-5	27.27 ± 1.85^{a}	4.88 ± 0.65^{a}	$7.16\pm0.65^{a,b}$	39.31 ± 2.87^{a}	1.59 ± 0.15^{a}

[a]Means in the same column with no letter in common are significantly different ($p < 0.05$) from the Tukey's HSD test. The letters (a-d) superscripts refer to the highest estimates to the least.
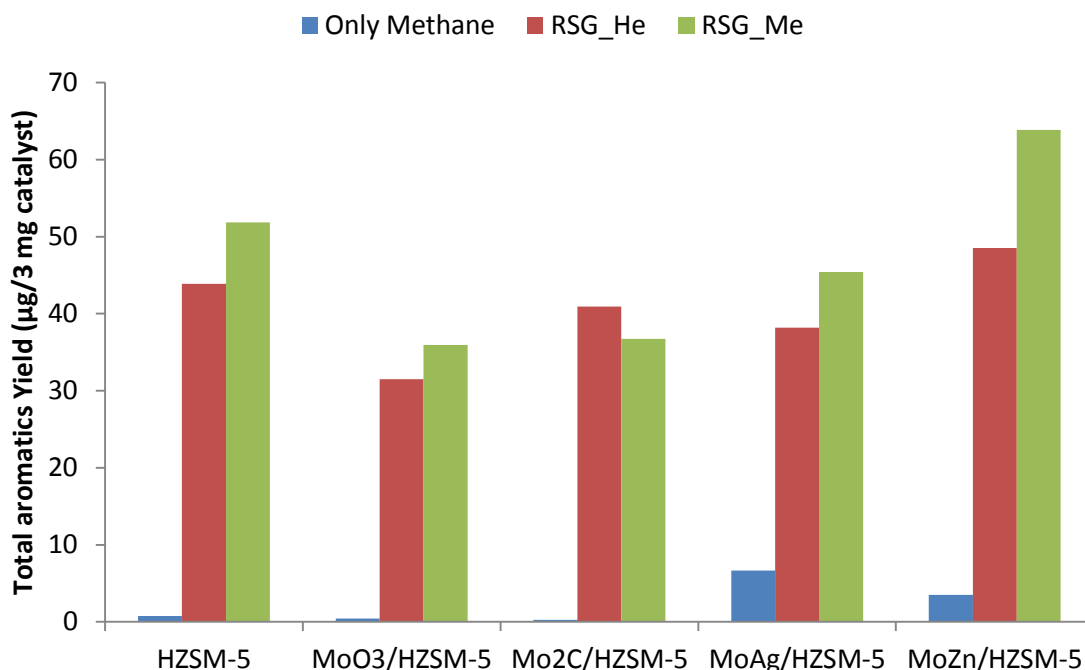
Figure 5.4 Total aromatics yield from methane, raw switchgrass under helium (RSG_He) and raw switchgrass under methane (RSG_Me) atmospheres

The aromatics selectivity (shown in Figure 5.5) of compounds obtained under helium with each catalyst was almost similar to that obtained under methane, indicating that methane had no significant effect on the selectivity of particular compounds during catalysis. The variations on aromatics selectivity across different HZSM-5 catalysts were obvious. MoAg/HZSM-5 yielded the highest benzene selectivity, which reached up to 24.53 and 26.97 % under helium and methane atmosphere, respectively. In return, the lowest selectivity of xylenes was also observed for MoAg/HZSM-5. Also, MoAg/HZSM-5 yielded the lowest selectivities of benzene derivatives and ethylbenzene among all the molybdenum modified catalysts. These results indicated that the active sites provided by Ag in MoAg/HZSM-5 system were responsible for the dealkylation of alkylated aromatics into benzene. Precious metal such as Pt, Pd and Ag are highly active for hydrogenation reactions. The detailed reaction mechanism [271] involves cleavage of alkyl side chains and simultaneous hydrogenation (Figure 5.6). In addition, the highest selectivity for polyaromatics was obtained with only the support, indicating that impregnation of metals could have suppressed polymerization of aromatics, leading to polyaromatics or coke deposition.

118
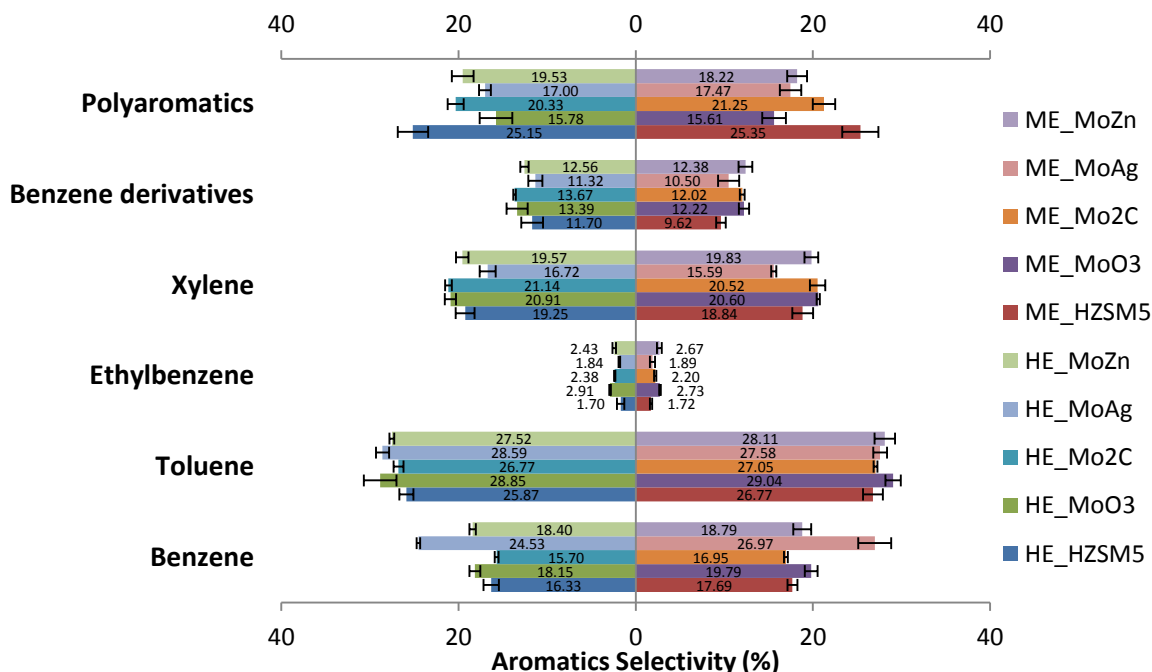
Figure 5.5 Aromatics selectivity of products from raw switchgrass in the presence of HZSM-5 supported catalysts.

The results of aromatics carbon yield show that single molybdenum modified HZSM-5 catalysts are not effective in catalyzing breakage of C-H bond in methane. The bimetallic catalysts (MoAg/HZSM-5 and MoZn/HZSM-5) behave as a bifunctional catalyst during the co-catalysis of biomass and methane. The HZSM-5 framework is mainly responsible for cracking of biomass-derived volatiles through a series of dehydration, decarboxylation, decarbonylation and oligomerization reactions to form aromatics. Whereas, the metals, especially the Ag and Zn species, provide active sites for methane activation, resulting in methyl radicals that can incorporate into the structure of biomass-derived organics, thus increase organics available for aromatization in the HZSM-5 channel. The aromatics yield with Mo-Ag was lower than that with Mo-Zn, but benzene selectivity followed opposite trend. This might be the outcome of competition between methane activation and hydrodealkylation of alkylated benzenes, since Ag provides active sites for both reactions. The reactions shown in Figure 5.6 indicated a carbon loss in the form of alkanes through dealkylation, and this might explain why the total yield of aromatics in presence of Mo-Ag loaded catalyst is lower than that in presence of Mo-Zn loaded

119

one. Therefore, taking the catalytic reactivity and aromatic loss into consideration, MoZn/HZSM-5 showed the best catalytic performance in co-conversion of biomass and methane.
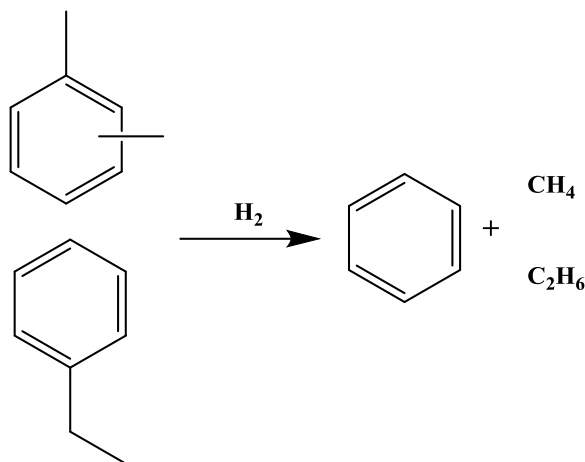
Figure 5.6 Reactions of hydrodealkylation of Xylenes and ethylbenzene.

5.3.3. Effects of reaction temperature on co-catalysis of biomass and methane

The effect of pyrolysis temperature on the carbon yield of different groups of aromatics from raw switchgrass catalysis in presence of MoZn/HZSM-5 was shown in Figure 5.7. It can be seen that the increase in temperature increased the carbon yield of aromatics at temperature starting from 400 and reached to peak at 700 °C and then dropped. Methane outperformed helium in producing aromatics across the whole reaction temperature range. In addition, the gap of the total aromatics yield (Figure 5.7 (a)) between helium and methane also increased as the reaction temperature increased and maximized at 600 °C (71 %). These results indicated that methane activation through incorporation with biomass catalysis could occur at a temperature (400 °C) much lower than that required in methane aromatization (700°C) [220]. He et al. [272, 273] also reported the synergistic effects of methane and biomass pyrolysis in promoting the yield and H/C ratio of bio-oil using Zn and Ag loaded catalysts at a lower temperature range of 300 to 600 °C.

The trends of different aromatic groups such as BTEX, polyaromatics and benzene derivatives versus temperature (Figure 5.7 (b ~ d)) were similar to that of total aromatics. The

sensitivity of carbon yield towards reaction temperature declined in the order of

BTEX>polyaromatics>benzene derivatives.
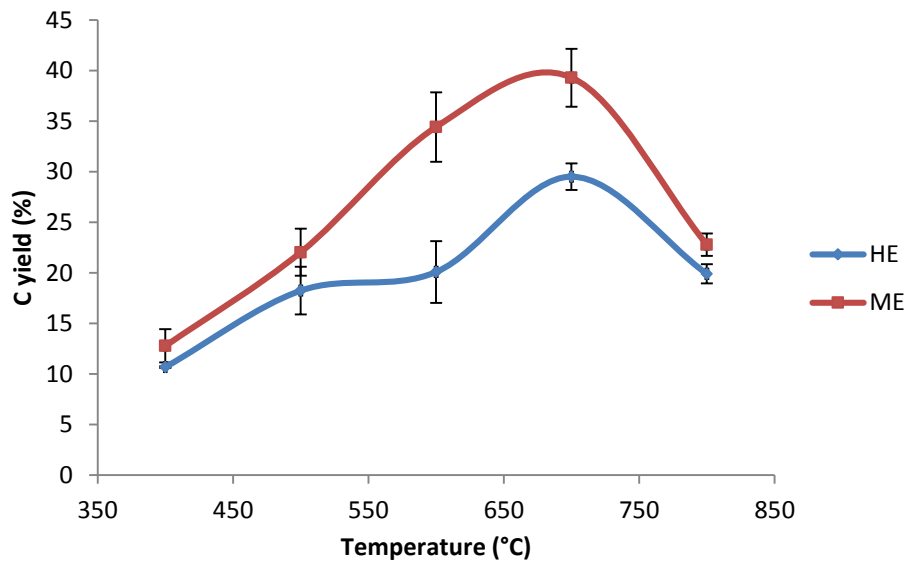
(a)
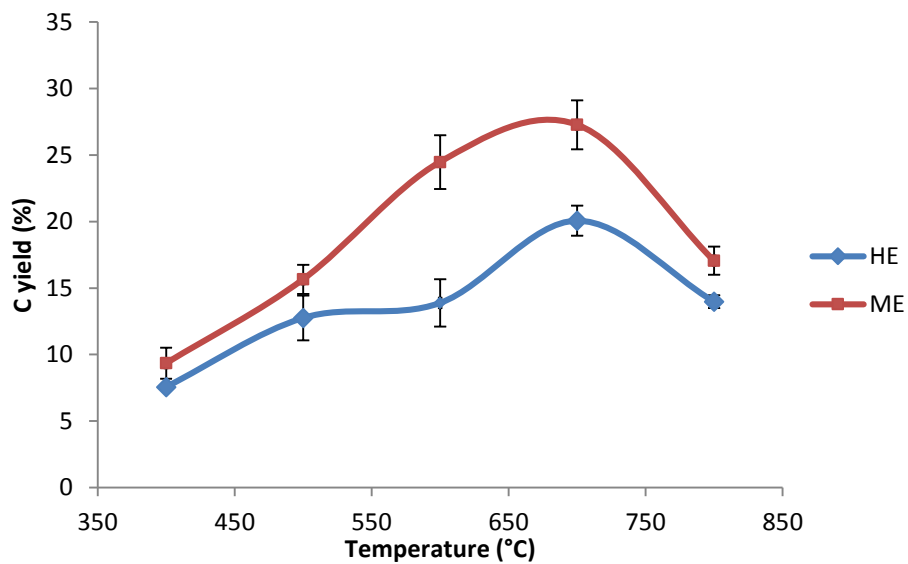
(b)
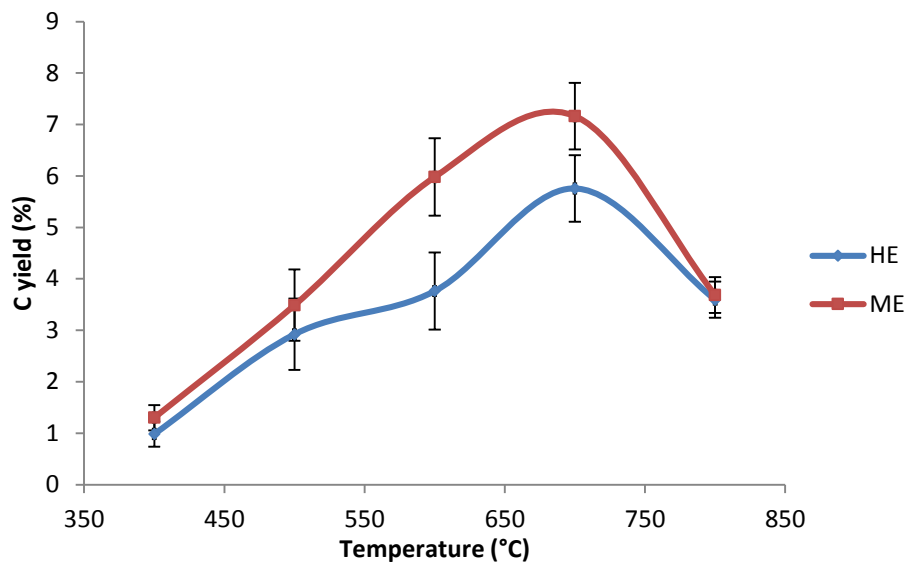
(c)
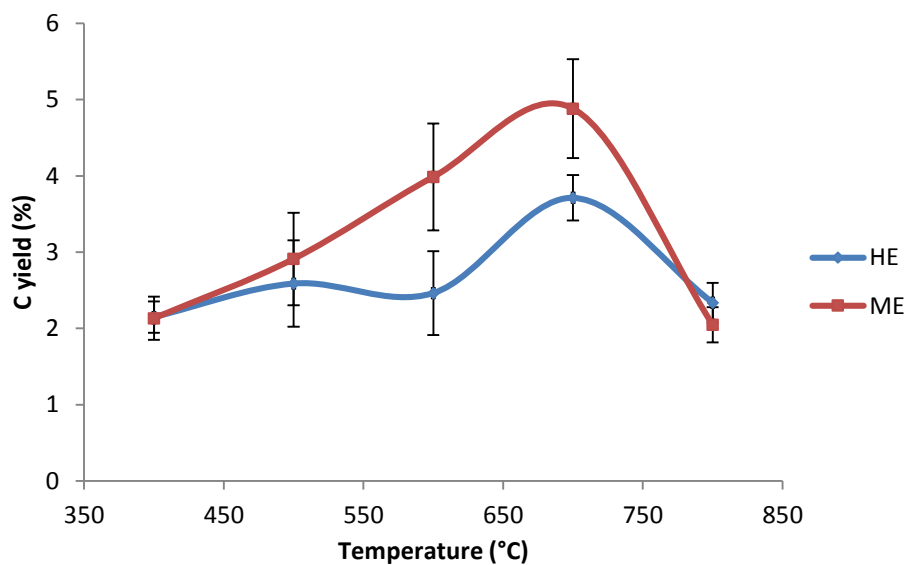
(d)

Figure 5.7 Carbon yield of aromatic hydrocarbons as a function of pyrolysis temperature (a) ~ (d): Total hydrocarbons, BTEX, Polyaromatics and Benzene derivatives.

The aromatics selectivity for the major compounds versus reaction temperature is plotted in Figure 5.8. As shown in Figure 5.8 (a), benzene selectivity increased steadily across the whole reaction temperature. Also, the difference between helium and methane atmosphere was not significant until the temperature reached 800 ℃. Toluene selectivity, fluctuating from 27.01 (400℃ under helium) to 29.10 % (600 ℃ under methane), was not sensitive to reaction temperature (Figure 5.8 (b)). However, reaction atmosphere does seem to affect toluene

selectivity. The selectivity of alkylated benzenes other than toluene, including ethylbenzene and xylenes, decreased as the reaction temperature increased as shown in Figure 5.8 (c) and (d). The opposite trends of benzene and C_8 alkylated benzenes with temperature suggested that dealkylation reactions were favored thermally, thus the equilibrium was driven forward to produce more benzene when temperature increased. Benzene derivatives selectivity (Figure 5.8 (e)) decreased sharply when temperature increased from 400 to 500 °C followed by no noticeable variation until 700 °C under both helium and methane atmosphere. At 800 °C, methane yielded even lower selectivity than that from 700 °C, whereas helium still yielded similar selectivity with that from 500 to 700 °C. The selectivity of polyaromatics (Figure 5.8 (f)) increased gradually and peaked at 700 °C. It was worth noting that the selectivity of polyaromatics under methane was lower than that under helium when temperature was equal to or higher than 600 °C. Polyaromatic compound, formed by the oligomerization of aromatic rings is considered as an indicator of catalyst coking. The results suggest that incorporation of methane into biomass catalysis pyrolysis could reduce the generation of polyaromatics and thus undermine catalyst coking.

(a)

(b)

(c)

(d)

(e)
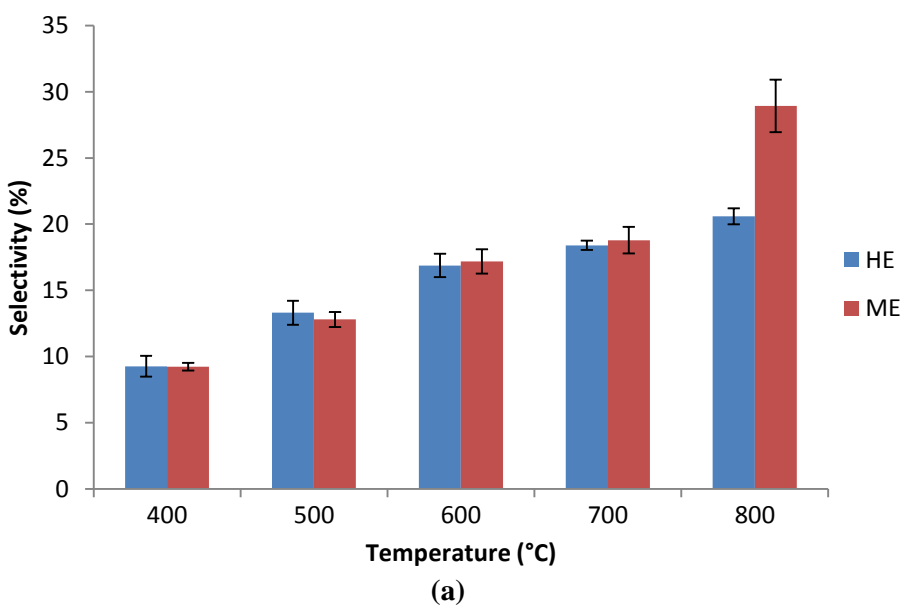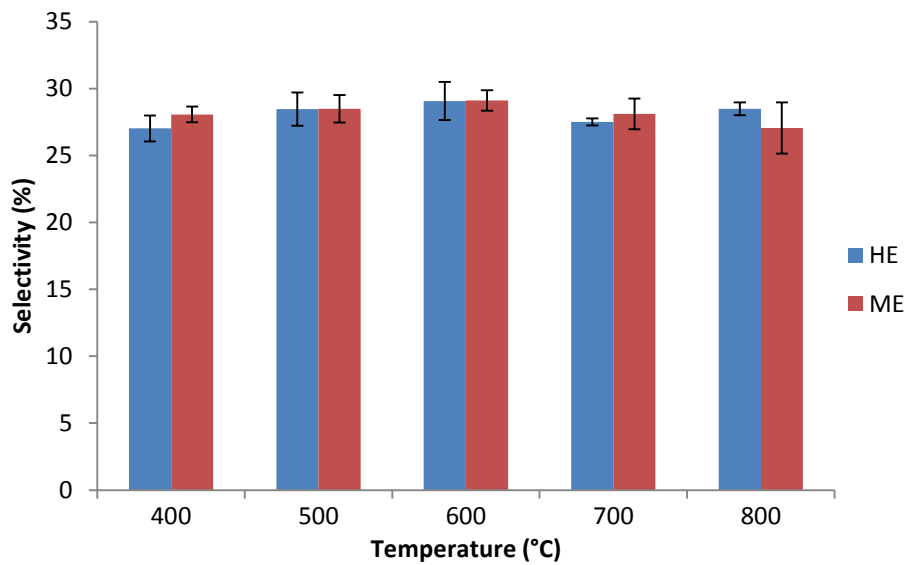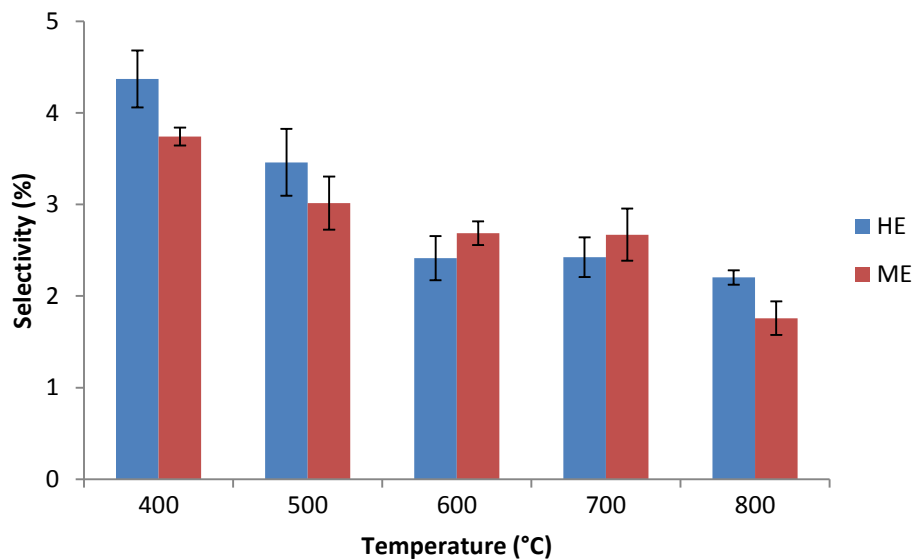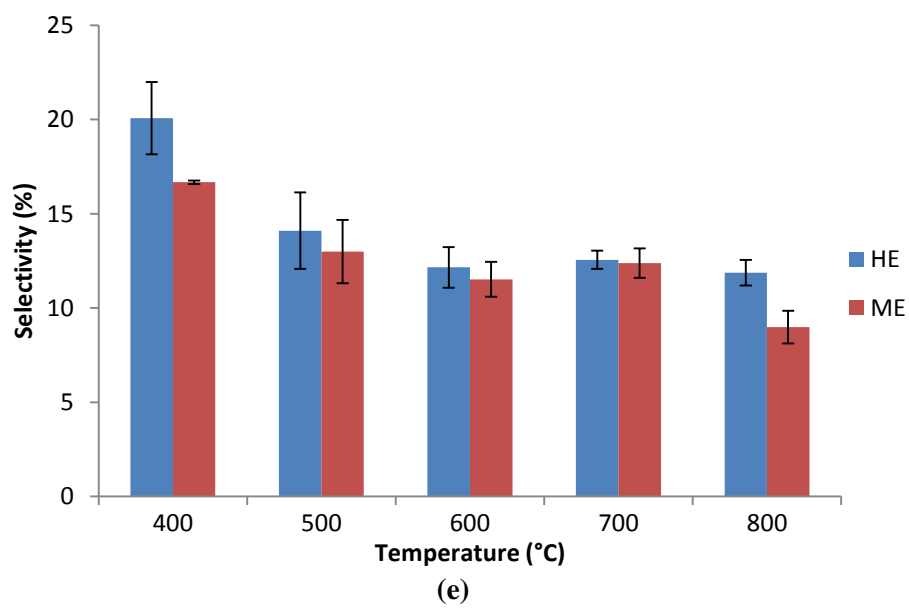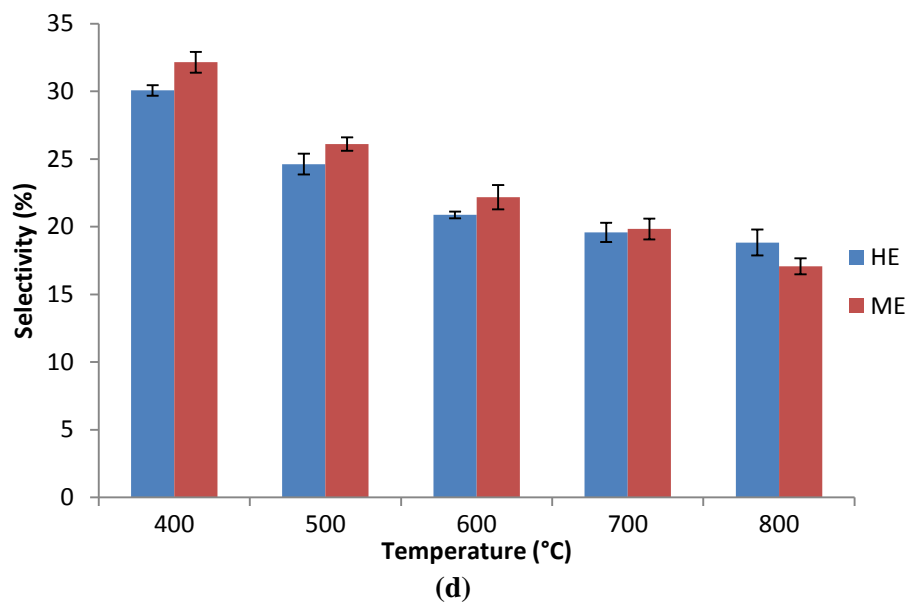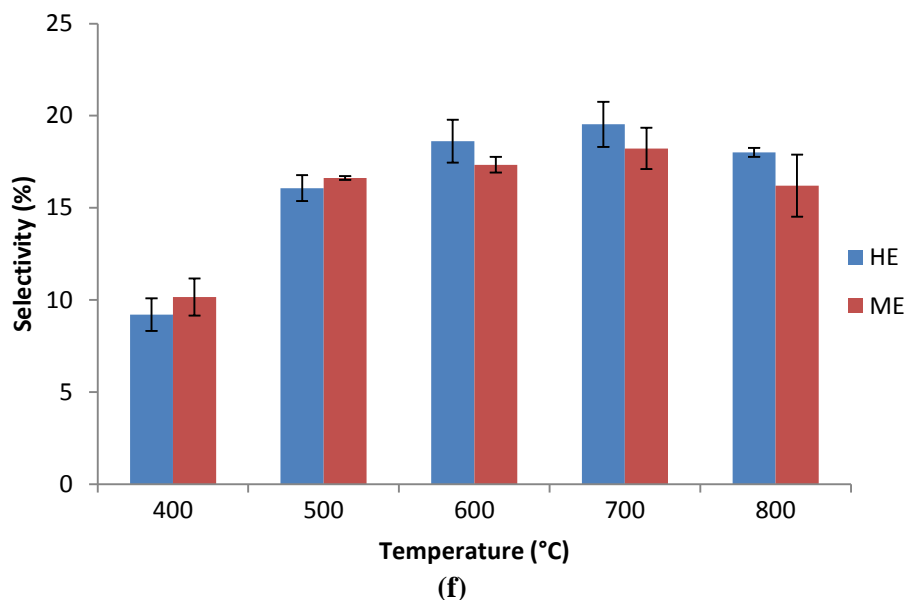
Figure 5.8. Aromatics selectivity of catalysis products of raw swichgrass as a function of operation temperature (a) ~ (f): Benzene, Toluene, Ethylbenzene, Xylenes, Benzene derivatives and Polyaromatics.

5.3.4. Effects of torrefaction on co-catalysis of biomass and methane

To investigate the impacts of torrefaction on the aromatics production from co-catalysis of biomass and methane, raw switchgrass, switchgrass torrefied at 230 °C and switchgrass torrefied at 270 °C were pyrolyzed at 700 °C in the presence of MoZn/HZSM-5 catalyst. The aromatics carbon yields are summarized in Table 5.3. The torrefied switchgrass did not yield more aromatics than raw switchgrass as expected, and the maximum aromatics carbon yield of 39.31 % was obtained from raw switchgrass under methane atmosphere. Furthermore, the aromatics carbon yield decreased sharply as the torrefaction temperature increased from 230 to 270 °C. In contrast, oxygenates yield decreased as the torrefaction temperature increased. Similar to raw switchgrass, the carbon yield of different groups of aromatics and total aromatics derived from torrefied switchgrass was also affected by co-feeding methane. However, the increase in aromatics carbon yield due to incorporation of methane decreased as the torrefaction temperature increased. The aromatics carbon yield from switchgrass torrefied at 230 °C was 22.40 % in helium, compared with 27.49 % in methane atmosphere. Similarly, the aromatics carbon yield

from switchgrass torrefied at 270 °C increased from 13.73 to 18.17 % when pyrolysis

environment switched from helium to methane. Neupane et al. [274] studied catalytic pyrolysis of

torrefied pine wood in presence of HZSM-5 (Si/Al=30) zeolite using Py-GC/MS at 550 °C. In

their study, weight loss during torrefaction at 225 °C for 45 min was 25.85 %, which was

comparable to weight loss of 25.01 % obtained in the current study. The torrefied pine wood

yielded a BTEX of 13.13 % [274], which was less than BTEX yield of 15.62 % obtained from

switchgrass in this study (Table 5.3). However, aromatics carbon yield of 26.68 % obtained from

torrefied pine wood was higher than that of 22.40 % obtained from switchgrass torrefied at 230

°C. The difference in aromatics carbon yield from switchgrass and pine wood with similar

torrefaction severity could be attributed to the difference in reaction temperature or the difference

in catalyst reactivity. Our results confirm that MoZn/HZSM-5 increased yield and selectivity of

BTEX (targeted aromatic hydrocarbons) as compared to only HZSM-5.

Table 5.3 Carbon yield of catalysis products of raw and torrefied switchgrass (C %)[a](SG=switchgrass, T230=torrefied at 230 °C, T270=torrefied at 270 °C, He=Helium, Me=Methane).

Trial	Aromatics			Total Aromatic HCs	Oxygenates
	BTEX	Benzene derivatives	Polyaromatics		
RSG, He	20.06±1.13[b]	3.71±0.30[a,b]	5.76±0.11[a,b]	29.53±1.31[b]	1.35±0.17[a,b]
RSG, Me	27.27±1.85[a]	4.88±0.65[a]	7.16±0.65[a]	39.31±2.87[a]	1.59±0.15[a]
T230, He	15.62±1.38[b,c]	2.42±0.19[c,d]	4.04±0.19[c,d]	22.40±1.69[c,d]	0.64±0.48[b,c]
T230, Me	19.38±0.53[b]	3.05±0.42[b,c]	5.06±0.72[b,c]	27.49±1.56[b,c]	0.92±0.28[a,b,c]
T270, He	10.33±1.02[d]	1.35±0.22[d]	2.05±0.18[e]	13.73±1.33[e]	0.48±0.20[c]
T270, Me	13.42±2.29[c,d]	1.73±0.60[d]	3.02±0.72[d,e]	18.17±3.61[d,e]	0.59±0.23[c]

[a]Means in the same column with no letter in common are significantly different ($p < 0.05$) from the Tukey's HSD test. The letters (a-e) superscripts refer to the highest estimates to the least.

The aromatics selectivity of raw and torrefied switchgrass in both helium and methane

atmosphere is illustrated in Figure 5.9. No difference in aromatics selectivity was observed

between helium and methane. The selectivity of BTEX from catalytic pyrolysis under helium was

67.91 % for raw switchgrass, compared with 70.69 and 75.25 % for switchgrass torrefied at 230

and 270 °C, respectively. For instance, the selectivity of benzene and toluene from catalysis of

raw switchgrass under helium was 18.40 and 27.52 %, respectively. As the torrefaction

temperature increased, the selectivity of benzene and toluene under helium increased from 20.21

and 29.21 %, respectively, at torrefaction temperature of 230 °C to 21.10 and 31.46 %,

respectively, at torrefaction temperature of 270 °C. On the contrary, the selectivity of

polyaromatics and benzene derivatives declined in the order of raw switchgrass>switchgrass

torrefied at 230 °C>switchgrass torrefied at 270 °C. The variation in aromatics selectivity with

torrefaction and torrefaction temperature are consistent with that reported in literature [199, 253].
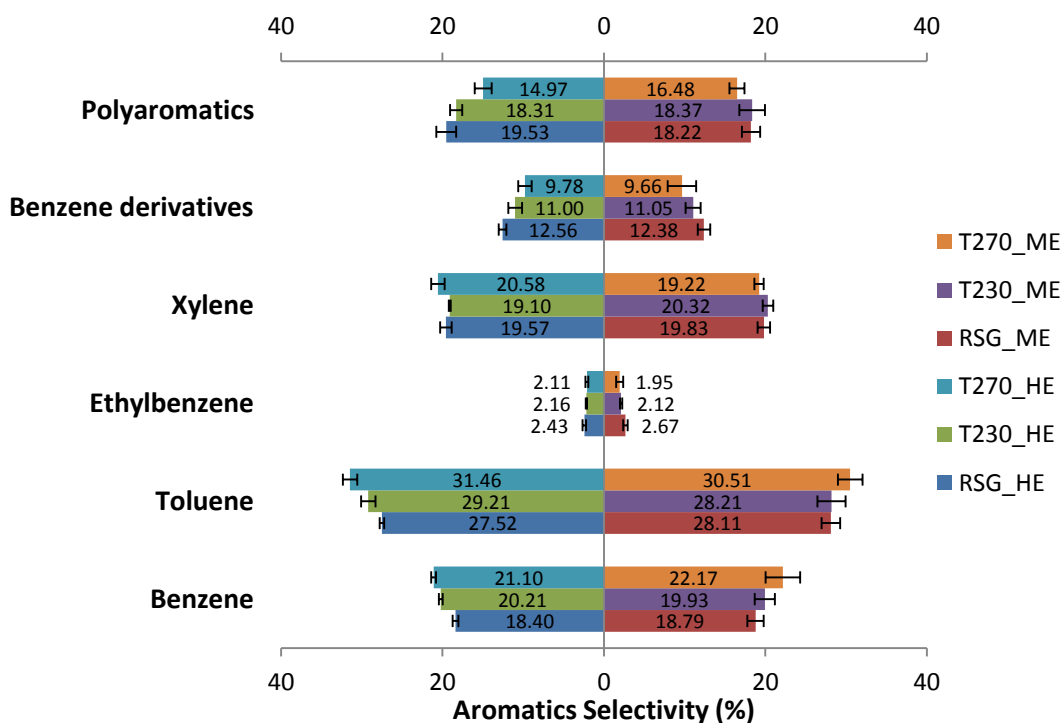
Figure 5.9 Aromatics selectivity of catalysis product from raw and torrefied switchgrass.

5.3.5. Effect of biomass components on co-catalysis of biomass and methane

To investigate the correlation between contents of biomass major components (cellulose,

hemicellulose and lignin) and its aromatics carbon yield from the catalytic pyrolysis, biomass

components (Table 5.1) was plotted against total aromatics yields (Table 5.3) in Figure 5.10. The

contents of two carbohydrates (cellulose and hemicellulose) were correlated positively with the

aromatics carbon yield. In contrast, content of lignin negatively correlated with the aromatics

yield. These results proved that aromatics yield from biomass components follow the order of cellulose > hemicellulose > lignin, which is consistent with the findings reported in previous studies [240, 241, 274]. Therefore, the lower aromatics yield obtained from torrefied switchgrass (as compared to raw switchgrass) could be attributed to the decrease in cellulose content and increase in lignin content during torrefaction. In order to maximize the aromatics yield from torrefied biomass, torrefaction reactor design and conditions should be optimized to increase the cellulose fraction and decrease the lignin fraction.

(a)

(b)
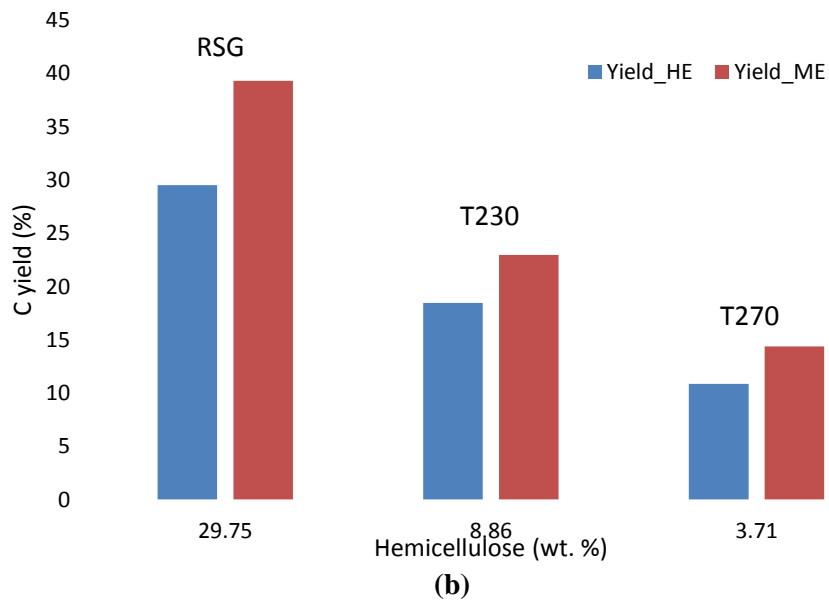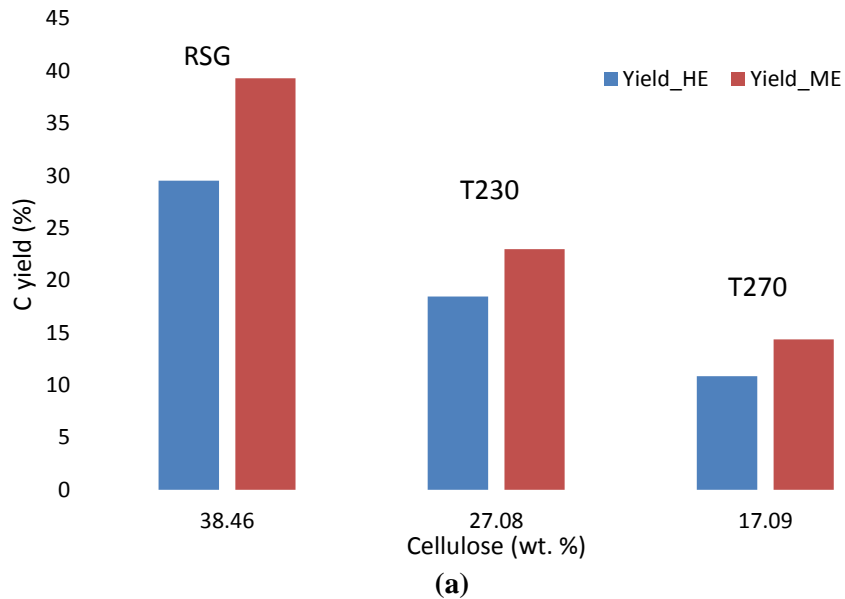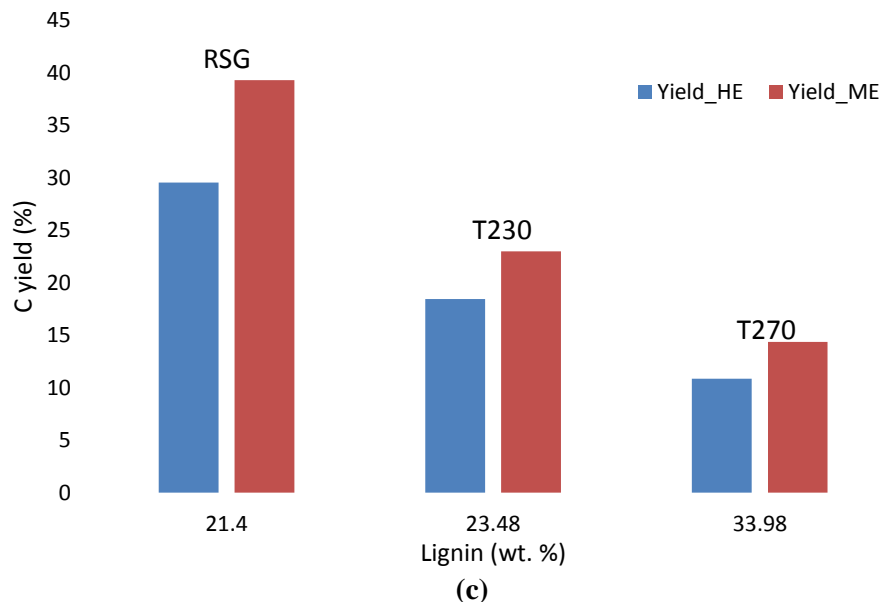
Figure 5.10 Aromatics carbon yield vs. weight percentages of cellulose (a), hemicellulose (b) and lignin (c) in samples pyrolyzed at 700 °C with MoZn/HZSM-5.

5.4. Conclusions

Co-catalysis of torrefied switchgrass and methane was investigated over molybdenum modified HZSM-5 catalysts. Bimetallic catalysts (MoAg/HZSM-5 and MoZn/HZSM-5) were more effective in catalyzing methane activation than molybdenum-only loaded (MoO$_3$/HZSM-5 and Mo$_2$C/HZSM-5) catalysts. A maximum aromatics yield obtained from raw switchgrass under methane atmosphere in presence of MoZn/HZSM-5 was 39.31 %, which was 33 % higher than that under helium atmosphere. Methane incorporation increased aromatics yield by up to 71 % at 600 °C. However, contrary to our expectation, torrefaction pretreatment did not increase the aromatics yield due to the reduced cellulose content and increased lignin content during torrefaction. The aromatic yield is highly dependent on the relative contents of cellulose, hemicellulose and lignin in biomass samples. Aromatic yield follows the trend of cellulose>hemicellulose>lignin.

130

CHAPTER VI

SUMMARY AND RECOMMENDATIONS FOR FUTURE WORK

6.1. Summary

The current study was conducted to improve the quality of the bio-oil produced from pyrolysis of lignocellulose biomass and to seek innovative pathways for producing renewable hydrocarbons. The pyrolytic behavior of eastern redcedar sapwood and heartwood were investigated under both fast and slow pyrolysis conditions at two temperatures (450 and 500 °C). Eastern redcedar wood demonstrated a G-H type lignin structure. The composition of bio-oil from fast pyrolysis condition was significantly affected by wood zones and reaction temperature; however, the interaction of these two effects was not significant for most bio-oil compounds. Slow pyrolysis yielded significantly more secondary pyrolysis products such as acetic acid, furfural and simple phenols than fast pyrolysis. In addition, slow pyrolysis turned out to be an alternative method to extract alpha/beta-cedrene, the major component of cedar oil.

Torrefaction and densification not only modified the physiochemical properties of switchgrass but also affected its pyrolysis product composition. Torrefaction enhanced the production of sugar-based compounds and phenols from pyrolysis. Densification enhanced the degradation of cellulose and hemicellulose thus promoted the production of secondary pyrolysis compounds, such as acetic acid, ketones and furans.

The final two chapters of this dissertation demonstrated an innovative biomass upgrading process with the intervention of low-cost methane to produce aromatic hydrocarbons in presence of molybdenum modified HZSM-5 zeolite. Of the three biomass constituents, cellulose was found to be the major contributor to the production of aromatics followed by hemicellulose and lignin. The introduction of methane enhanced the hydrodeoxygenation of lignin-derived phenols into aromatics. However, methane did not show any effect on improving production of aromatics from catalysis of cellulose or hemicellulose in presence of molybdenum-only modified HZSM-5 zeolites. The molybdenum modified HZSM-5 zeolites enhanced the deoxygenation of phenols thus inhibited the generation of polyaromatics during catalysis of lignin.

To improve the performance of the co-catalysis of biomass and methane, HZSM-5 zeolite was modified by loading bimetallic molybdenum-containing compounds, resulting two new catalysts MoAg/HZSM-5 and MoZn/HZSM-5, respectively. Both catalysts showed higher reactivity towards methane activation than molybdenum-only loaded catalysts. MoAg/HZSM-5 tended to catalyze dealkylation of alkylated benzenes thus yielded a product with high selectivity towards benzene. A dramatic increase in the yield of aromatic hydrocarbons was noticed when MoZn/HZSM-5 was used for catalysis of switchgrass under methane atmosphere. The maximum carbon yield of total aromatics of 39.31 % was obtained from catalysis of raw switchgrass under methane at 700 °C. The yield of aromatic hydrocarbons from catalysis was not further improved by pretreating the biomass feedstock via torrefaction as expected, because the significant loss of cellulose and concentration of lignin during torrefaction.

The present study provided a conceptual methodology on biomass-to-liquid process (BTL) through the integration of multiple upgrading processes, such as torrefaction, catalytic fast pyrolysis, and methane aromatization. Catalytic pyrolysis of biomass with the intervention of methane is a very promising technique for the hydrocarbon production. This combined conversion process has many benefits. Methane can be activated and incorporated into the carbon chain of biomass derived volatiles and thus improve the yield and quality of liquid product. In addition, the operational cost for bio-oil upgrading could be significantly reduced by switching from conventional hydrotreating processes to this combined process with the intervention of methane. The research and development on this co-conversion process is still at an early stage.

6.2. Future work

Recommendations for further exploration are:

I.   Reaction mechanisms and kinetics study

Although the current study proved the synergistic effect of methane activation and catalysis of biomass in presence of metal modified HZSM-5 zeolite, the detailed reaction

mechanisms associated with methane activation and the incorporation of methyl intermediates into the carbon chain of biomass-derived molecules are not fully understood. More advanced analytical techniques, such as isotopic labeling can be employed. In addition, methane activation appears to be the rate limiting step of the whole combined process. The kinetic study on methane activation is required to provide guidance on the selection of operation parameters for optimization.

II.   Lab-scale operational study

The current study demonstrated proof-of-concept of an innovative process which synergistically converted biomass and methane into liquid hydrocarbon fuels. A study is needed to determine how this new concept fits industry. The proposed process should be tested on a lab-scale experiment unit to obtain operational data to support the feasibility of this new technology.

III.   Techonoeconomic study on production of aromatics

An economic analysis of this synergistic process can be performed to estimate the yield of aromatic products and the production costs based on the experimental data obtained from the lab-scale study. Sensitivity analysis is required to understand the effects of operational parameters during production on the product yield and costs thus to maximize the profits of this process.

REFERENCES

[1] R. Venderbosch, W. Prins, Fast pyrolysis technology development, Biofuels, Bioproducts and Biorefining, 4 (2010) 178-208.

[2] A. Bridgwater, D. Meier, D. Radlein, An overview of fast pyrolysis of biomass, Organic Geochemistry, 30 (1999) 1479-1493.

[3] A.V. Bridgwater, Review of fast pyrolysis of biomass and product upgrading, Biomass and Bioenergy, 38 (2012) 68-94.

[4] M. Balat, An overview of the properties and applications of biomass pyrolysis oils, Energy Sources, Part A: Recovery, Utilization, and Environmental Effects, 33 (2011) 674-689.

[5] C.J. Deng, R.H. Liu, J.M. Cai, State of art of biomass fast pyrolysis for bio-oil in China: a review, Journal of the Energy Institute, 81 (2008) 211-217.

[6] D. Mohan, C.U. Pittman Jr, P.H. Steele, Pyrolysis of wood/biomass for bio-oil: a critical review, Energy & Fuels, 20 (2006) 848-889.

[7] D. Meier, O. Faix, State of the art of applied fast pyrolysis of lignocellulosic materials—a review, Bioresource Technology, 68 (1999) 71-77.

[8] S. Xiu, A. Shahbazi, Bio-oil production and upgrading research: A review, Renewable and Sustainable Energy Reviews, 16 (2012) 4406-4414.

[9] A.A. Boateng, D.E. Daugaard, N.M. Goldberg, K.B. Hicks, Bench-scale fluidized-bed pyrolysis of switchgrass for bio-oil production, Industrial & Engineering Chemistry Research, 46 (2007) 1891-1897.

[10] C.U. Pittman Jr, D. Mohan, A. Eseyin, Q. Li, L. Ingram, E.B.M. Hassan, B. Mitchell, H. Guo, P.H. Steele, Characterization of bio-oils produced from fast pyrolysis of corn stalks in an auger reactor, Energy & Fuels, 26 (2012) 3816-3825

[11] R. Li, Z.P. Zhong, B.S. Jin, X.X. Jiang, C.H. Wang, A.J. Zheng, Influence of reaction conditions and red brick on fast pyrolysis of rice residue (husk and straw) in a spout‐fluid bed, The Canadian Journal of Chemical Engineering, 90 (2011) 1202-1211.

[12] M. Bertero, G. de la Puente, U. Sedran, Fuels from bio-oils: Bio-oil production from different residual sources, characterization and thermal conditioning, Fuel, 95 (2012) 263-271.

[13] Q. Zhang, J. Chang, T. Wang, Y. Xu, Review of biomass pyrolysis oil properties and upgrading research, Energy conversion and management, 48 (2007) 87-92.

[14] S. Czernik, A. Bridgwater, Overview of applications of biomass fast pyrolysis oil, Energy & Fuels, 18 (2004) 590-598.

[15] A. Oasmaa, J. Korhonen, E. Kuoppala, An approach for stability measurement of wood-based fast pyrolysis bio-oils, Energy & Fuels, 25 (2011) 3307-3313.

[16] S. Czernik, Storage of biomass pyrolysis oils, in: Proceedings of Specialist Workshop on Biomass Pyrolysis Oil Properties and Combustion, 1994, pp. 26-28.

[17] M. Boucher, A. Chaala, H. Pakdel, C. Roy, Bio-oils obtained by vacuum pyrolysis of softwood bark as a liquid fuel for gas turbines. Part II: Stability and ageing of bio-oil and its blends with methanol and a pyrolytic aqueous phase, Biomass and Bioenergy, 19 (2000) 351-361.

[18] T. Ba, A. Chaala, M. Garcia-Perez, C. Roy, Colloidal properties of bio-oils obtained by vacuum pyrolysis of softwood bark. Storage stability, Energy & fuels, 18 (2004) 188-201.

[19] Upgrading of Biomass Fast Pyrolysis Oil (Bio-oil) Funding Opportunity Announcement Number: DE-FOA-0000342, in, U.S Department of Energy, 2010, pp. 33.

[20] D. Meier, B. van de Beld, A.V. Bridgwater, D.C. Elliott, A. Oasmaa, F. Preto, State-of-the-art of fast pyrolysis in IEA bioenergy member countries, Renewable and Sustainable Energy Reviews, 20 (2013) 619-641.

[21] D.C. Elliott, A. Oasmaa, F. Preto, D. Meier, A.V. Bridgwater, Results of the IEA round robin on viscosity and stability of fast pyrolysis bio-oils, Energy & Fuels, 26 (2012) 3769-3776.

[22] A.V. Bridgwater, Upgrading biomass fast pyrolysis liquids, Environ. Progress & Sustainable Energy, 31 (2012) 261-268.

[23] J. Manganaro, B. Chen, J. Adeosun, S. Lakhapatri, D. Favetta, A. Lawal, R. Farrauto, L. Dorazio, D. Rosse, Conversion of residual biomass into liquid transportation fuel: An energy analysis, Energy & Fuels, 25 (2011) 2711-2720.

[24] A. Oasmaa, C. Peacocke, S. Gust, D. Meier, R. McLellan, Norms and standards for pyrolysis liquids. End-user requirements and specifications, Energy & Fuels, 19 (2005) 2155-2163.

[25] A.V. Bridgewater, Biomass fast pyrolysis, Thermal Science, 8 (2004) 21-50.

[26] M. Garcıa-Perez, A. Chaala, C. Roy, Vacuum pyrolysis of sugarcane bagasse, Journal of Analytical and Applied Pyrolysis, 65 (2002) 111-136.

[27] A. Demirbas, Chemical Valorization of Wood for Bio-fuels and Bio-chemicals, Energy Sources, Part A: Recovery, Utilization, and Environmental Effects, 32 (2009) 1-9.

[28] J. Scahill, J. Diebold, C. Feik, Removal of residual char fines from pyrolysis vapors by hot gas filtration, Developments in thermochemical biomass conversion, (1997) 253-266.

[29] S. Czernik, D.K. Johnson, S. Black, Stability of wood fast pyrolysis oil, Biomass and Bioenergy, 7 (1994) 187-192.

[30] X. Hu, Y. Wang, D. Mourant, R. Gunawan, C. Lievens, W. Chaiwat, M. Gholizadeh, L. Wu, X. Li, C.-Z. Li, Polymerization on heating up of bio-oil: A model compound study, AIChE Journal, 59 (2012) 888-900.

[31] J.P. Diebold, A review of the chemical and physical mechanisms of the storage stability of fast pyrolysis bio-oils, National Renewable Energy Laboratory Golden, CO, 2000.

[32] A. Oasmaa, Fuel oil quality properties of wood-based pyrolysis liquids, University of Jyväskylä, 2003.

[33] A. Oasmaa, C. Peacocke, A guide to physical property characterisation of biomass-derived fast pyrolysis liquids, Technical Research Centre of Finland Espoo, 2001.

[34] D. Elliott, S. Lee, T. Hart, Stabilization of Fast Pyrolysis Oil: Post Processing, (2012).

[35] T.-S. Kim, J.-Y. Kim, K.-H. Kim, S. Lee, D. Choi, I.-G. Choi, J.W. Choi, The effect of storage duration on bio-oil properties, Journal of Analytical and Applied Pyrolysis, 95 (2012) 118-125.

[36] W. He, Q. Liu, L. Shi, Z. Liu, D. Ci, C. Lievens, X. Guo, M. Liu, Understanding the stability of pyrolysis tars from biomass in a view point of free radicals, Bioresource technology, 156 (2014) 372-375.

[37] J. Meng, T.I. Smirnova, X. Song, A. Moore, X. Ren, S. Kelley, S. Park, D. Tilotta, Identification of free radicals in pyrolysis oil and their impact on bio-oil stability, RSC Advances, 4 (2014) 29840-29846.

[38] J. Samanya, Thermal stability of sewage sludge pyrolysis oil, International Journal of Renewable Energy Research (IJRER), 1 (2011) 175-183.

[39] B. Batts, A.Z. Fathoni, A literature review on fuel stability studies with particular emphasis on diesel oil, Energy & Fuels, 5 (1991) 2-21.

[40] A. Siriwardhana, Aging and Stabilization of Pyrolitic Bio-Oils and Model Compounds, (2013).

[41] ASTM Standard D6468 − 08 Standard Test Method for High Temperature Stability of Middle Distillate Fuels, in, ASTM International, West Conshohocken, PA, 2013.

[42] ASTM D873 − 12 Standard Test Method for Oxidation Stability of Aviation Fuels (Potential Residue Method), in, ASTM International, West Conshohocken, PA, 2012.

[43] ASTM D2274 − 14 Standard Test Method for Oxidation Stability of Distillate Fuel Oil (Accelerated Method), in, ASTM International, West Conshohocken, PA, 2015.

[44] ASTM D525 − 12a Standard Test Method for Oxidation Stability of Gasoline (Induction Period Method), in, ASTM International, West Conshohocken, PA, 2012.

[45] R.N. Hilten, K. Das, Comparison of three accelerated aging procedures to assess bio-oil stability, Fuel, 89 (2010) 2741-2749.

[46] J.P. Diebold, S. Czernik, Additives to lower and stabilize the viscosity of pyrolysis oils during storage, Energy & Fuels, 11 (1997) 1081-1091.

[47] E. Alsbou, B. Helleur, Accelerated Aging of Bio-oil from Fast Pyrolysis of Hardwood, Energy & Fuels, 28 (2014) 3224-3235.

[48] J. Meng, A. Moore, D. Tilotta, S. Kelley, S. Park, Toward Understanding of Bio-Oil Aging: Accelerated Aging of Bio-Oil Fractions, ACS Sustainable Chemistry & Engineering, 2 (2014) 2011-2018.

[49] E.A. Smith, C. Thompson, Y.J. Lee, Petroleomic Characterization of Bio-Oil Aging using Fourier-Transform Ion Cyclotron Resonance Mass Spectrometry, Bull. Korean Chem. Soc, 35 (2014) 811.

[50] M. Cordella, C. Berrueco, F. Santarelli, N. Paterson, R. Kandiyoti, M. Millan, Yields and ageing of the liquids obtained by slow pyrolysis of sorghum, switchgrass and corn stalks, Journal of Analytical and Applied Pyrolysis, 104 (2013) 316-324.

[51] M. Garcia-Perez, T.T. Adams, J.W. Goodrum, K. Das, D.P. Geller, DSC studies to evaluate the impact of bio-oil on cold flow properties and oxidation stability of bio-diesel, Bioresource technology, 101 (2010) 6219-6224.

[52] U. Jena, K. Das, Comparative evaluation of thermochemical liquefaction and pyrolysis for bio-oil production from microalgae, Energy & Fuels, 25 (2011) 5472-5482.

[53] A. Oasmaa, E. Kuoppala, Fast pyrolysis of forestry residue. 3. Storage stability of liquid fuel, Energy & Fuels, 17 (2003) 1075-1084.

[54] M.W. Nolte, M.W. Liberatore, Real-time viscosity measurements during the accelerated aging of biomass pyrolysis oil, Energy & Fuels, 25 (2011) 3314-3317.

[55] J.V. Ortega, A.M. Renehan, M.W. Liberatore, A.M. Herring, Physical and chemical characteristics of aging pyrolysis oils produced from hardwood and softwood feedstocks, Journal of Analytical and Applied Pyrolysis, 91 (2011) 190-198.

[56] X. Jiang, Z. Zhong, N. Ellis, Q. Wang, Aging and Thermal Stability of the Mixed Product of the Ether‑Soluble Fraction of Bio‑Oil and Bio‑Diesel, Chemical Engineering & Technology, 34 (2011) 727-736.

[57] E. Hoekstra, S.R.A. Kersten, A. Tudos, D. Meier, K.J.A. Hogendoorn, Possibilities and pitfalls in analyzing (upgraded) pyrolysis oil by size exclusion chromatography (SEC), Journal of Analytical and Applied Pyrolysis, 91 (2011) 76-88.

[58] A. Oasmaa, E. Kuoppala, D.C. Elliott, Development of the basis for an analytical protocol for feeds and products of bio-oil hydrotreatment, Energy & Fuels, 26 (2012) 2454-2460.

[59] N.-E. El Mansouri, J. Salvadó, Analytical methods for determining functional groups in various technical lignins, Industrial Crops and Products, 26 (2007) 116-124.

[60] G.H. Schenk, Organic Functional Group Analysis: Theory and Development, Pergamon Press, 1968.

[61] B. Scholze, D. Meier, Characterization of the water-insoluble fraction from pyrolysis oil (pyrolytic lignin). Part I. PY–GC/MS, FTIR, and functional groups, Journal of Analytical and Applied Pyrolysis, 60 (2001) 41-54.

[62] B. Scholze, C. Hanser, D. Meier, Characterization of the water-insoluble fraction from fast pyrolysis liquids (pyrolytic lignin): Part II. GPC, carbonyl goups, and 13C-NMR, Journal of Analytical and Applied Pyrolysis, 58 (2001) 387-400.

[63] C.A. Mullen, G.D. Strahan, A.A. Boateng, Characterization of Various Fast-Pyrolysis Bio-Oils by NMR Spectroscopy†, Energy & fuels, 23 (2009) 2707-2718.

[64] G.D. Strahan, C.A. Mullen, A.A. Boateng, Characterizing biomass fast pyrolysis oils by 13C NMR and chemometric analysis, Energy & Fuels, 25 (2011) 5452-5461.

[65] O.D. Mante, F.A. Agblevor, Storage stability of biocrude oils from fast pyrolysis of poultry litter, Waste management, 32 (2012) 67-76.

[66] ASTM D 5304-06 Standard test method for assessing middle distillate fuel storage stability by oxygen overpressure, in, American Society for Testing and Materials, Easton, MD, 2006.

[67] ASTM E 2009-02 Standard test method for oxidation onset temperature of hydrocarbons by differential scanning calorimetry, in, American Society for Testing and Materials, Easton, MD, 2002.

[68] A. Oasmaa, E. Kuoppala, J.-F. Selin, S. Gust, Y. Solantausta, Fast pyrolysis of forestry residue and pine. 4. Improvement of the product quality by solvent addition, Energy & Fuels, 18 (2004) 1578-1583.

[69] A. Oasmaa, S. Czernik, Fuel oil quality of biomass pyrolysis oils state of the art for the end users, Energy & Fuels, 13 (1999) 914-921.

[70] R. Liu, W. Fei, C. Shen, Influence of acetone addition on the physicochemical properties of bio-oils, Journal of the Energy Institute, 87 (2014) 127-133.

[71] F. Wenting, L. Ronghou, Z. Weiqi, M. Yuanfei, Y. Renzhan, Influence of methanol additive on bio-oil stability, International Journal of Agricultural and Biological Engineering, 7 (2014) 83-92.

[72] J.A. Martin, C.A. Mullen, A.A. Boateng, Maximizing the stability of pyrolysis oil/diesel fuel emulsions, Energy & Fuels, 28 (2014) 5918-5929.

[73] M. Ikura, M. Stanciulescu, E. Hogan, Emulsification of pyrolysis derived bio-oil in diesel fuel, Biomass and bioenergy, 24 (2003) 221-232.

[74] X. Jiang, N. Ellis, Upgrading bio-oil through emulsification with biodiesel: mixture production, Energy & Fuels, 24 (2009) 1358-1364.

[75] X. Jiang, N. Ellis, Upgrading bio-oil through emulsification with biodiesel: thermal stability, Energy & Fuels, 24 (2010) 2699-2706.

[76] M. Garcia-Perez, T.T. Adams, J.W. Goodrum, D.P. Geller, K. Das, Production and fuel properties of pine chip bio-oil/biodiesel blends, Energy & Fuels, 21 (2007) 2363-2372.

[77] P.A. Zapata, J. Faria, M.P. Ruiz, D.E. Resasco, Condensation/hydrogenation of biomass-derived oxygenates in water/oil emulsions stabilized by nanohybrid catalysts, Topics in Catalysis, 55 (2012) 38-52.

[78] J.-L. Zheng, Q. Wei, Improving the quality of fast pyrolysis bio-oil by reduced pressure distillation, Biomass and Bioenergy, 35 (2011) 1804-1810.

[79] B.-S. Kang, K.H. Lee, H.J. Park, Y.-K. Park, J.-S. Kim, Fast pyrolysis of radiata pine in a bench scale plant with a fluidized bed: Influence of a char separation system and reaction conditions on the production of bio-oil, Journal of Analytical and Applied Pyrolysis, 76 (2006) 32-37.

[80] E. Hoekstra, K.J. Hogendoorn, X. Wang, R.J. Westerhof, S.R. Kersten, W.P. van Swaaij, M.J. Groeneveld, Fast pyrolysis of biomass in a fluidized bed reactor: in situ filtering of the vapors, Industrial & Engineering Chemistry Research, 48 (2009) 4744-4756.

[81] A. Pattiya, S. Suttibak, Influence of a glass wool hot vapour filter on yields and properties of bio-oil derived from rapid pyrolysis of paddy residues, Bioresource Technology, 116 (2012) 107-113.

[82] T. Chen, C. Wu, R. Liu, W. Fei, S. Liu, Effect of hot vapor filtration on the characterization of bio-oil from rice husks with fast pyrolysis in a fluidized-bed reactor, Bioresource Technology, 102 (2011) 6178-6185.

[83] R.M. Baldwin, C.J. Feik, Bio-oil Stabilization and Upgrading by Hot Gas Filtration, Energy & Fuels, 27 (2013) 3224-3238.

[84] M. Takht Ravanchi, T. Kaghazchi, A. Kargari, Application of membrane separation processes in petrochemical industry: a review, Desalination, 235 (2009) 199-244.

[85] A. Javaid, T. Ryan, G. Berg, X. Pan, T. Vispute, S.R. Bhatia, G.W. Huber, D.M. Ford, Removal of char particles from fast pyrolysis bio-oil by microfiltration, Journal of Membrane Science, 363 (2010) 120-127.

[86] C. Chiemchaisri, W. Chiemchaisri, T. Kornboonraksa, C. Dumrongsukit, S. Threedeach, H. Ngo, S. Vigneswaran, Particle and microorganism removal in floating plastic media coupled with microfiltration membrane for surface water treatment, Water Science & Technology, 51 (2005) 93-100.

[87] P. Paquin, Technological properties of high pressure homogenizers: the effect of fat globules, milk proteins, and polysaccharides, International Dairy Journal, 9 (1999) 329-335.

[88] R. He, X.P. Ye, F. Harte, B. English, Effects of high-pressure homogenization on physicochemical properties and storage stability of switchgrass bio-oil, Fuel Processing Technology, 90 (2009) 415-421.

[89] Y. Xu, T. Wang, L. Ma, Q. Zhang, L. Wang, Upgrading of liquid fuel from the vacuum pyrolysis of biomass over the Mo–Ni/γ-Al$_2$O$_3$ catalysts, Biomass and Bioenergy, 33 (2009) 1030-1036.

[90] Y.T. Cheng, J. Jae, J. Shi, W. Fan, G.W. Huber, Production of Renewable Aromatic Compounds by Catalytic Fast Pyrolysis of Lignocellulosic Biomass with Bifunctional Ga/ZSM‑5 Catalysts, Angewandte Chemie, 124 (2012) 1416-1419.

[91] T.R. Carlson, Y.-T. Cheng, J. Jae, G.W. Huber, Production of green aromatics and olefins by catalytic fast pyrolysis of wood sawdust, Energy & Environmental Science, 4 (2011) 145-161.

[92] R. Olcese, M. Bettahar, D. Petitjean, B. Malaman, F. Giovanella, A. Dufour, Gas-phase hydrodeoxygenation of guaiacol over Fe/SiO$_2$ catalyst, Applied Catalysis B: Environmental, 115 (2012) 63-73.

[93] R.J. French, J. Hrdlicka, R. Baldwin, Mild hydrotreating of biomass pyrolysis oils to produce a suitable refinery feedstock, Environmental Progress & Sustainable Energy, 29 (2010) 142-150.

[94] S. Fernando, D.A. Gunawardena, Deoxygenation of biomass derived oxygenates to hydrocarbons via direct methane intervention, in, Google Patents, 2011.

[95] W.-M. Xiong, M.-Z. Zhu, L. Deng, Y. Fu, Q.-X. Guo, Esterification of organic acid in bio-oil using acidic ionic liquid catalysts, Energy & Fuels, 23 (2009) 2278-2283.

[96] P. Weerachanchai, C. Tangsathitkulchai, M. Tangsathitkulchai, Effect of reaction conditions on the catalytic esterification of bio-oil, Korean Journal of Chemical Engineering, 29 (2012) 182-189.

[97] X. Li, R. Gunawan, C. Lievens, Y. Wang, D. Mourant, S. Wang, H. Wu, M. Garcia-Perez, C.-Z. Li, Simultaneous catalytic esterification of carboxylic acids and acetalisation of aldehydes in a fast pyrolysis bio-oil from mallee biomass, Fuel, 90 (2011) 2530-2537.

[98] N. Lohitharn, B.H. Shanks, Upgrading of bio-oil: Effect of light aldehydes on acetic acid removal via esterification, Catalysis Communications, 11 (2009) 96-99.

[99] T. Dickerson, J. Soria, Catalytic Fast Pyrolysis: A Review, Energies, 6 (2013) 514-538.

[100] E.G. Baker, D.C. Elliott, Catalytic Upgrading of Biomass Pyrolysis Oils, in: A.V. Bridgwater, J.L. Kuester (Eds.) Research in Thermochemical Biomass Conversion, Springer Netherlands, 1988, pp. 883-895.

[101] R.J. French, J. Stunkel, R.M. Baldwin, Mild Hydrotreating of Bio-Oil: Effect of Reaction Severity and Fate of Oxygenated Species, Energy & Fuels, 25 (2011) 3266-3274.

[102] L. Zhang, R. Liu, R. Yin, Y. Mei, Upgrading of bio-oil from biomass fast pyrolysis in China: A review, Renewable and Sustainable Energy Reviews, 24 (2013) 66-72.

[103] Y. Tang, S. Miao, B.H. Shanks, X. Zheng, Bifunctional mesoporous organic–inorganic hybrid silica for combined one-step hydrogenation/esterification, Applied Catalysis A: General, 375 (2010) 310-317.

[104] Y. Tang, S. Miao, L. Mo, X. Zheng, B.H. Shanks, One-Step Hydrogenation/Esterification Activity Enhancement Over Bifunctional Mesoporous Organic–Inorganic Hybrid Silicas, Topics in Catalysis, 56 (2013) 1804-1813.

[105] Z. Li, S. Kelkar, L. Raycraft, M. Garedew, J.E. Jackson, D.J. Miller, C.M. Saffron, A mild approach for bio-oil stabilization and upgrading: electrocatalytic hydrogenation using ruthenium supported on activated carbon cloth, Green Chemistry, 16 (2014) 844-852.

[106] Z. Guo, S. Wang, X. Wang, Stability mechanism investigation of emulsion fuels from biomass pyrolysis oil and diesel, Energy, 66 (2014) 250-255.

[107] A. Sanna, T.P. Vispute, G.W. Huber, Hydrodeoxygenation of the aqueous fraction of bio-oil with Ru/C and Pt/C catalysts, Applied Catalysis B: Environmental, 165 (2015) 446-456.

[108] Z. Tang, Y. Zhang, Q. Guo, Catalytic hydrocracking of pyrolytic lignin to liquid fuel in supercritical ethanol, Industrial & Engineering Chemistry Research, 49 (2010) 2040-2046.

[109] W. Qu, L. Wei, J. Julson, An Exploration of Improving the Properties of Heavy Bio-oil, Energy & Fuels, 27 (2013) 4717-4722.

[110] S. Thangalazhy-Gopakumar, S. Adhikari, R.B. Gupta, M. Tu, S. Taylor, Production of hydrocarbon fuels from biomass using catalytic pyrolysis under helium and hydrogen environments, Bioresour Technol, 102 (2011) 6742-6749.

[111] K. Iisa, A.R. Stanton, S. Czernik, Production of Hydrocarbon Fuels from Biomass by Catalytic Fast Pyrolysis, in, National Renewable Energy Laboratory (NREL), Golden, CO., 2012.

[112] C.A. Mullen, A.A. Boateng, Catalytic pyrolysis-GC/MS of lignin from several sources, Fuel Processing Technology, 91 (2010) 1446-1458.

[113] R. French, S. Czernik, Catalytic pyrolysis of biomass for biofuels production, Fuel Processing Technology, 91 (2010) 25-32.

[114] M. Milina, S. Mitchell, J. Pérez-Ramírez, Prospectives for bio-oil upgrading via esterification over zeolite catalysts, Catalysis Today, 235 (2014) 176-183.

[115] G.W. Huber, S. Iborra, A. Corma, Synthesis of transportation fuels from biomass: chemistry, catalysts, and engineering, Chemical reviews, 106 (2006) 4044-4098.

[116] N. Li, G.A. Tompsett, G.W. Huber, Renewable High‐Octane Gasoline by Aqueous‐Phase Hydrodeoxygenation of C5 and C6 Carbohydrates over Pt/Zirconium Phosphate Catalysts, ChemSusChem, 3 (2010) 1154-1157.

[117] N. Li, G.W. Huber, Aqueous-phase hydrodeoxygenation of sorbitol with Pt/SiO2–Al2O3: Identification of reaction intermediates, Journal of Catalysis, 270 (2010) 48-59.

[118] H. Wang, J. Male, Y. Wang, Recent advances in hydrotreating of pyrolysis bio-oil and its oxygen-containing model compounds, Acs Catalysis, 3 (2013) 1047-1070.

[119] D.C. Elliott, T.R. Hart, Catalytic hydroprocessing of chemical models for bio-oil, Energy & Fuels, 23 (2008) 631-637.

[120] D.C. Elliott, Historical developments in hydroprocessing bio-oils, Energy & Fuels, 21 (2007) 1792-1815.

[121] P.M. Mortensen, J.-D. Grunwaldt, P.A. Jensen, K. Knudsen, A.D. Jensen, A review of catalytic upgrading of bio-oil to engine fuels, Applied Catalysis A: General, 407 (2011) 1-19.

[122] A.G. Gayubo, A.T. Aguayo, A. Atutxa, R. Aguado, M. Olazar, J. Bilbao, Transformation of oxygenate components of biomass pyrolysis oil on a HZSM-5 zeolite. II. Aldehydes, ketones, and acids, Industrial & Engineering Chemistry Research, 43 (2004) 2619-2626.

[123] M.A. Patel, M. Baldanza, V. Teixeira da Silva, A. Bridgwater, In situ catalytic upgrading of bio-oil using supported molybdenum carbide, Applied Catalysis A: General, 458 (2013) 48-54.

[124] A. Demirbaş, Biomass resource facilities and biomass conversion processing for fuels and chemicals, Energy conversion and management, 42 (2001) 1357-1378.

[125] A. Kumar, D.D. Jones, M.A. Hanna, Thermochemical biomass gasification: A review of the current status of the technology, Energies, 2 (2009) 556-581.

[126] M. Paster, J.L. Pellegrino, T.M. Carole, Industrial bioproducts; today and tomorrow, in: Industrial bioproducts; today and tomorrow, DOE-EERE, 2003.

[127] C.A. Mullen, A.A. Boateng, N.M. Goldberg, I.M. Lima, D.A. Laird, K.B. Hicks, Bio-oil and bio-char production from corn cobs and stover by fast pyrolysis, Biomass and Bioenergy, 34 (2010) 67-74.

[128] A. Effendi, H. Gerhauser, A.V. Bridgwater, Production of renewable phenolic resins by thermochemical conversion of biomass: A review, Renewable and Sustainable Energy Reviews, 12 (2008) 2092-2116.

[129] V. Goia, C.-C. Cormos, P.S. Agachi, Influence of temperature and heating rate on biomass pyrolysis in a fixed-bed reactor, Studia Universitatis Babes-Bolyai Chemia, 56 (2011) 49-56.

[130] D. Chen, J. Zhou, Q. Zhang, Effects of heating rate on slow pyrolysis behavior, kinetic parameters and products properties of moso bamboo, Bioresource Technology, 169 (2014) 313-319.

[131] Y.-K. Park, M.L. Yoo, H.W. Lee, S.H. Park, S.-C. Jung, S.-S. Park, S.-C. Kim, Effects of operation conditions on pyrolysis characteristics of agricultural residues, Renewable Energy, 42 (2012) 125-130.

[132] J. Shen, X.S. Wang, M. Garcia-Perez, D. Mourant, M.J. Rhodes, C.Z. Li, Effects of particle size on the fast pyrolysis of oil mallee woody biomass, Fuel, 88 (2009) 1810-1817.

[133] J. Akhtar, N.S. Amin, A review on operating parameters for optimum liquid oil yield in biomass pyrolysis, Renewable & Sustainable Energy Reviews, 16 (2012) 5101-5109.

[134] R. He, X.P. Ye, B.C. English, J.A. Satrio, Influence of pyrolysis condition on switchgrass bio-oil yield and physicochemical properties, Bioresource Technology, 100 (2009) 5305-5311.

[135] L. Ingram, D. Mohan, M. Bricka, P. Steele, D. Strobel, D. Crocker, B. Mitchell, J. Mohammad, K. Cantrell, C.U. Pittman Jr, Pyrolysis of wood and bark in an auger reactor: physical properties and chemical analysis of the produced bio-oils, Energy & Fuels, 22 (2007) 614-625.

[136] R.A. Jordan, L.A.B. Cortez, J.M.M. Perez, H.R.M. Mesa, J.D. Rocha, Operationalization of a fast pyrolysis plant of biomass with fluidized bed reactor, Engenharia na Agricultura, 18 (2010) 472-479.

[137] A.R. Fernandez-Akarregi, J. Makibar, G. Lopez, M. Amutio, M. Olazar, Design and operation of a conical spouted bed reactor pilot plant (25 kg/h) for biomass fast pyrolysis, Fuel Processing Technology, 112 (2013) 48-56.

[138] Y.-C. Lin, J. Cho, G.A. Tompsett, P.R. Westmoreland, G.W. Huber, Kinetics and mechanism of cellulose pyrolysis, The Journal of Physical Chemistry C, 113 (2009) 20097-20107.

[139] A. Lourenco, D.M. Neiva, J. Gominho, A.V. Marques, H. Pereira, Characterization of lignin in heartwood, sapwood and bark from Tectona grandis using Py-GC-MS/FID, Wood Science and Technology, 49 (2015) 159-175.

[140] D. Fengel, G. Wegener, Wood: chemistry, ultrastructure, reactions, Walter de Gruyter, 1983.

[141] A. Lourenço, I. Baptista, J. Gominho, H. Pereira, The influence of heartwood on the pulping properties of Acacia melanoxylon wood, Journal of wood science, 54 (2008) 464-469.

[142] Y. Atac, H. Eroğlu, The effects of heartwood and sapwood on kraft pulp properties of Pinus nigra JF Arnold and Abies bornmuelleriana Mattf, Turkish Journal of Agriculture and Forestry, 37 (2013) 243-248.

[143] R.W. Lykins, Estimation of aboveground eastern redcedar biomass, in, Oklahoma State University, 1995.

[144] K. Price, J. Brooks, D. Dobbeleare, T. Gaines-Bey, K. Loftus, K. Starzec, The susceptibility of native grasslands to woody plant encroachment: A study of juniperus virginiana, (2010).

[145] E. Semen, S. Hiziroglu, Production, yield and derivatives of volatile oils from eastern redcedar (< i> juniperus virginiana</i> l.), American Journal of Environmental Sciences, 1 (2005) 133-138.

[146] M.L. Wine, T.E. Ochsner, A. Sutradhar, R. Pepin, Effects of eastern redcedar encroachment on soil hydraulic properties along Oklahoma's grassland‐forest ecotone, Hydrological Processes, 26 (2012) 1720-1728.

[147] D. Engle, J. Stritzke, P. Claypool, Herbage standing crop around eastern redcedar trees, Journal of Range Management, (1987) 237-239.

[148] J.R. Weir, D.M. Engle, Cedar control by individual scorched-tree ignition following fire, Division of Agricultural Sciences and Natural Resources, Oklahoma State University, 2011.

[149] A.J. Gawde, V.D. Zheljazkov, V. Maddox, C.L. Cantrell, Bioprospection of Eastern red cedar from nine physiographic regions in Mississippi, Industrial Crops and Products, 30 (2009) 59-64.

[150] F.J. Eller, J.W. King, Supercritical carbon dioxide extraction of cedarwood oil: a study of extraction parameters and oil characteristics, Phytochemical Analysis, 11 (2000) 226-231.

[151] K. Qian, A. Kumar, H. Zhang, D. Bellmer, R. Huhnke, Recent advances in utilization of biochar, Renewable and Sustainable Energy Reviews, 42 (2015) 1055-1064.

[152] A. Sluiter, B. Hames, R. Ruiz, C. Scarlata, J. Sluiter, D. Templeton, D. Crocker, Determination of structural carbohydrates and lignin in biomass, Laboratory analytical procedure, (2008).

[153] A. Sluiter, R. Ruiz, C. Scarlata, J. Sluiter, D. Templeton, Determination of extractives in biomass, Laboratory Analytical Procedure (LAP), 1617 (2005).

[154] K.D. Ramachandriya, M. Wilkins, O. Pardo-Planas, H.K. Atiyeh, N.T. Dunford, S. Hiziroglu, Simultaneous saccharification and fermentation of Eastern redcedar heartwood and sapwood using a novel size reduction technique, Bioresource Technology, 161 (2014) 1-9.

[155] V. Pasangulapati, K.D. Ramachandriya, A. Kumar, M.R. Wilkins, C.L. Jones, R.L. Huhnke, Effects of cellulose, hemicellulose and lignin on thermochemical conversion characteristics of the selected biomass, Bioresource Technology, 114 (2012) 663-669.

[156] S. Thangalazhy-Gopakumar, S. Adhikari, R.B. Gupta, S.D. Fernando, Influence of pyrolysis operating conditions on bio-oil components: a microscale study in a pyroprobe, Energy & Fuels, 25 (2011) 1191-1199.

[157] V. Srinivasan, S. Adhikari, S.A. Chattanathan, S. Park, Catalytic pyrolysis of torrefied biomass for hydrocarbons production, Energy & Fuels, 26 (2012) 7347-7353.

[158] A. Wiedenhoeft, Structure and function of wood, Wood Technology, 3 (2010) 12.

[159] K. Wang, K.H. Kim, R.C. Brown, Catalytic pyrolysis of individual components of lignocellulosic biomass, Green Chemistry, 16 (2014) 727-735.

[160] F. Shafizadeh, Introduction to pyrolysis of biomass, Journal of Analytical and Applied Pyrolysis, 3 (1982) 283-305.

[161] C. Popescu, C. Vasile, M. Popescu, G. Singurel, V. Popa, B. Munteanu, Analytical methods for lignin characterization. II. Spectroscopic studies, Cellulose chemistry and technology, 40 (2006) 597.

[162] M. Garcia-Perez, S. Wang, J. Shen, M. Rhodes, W.J. Lee, C.-Z. Li, Effects of Temperature on the Formation of Lignin-Derived Oligomers during the Fast Pyrolysis of Mallee Woody Biomass, Energy & Fuels, 22 (2008) 2022-2032.

[163] M. Amutio, G. Lopez, M. Artetxe, G. Elordi, M. Olazar, J. Bilbao, Influence of temperature on biomass pyrolysis in a conical spouted bed reactor, Resources, Conservation and Recycling, 59 (2012) 23-31.

[164] A. Zhurinsh, J. Zandersons, G. Dobele, Slow pyrolysis studies for utilization of impregnated waste timber materials, Journal of Analytical and Applied Pyrolysis, 74 (2005) 439-444.

[165] T.R. Kosanic, M.B. Ceranic, S.N. Duric, V.R. Grkovic, M.M. Milotic, S.D. Brankov, Experimental investigation of pyrolysis process of woody biomass mixture, Journal of Thermal Science, 23 (2014) 290-296.

[166] A.N. Phan, C. Ryu, V.N. Sharifi, J. Swithenbank, Characterisation of slow pyrolysis products from segregated wastes for energy production, Journal of Analytical and Applied Pyrolysis, 81 (2008) 65-71.

[167] S. Uçar, S. Karagöz, The slow pyrolysis of pomegranate seeds: the effect of temperature on the product yields and bio-oil properties, Journal of analytical and applied Pyrolysis, 84 (2009) 151-156.

[168] K.H. Kim, T.-S. Kim, S.-M. Lee, D. Choi, H. Yeo, I.-G. Choi, J.W. Choi, Comparison of physicochemical features of biooils and biochars produced from various woody biomasses by fast pyrolysis, Renewable Energy, 50 (2013) 188-195.

[169] S.-S. Liaw, Z. Wang, P. Ndegwa, C. Frear, S. Ha, C.-Z. Li, M. Garcia-Perez, Effect of pyrolysis temperature on the yield and properties of bio-oils obtained from the auger pyrolysis of Douglas Fir wood, Journal of Analytical and Applied Pyrolysis, 93 (2012) 52-62.

[170] V. Strezov, B. Moghtaderi, J. Lucas, Thermal study of decomposition of selected biomass samples, Journal of thermal analysis and calorimetry, 72 (2003) 1041-1048.

[171] D. Mohan, C.U. Pittman, P.H. Steele, Pyrolysis of wood/biomass for bio-oil: a critical review, Energy & Fuels, 20 (2006) 848-889.

[172] M. Garcia-Perez, X.S. Wang, J. Shen, M.J. Rhodes, F. Tian, W.-J. Lee, H. Wu, C.-Z. Li, Fast pyrolysis of oil mallee woody biomass: effect of temperature on the yield and quality of pyrolysis products, Industrial & Engineering Chemistry Research, 47 (2008) 1846-1854.

[173] M. Bajus, Pyrolysis of woody material, Petroleum & Coal, 52 (2010) 207-214.

[174] D.K. Shen, S. Gu, A.V. Bridgwater, Study on the pyrolytic behaviour of xylan-based hemicellulose using TG–FTIR and Py–GC–FTIR, Journal of Analytical and Applied Pyrolysis, 87 (2010) 199-206.

[175] C.A. Mullen, A.A. Boateng, Chemical composition of bio-oils produced by fast pyrolysis of two energy crops, Energy & Fuels, 22 (2008) 2104-2109.

[176] M.-J. Jeon, J.-K. Jeon, D.J. Suh, S.H. Park, Y.J. Sa, S.H. Joo, Y.-K. Park, Catalytic pyrolysis of biomass components over mesoporous catalysts using Py-GC/MS, Catalysis Today, 204 (2013) 170-178.

[177] R.P. Adams, Identification of essential oils by ion trap mass spectroscopy, Academic Press, 2012.

[178] L. Waldheim, T. Nilsson, Heating value of gases from biomass gasification, Report prepared for: IEA Bioenergy Agreement, Task, 20 (2001).

[179] V.L. Budarin, J.H. Clark, B.A. Lanigan, P. Shuttleworth, S.W. Breeden, A.J. Wilson, D.J. Macquarrie, K. Milkowski, J. Jones, T. Bridgeman, The preparation of high-grade bio-oils through the controlled, low temperature microwave activation of wheat straw, Bioresour Technol, 100 (2009) 6064-6068.

[180] X. Wu, J. McLaren, R. Madl, D. Wang, Biofuels from lignocellulosic biomass, in: Sustainable Biotechnology, Springer, 2010, pp. 19-41.

[181] S. Sokhansanj, S. Mani, A. Turhollow, A. Kumar, D. Bransby, L. Lynd, M. Laser, Large‐scale production, harvest and logistics of switchgrass (Panicum virgatum L.)‐current technology and envisioning a mature technology, Biofuels, Bioproducts and Biorefining, 3 (2009) 124-141.

[182] A.M. Roth, D.W. Sample, C.A. Ribic, L. Paine, D.J. Undersander, G.A. Bartelt, Grassland bird response to harvesting switchgrass as a biomass energy crop, Biomass and Bioenergy, 28 (2005) 490-498.

[183] A.J.R. Kasi David, Switchgrass as an energy crop for biofuel production: A review of its lignocellulosic chemical properties, Energy and Environmental Science, 3 (2010) 1182-1190.

[184] C. Karunanithy, Y. Wang, K. Muthukumarappan, S. Pugalendhi, Physiochemical characterization of briquettes made from different feedstocks, Biotechnology research international, 2012 (2012).

[185] X. Yang, Y. Zeng, F. Ma, X. Zhang, H. Yu, Effect of biopretreatment on thermogravimetric and chemical characteristics of corn stover by different white-rot fungi, Bioresource Technology, 101 (2010) 5475-5479.

[186] J. Shankar Tumuluru, S. Sokhansanj, J.R. Hess, C.T. Wright, R.D. Boardman, REVIEW: A review on biomass torrefaction process and product properties for energy applications, Industrial Biotechnology, 7 (2011) 384-401.

[187] J.S. Tumuluru, Effect of process variables on the density and durability of the pellets made from high moisture corn stover, Biosystems Engineering, 119 (2014) 44-57.

[188] S. Vichaphund, D. Aht-ong, V. Sricharoenchaikul, D. Atong, Catalytic upgrading pyrolysis vapors of Jatropha waste using metal promoted ZSM-5 catalysts: An analytical PY-GC/MS, Renewable energy, 65 (2014) 70-77.

[189] J. Meng, J. Park, D. Tilotta, S. Park, The effect of torrefaction on the chemistry of fast-pyrolysis bio-oil, Bioresour Technol, 111 (2012) 439-446.

[190] W. De Jong, A. Pirone, M. Wojtowicz, Pyrolysis of Miscanthus Giganteus and wood pellets: TG-FTIR analysis and reaction kinetics, Fuel, 82 (2003) 1139-1147.

[191] M. Sarkar, A. Kumar, J.S. Tumuluru, K.N. Patil, D.D. Bellmer, Gasification performance of switchgrass pretreated with torrefaction and densification, Applied Energy, 127 (2014) 194-201.

[192] A. Boateng, C. Mullen, Fast pyrolysis of biomass thermally pretreated by torrefaction, Journal of Analytical and Applied Pyrolysis, 100 (2013) 95-102.

[193] S. Ren, H. Lei, L. Wang, Q. Bu, S. Chen, J. Wu, J. Julson, R. Ruan, The effects of torrefaction on compositions of bio-oil and syngas from biomass pyrolysis by microwave heating, Bioresource technology, 135 (2013) 659-664.

[194] V. Pasangulapati, K.D. Ramachandriya, A. Kumar, M.R. Wilkins, C.L. Jones, R.L. Huhnke, Effects of cellulose, hemicellulose and lignin on thermochemical conversion characteristics of the selected biomass, Bioresource technology, 114 (2012) 663-669.

[195] H. Yang, R. Yan, H. Chen, D.H. Lee, C. Zheng, Characteristics of hemicellulose, cellulose and lignin pyrolysis, Fuel, 86 (2007) 1781-1788.

[196] T. Hosoya, H. Kawamoto, S. Saka, Cellulose–hemicellulose and cellulose–lignin interactions in wood pyrolysis at gasification temperature, Journal of analytical and applied pyrolysis, 80 (2007) 118-125.

[197] S. Wang, X. Guo, K. Wang, Z. Luo, Influence of the interaction of components on the pyrolysis behavior of biomass, Journal of Analytical and Applied Pyrolysis, 91 (2011) 183-189.

[198] T. Hosoya, H. Kawamoto, S. Saka, Solid/liquid-and vapor-phase interactions between cellulose-and lignin-derived pyrolysis products, Journal of Analytical and Applied Pyrolysis, 85 (2009) 237-246.

[199] A. Zheng, Z. Zhao, S. Chang, Z. Huang, F. He, H. Li, Effect of torrefaction temperature on product distribution from two-staged pyrolysis of biomass, Energy & Fuels, 26 (2012) 2968-2974.

[200] M.J.J. Antal, G. Varhegyi, Cellulose pyrolysis kinetics: the current state of knowledge, Industrial & Engineering Chemistry Research, 34 (1995) 703-717.

[201] A. Demirbaş, Mechanisms of liquefaction and pyrolysis reactions of biomass, Energy Conversion and Management, 41 (2000) 633-646.

[202] O. Boutin, M. Ferrer, J. Lédé, Radiant flash pyrolysis of cellulose—Evidence for the formation of short life time intermediate liquid species, Journal of Analytical and Applied Pyrolysis, 47 (1998) 13-31.

[203] X. Zhu, Q. Lu, Production of chemicals from selective fast pyrolysis of biomass, SCIYO. COM, (2010) 147.

[204] J. Piskorz, D.S.A.G. Radlein, D.S. Scott, S. Czernik, Pretreatment of wood and cellulose for production of sugars by fast pyrolysis, Journal of Analytical and Applied Pyrolysis, 16 (1989) 127-142.

[205] B. Rijal, C. Igathinathane, B. Karki, M. Yu, S.W. Pryor, Combined effect of pelleting and pretreatment on enzymatic hydrolysis of switchgrass, Bioresource Technology, 116 (2012) 36-41.

[206] P. McKendry, Energy production from biomass (part 1): overview of biomass, Bioresour. Tech., 83 (2002) 37-46.

[207] A.V. Bridgewater, Biomass fast pyrolysis, Thermal Sci., 8 (2004) 21-50.

[208] R. Venderbosch, W. Prins, Fast pyrolysis technology development, Biofuels, Bioprod. and Biorefining, 4 (2010) 178-208.

[209] T. Dickerson, J. Soria, Catalytic Fast Pyrolysis: A Rev., Energies, 6 (2013) 514-538.

[210] H. Zhang, T.R. Carlson, R. Xiao, G.W. Huber, Catalytic fast pyrolysis of wood and alcohol mixtures in a fluidized bed reactor, Green Chem., 14 (2012) 98-110.

[211] T.R. Carlson, G.A. Tompsett, W.C. Conner, G.W. Huber, Aromatic production from catalytic fast pyrolysis of biomass-derived feedstocks, Topics in Catalysis, 52 (2009) 241-252.

[212] T.R. Carlson, Y.-T. Cheng, J. Jae, G.W. Huber, Production of green aromatics and olefins by catalytic fast pyrolysis of wood sawdust, Energy & Environ. Sci., 4 (2011) 145-161.

[213] S. Thangalazhy-Gopakumar, S. Adhikari, R.B. Gupta, Catalytic pyrolysis of biomass over H+ ZSM-5 under hydrogen pressure, Energy & Fuels, 26 (2012) 5300-5306.

[214] C.A. Mullen, A.A. Boateng, Catalytic pyrolysis-GC/MS of lignin from several sources, Fuel Proc. Tech., 91 (2010) 1446-1458.

[215] D.A. Gunawardena, S.D. Fernando, Deoxygenation of Methanol over ZSM‐5 in a High‐Pressure Catalytic Pyroprobe, Chem. eng. & tech., 34 (2011) 173-178.

[216] S. Thangalazhy-Gopakumar, S. Adhikari, R.B. Gupta, M. Tu, S. Taylor, Production of hydrocarbon fuels from biomass using catalytic pyrolysis under helium and hydrogen environments, Bioresour. Tech., 102 (2011) 6742-6749.

[217] H. Zhang, Y.-T. Cheng, T.P. Vispute, R. Xiao, G.W. Huber, Catalytic conversion of biomass-derived feedstocks into olefins and aromatics with ZSM-5: the hydrogen to carbon effective ratio, Energy & Environ. Sci., 4 (2011) 2297-2307.

[218] A. Zheng, Z. Zhao, S. Chang, Z. Huang, K. Zhao, H. Wu, X. Wang, F. He, H. Li, Maximum synergistic effect in the coupling conversion of bio-derived furans and methanol over ZSM-5 for enhancing aromatic production, Green Chem., 16 (2014) 2580-2586.

[219] P.A. Horne, N. Nugranad, P.T. Williams, Catalytic coprocessing of biomass-derived pyrolysis vapours and methanol, J. of Analytical and Appl. Pyrolysis, 34 (1995) 87-108.

[220] J.J. Spivey, G. Hutchings, Catalytic aromatization of methane, Chem. Soc. Rev., 43 (2014) 792-803.

[221] N. Mamonov, E. Fadeeva, D. Grigoriev, M. Mikhailov, L.M. Kustov, S. Alkhimov, Metal/zeolite catalysts of methane dehydroaromatization, Russian Chem. Rev., 82 (2013) 567.

[222] A. Holmen, Direct conversion of methane to fuels and chemicals, Catalysis Today, 142 (2009) 2-8.

[223] Z.R. Ismagilov, E.V. Matus, L.T. Tsikoza, Direct conversion of methane on Mo/ZSM-5 catalysts to produce benzene and hydrogen: achievements and perspectives, Energy & Environ. Sci., 1 (2008) 526-541.

[224] M.C. Iliuta, I. Iliuta, B.P. Grandjean, F. Larachi, Kinetics of methane nonoxidative aromatization over Ru-Mo/HZSM-5 catalyst, Ind. & eng. chem. res., 42 (2003) 3203-3209.

[225] R. Ohnishi, S.T. Liu, Q. Dong, L. Wang, M. Ichikawa, Catalytic dehydrocondensation of methane with CO and CO2 toward benzene and naphthalene on Mo/HZSM-5 and Fe/Co-modified Mo/HZSM-5, J. of Catalysis, 182 (1999) 92-103.

[226] Y.G. Li, T.H. Wu, W.J. Shen, X.H. Bao, Y.D. Xu, Combined single-pass conversion of methane via oxidative coupling and dehydro-aromatization, Catalysis Letters, 105 (2005) 77-82.

[227] Z. Liu, M.A. Nutt, E. Iglesia, The effects of CO2, CO and H-2 co-reactants on methane reactions catalyzed by Mo/H-ZSM-5, Catalysis Letters, 81 (2002) 271-279.

[228] J. Bedard, D.-Y. Hong, A. Bhan, Co-processing CH 4 and oxygenates on Mo/H-ZSM-5: 2. CH 4–CO 2 and CH 4–HCOOH mixtures, Physical Chemistry Chemical Physics, 15 (2013) 12173-12179.

[229] L. Jin, X. Zhou, X. He, H. Hu, Integrated coal pyrolysis with methane aromatization over Mo/HZSM-5 for improving tar yield, Fuel, 114 (2013) 187-190.

[230] J. Liu, H. Hu, L. Jin, P. Wang, S. Zhu, Integrated coal pyrolysis with CO_2 reforming of methane over Ni/MgO catalyst for improving tar yield, Fuel Proc. Tech., 91 (2010) 419-423.

[231] P. Wang, L. Jin, J. Liu, S. Zhu, H. Hu, Isotope analysis for understanding the tar formation in the integrated process of coal pyrolysis with CO2 reforming of methane, Energy & Fuels, 24 (2010) 4402-4407.

[232] Y.-C. Lin, J. Cho, G.A. Tompsett, P.R. Westmoreland, G.W. Huber, Kinetics and mechanism of cellulose pyrolysis, The J. of Physical Chem. C, 113 (2009) 20097-20107.

[233] T.E. Tshabalala, Non-oxidative conversion of methane into aromatic hydrocarbons over molybdenum modified H-ZSM-5 zeolite catalysts, in, University of the Witwatersrand, Johannesburg, 2013.

[234] H.-M. Wang, X.-H. Wang, M.-H. Zhang, X.-Y. Du, W. Li, K.-Y. Tao, Synthesis of bulk and supported molybdenum carbide by a single-step thermal carburization method, Chem. of Materials, 19 (2007) 1801-1807.

[235] P. Voogd, J.J.F. Scholten, H. van Bekkum, Use of the t-plot—De Boer method in pore volume determinations of ZSM-5 type zeolites, Colloids and Surfaces, 55 (1991) 163-171.

[236] Z. Yang, M. Sarkar, A. Kumar, J.S. Tumuluru, R.L. Huhnke, Effects of torrefaction and densification on switchgrass pyrolysis products, Bioresour. Technol., (2014).

[237] M.M. Treacy, J.B. Higgins, Collection of Simulated XRD Powder Patterns for Zeolites Fifth (5th) Revised Edition, Elsevier, 2007.

[238] A.S. Al-Dughaither, H. de Lasa, HZSM-5 zeolites with different SiO2/Al2O3 ratios. Characterization and NH3 desorption kinetics, Ind. & eng. chem. res., 53 (2014) 15303-15316.

[239] A. International, ASTM D5758 - 01: Standard Test Method for Determination of Relative Crystallinity of Zeolite ZSM-5 by X-Ray Diffraction, in, West Conshohocken, PA, United States, 2011, pp. 1-4.

[240] K. Wang, K.H. Kim, R.C. Brown, Catalytic pyrolysis of individual components of lignocellulosic biomass, Green Chem., 16 (2014) 727-735.

[241] A. Zheng, Z. Zhao, S. Chang, Z. Huang, H. Wu, X. Wang, F. He, H. Li, Effect of crystal size of ZSM-5 on the aromatic yield and selectivity from catalytic fast pyrolysis of biomass, J. of Molecular Catalysis A: Chem., 383–384 (2014) 23-30.

[242] Q. Bu, H. Lei, A.H. Zacher, L. Wang, S. Ren, J. Liang, Y. Wei, Y. Liu, J. Tang, Q. Zhang, R. Ruan, A review of catalytic hydrodeoxygenation of lignin-derived phenols from biomass pyrolysis, Bioresour. Tech., 124 (2012) 470-477.

[243] H. Shafaghat, P.S. Rezaei, W.M.A.W. Daud, Effective parameters on selective catalytic hydrodeoxygenation of phenolic compounds of pyrolysis bio-oil to high-value hydrocarbons, RSC Advances, 5 (2015) 103999-104042.

[244] Y. Zheng, D. Chen, X. Zhu, Aromatic hydrocarbon production by the online catalytic cracking of lignin fast pyrolysis vapors using Mo2N/γ-Al2O3, J. of Analytical and Appl. Pyrolysis, 104 (2013) 514-520.

[245] J.C. Serrano-Ruiz, J.A. Dumesic, Catalytic routes for the conversion of biomass into liquid hydrocarbon transportation fuels, Energy & Environmental Science, 4 (2011) 83-99.

[246] X.-f. Zhu, Q. Lu, Production of chemicals from selective fast pyrolysis of biomass, SCIYO. COM, (2010) 147.

[247] S. Sadaka, S. Negi, Improvements of biomass physical and thermochemical characteristics via torrefaction process, Environmental Progress & Sustainable Energy, 28 (2009) 427-434.

[248] Z. Yang, M. Sarkar, A. Kumar, J.S. Tumuluru, R.L. Huhnke, Effects of torrefaction and densification on switchgrass pyrolysis products, Bioresource Technology, 174 (2014) 266-273.

[249] J. Meng, J. Park, D. Tilotta, S. Park, The effect of torrefaction on the chemistry of fast-pyrolysis bio-oil, Bioresource Technology, 111 (2012) 439-446.

[250] S.J. Ren, H.W. Lei, L. Wang, Q. Bu, S.L. Chen, J. Wu, J. Julson, R. Ruan, The effects of torrefaction on compositions of bio-oil and syngas from biomass pyrolysis by microwave heating, Bioresource Technology, 135 (2013) 659-664.

[251] R.N. Hilten, R.A. Speir, J.R. Kastner, S. Mani, K. Das, Effect of torrefaction on bio-oil upgrading over HZSM-5. Part 2: Byproduct formation and catalyst properties and function, Energy & Fuels, 27 (2012) 844-856.

[252] R.N. Hilten, R.A. Speir, J.R. Kastner, S. Mani, K. Das, Effect of Torrefaction on Bio-oil Upgrading over HZSM-5. Part 1: Product Yield, Product Quality, and Catalyst Effectiveness for Benzene, Toluene, Ethylbenzene, and Xylene Production, Energy & Fuels, 27 (2013) 830-843.

[253] A. Zheng, Z. Zhao, Z. Huang, K. Zhao, G. Wei, X. Wang, F. He, H. Li, Catalytic fast pyrolysis of biomass pretreated by torrefaction with varying severity, Energy & Fuels, 28 (2014) 5804-5811.

[254] V. Srinivasan, S. Adhikari, S.A. Chattanathan, M. Tu, S. Park, Catalytic Pyrolysis of Raw and Thermally Treated Cellulose Using Different Acidic Zeolites, BioEnergy Research, (2014) 1-9.

[255] S. Adhikari, V. Srinivasan, O. Fasina, Catalytic Pyrolysis of Raw and Thermally Treated Lignin using Different Acidic Zeolites, Energy & Fuels, (2014).

[256] Y. Xu, X. Bao, L. Lin, Direct conversion of methane under nonoxidative conditions, Journal of Catalysis, 216 (2003) 386-395.

[257] G.E. Keller, M.M. Bhasin, Synthesis of ethylene via oxidative coupling of methane: I. Determination of active catalysts, Journal of Catalysis, 73 (1982) 9-19.

[258] K. Otsuka, K. Jinno, A. Morikawa, Active and selective catalysts for the synthesis of C2H4 and C2H6 via oxidative coupling of methane, Journal of Catalysis, 100 (1986) 353-359.

[259] S. Majhi, P. Mohanty, H. Wang, K.K. Pant, Direct conversion of natural gas to higher hydrocarbons: A review, Journal of Energy Chemistry, 22 (2013) 543-554.

[260] H. Jiang, L. Wang, W. Cui, Y. Xu, Study on the induction period of methane aromatization over Mo/HZSM-5: partial reduction of Mo species and formation of carbonaceous deposit, Catalysis Letters, 57 (1999) 95-102.

[261] Y. Xu, L. Lin, Recent advances in methane dehydro-aromatization over transition metal ion-modified zeolite catalysts under non-oxidative conditions, Applied Catalysis A: General, 188 (1999) 53-67.

[262] Y. Shu, Y. Xu, S.-T. Wong, L. Wang, X. Guo, Promotional Effect of Ru on the Dehydrogenation and Aromatization of Methane in the Absence of Oxygen over Mo/HZSM-5 Catalysts, Journal of Catalysis, 170 (1997) 11-19.

[263] D. Ma, Y. Shu, M. Cheng, Y. Xu, X. Bao, On the Induction Period of Methane Aromatization over Mo-Based Catalysts, Journal of Catalysis, 194 (2000) 105-114.

[264] V.R. Choudhary, A.K. Kinage, T.V. Choudhary, Low-temperature nonoxidative activation of methane over H-galloaluminosilicate (MFI) zeolite, Science, 275 (1997) 1286-1288.

[265] H. Zhang, A. Kong, Y. Ding, C. Dai, Y. Shan, Low-temperature activation of methane over rare earth metals promoted Zn/HZSM-5 zeolite catalysts in the presence of ethylene, Journal of Natural Gas Chemistry, 20 (2011) 243-248.

[266] A.A. Gabrienko, S.S. Arzumanov, I.B. Moroz, A.V. Toktarev, W. Wang, A.G. Stepanov, Methane Activation and Transformation on Ag/H-ZSM-5 Zeolite Studied with Solid-State NMR, The Journal of Physical Chemistry C, 117 (2013) 7690-7702.

[267] T.V. Choudhary, E. Aksoylu, D. Wayne Goodman, Nonoxidative activation of methane, Catalysis reviews, 45 (2003) 151-203.

[268] A. Sluiter, B. Hames, R. Ruiz, C. Scarlata, J. Sluiter, D. Templeton, D. Crocker, Determination of Structural Carbohydrates and Lignin in Biomass, in, NREL, 2011.

160

[269] A.M. Moneeb, A.M. Alabdulrahman, A.A. Bagabas, C.K. Perkins, A.W. Apblett, Bimetallic single-source precursor for the synthesis of pure nanocrystalline room temperature-stabilized β-NiMoO 4, Ceramics International, 42 (2016) 1366-1372.

[270] A. Bridgwater, G.W.E. Kommission, Thermal biomass conversion and utilization: biomass information system, Office for Official Publications of the European Communities, 1996.

[271] C. Hu, J. Li, W. Jia, M. Liu, Z. Hao, Z. Zhu, Influence of Metallic Modification on Ethylbenzene Dealkylation over ZSM‑5 Zeolites, Chinese Journal of Chemistry, 33 (2015) 247-252.

[272] P. He, H. Song, Catalytic Conversion of Biomass by Natural Gas for Oil Quality Upgrading, Industrial & Engineering Chemistry Research, 53 (2014) 15862-15870.

[273] P. He, W. Shan, Y. Xiao, H. Song, Performance of Zn/ZSM-5 for In Situ Catalytic Upgrading of Pyrolysis Bio-oil by Methane, Topics in Catalysis, 59 (2016) 86-93.

[274] S. Neupane, S. Adhikari, Z. Wang, A. Ragauskas, Y. Pu, Effect of torrefaction on biomass structure and hydrocarbon production from fast pyrolysis, Green Chemistry, 17 (2015) 2406-2417.

VITA

ZIXU YANG
Candidate for the Degree of
Doctor of Philosophy

Thesis: SYNERGISTIC CO-PYROLYSIS OF BIOMASS AND NATURAL GAS OVER
HZSM-5 CATALYSTS

Major Field: Biosystems Engineering

Biographical:

Education:

Completed the requirements for the Doctor of Philosophy in Biosystems Engineering at
Oklahoma State University, Stillwater, Oklahoma in May, 2016.

Completed the requirements for the Masters of Engineering in Thermal Engineering at Huazhong
University of Science and Technology, Wuhan, China in March 2012.

Completed the requirements for the Bachelors of Engineering in Thermal and Power Engineering
at Huazhong University of Science and Technology, Wuhan, China in June 2009.

Experience:

Research Assistant (Biomass Thermochemical Conversion), Oklahoma State University,
Stillwater, Oklahoma, August 2012 to Present.

Research Assistant (State key laboratory of coal combustion), Huazhong University of Science
and Technology, Wuhan, China in September 2009 - June 2012.

Professional Memberships:
American Society of Agricultural and Biological Engineers (ASABE)
American Chemical Society (ACS)